dramatically different ICP-MS

Thermo SCIENTIFIC

Experience class-leading performance and ease of use with the all-new Thermo Scientific iCAP Q ICP-MS.

Explore the latest technological advances and applications capabilities at our ICP-MS Launch Centre:

- Download application notes
- Watch videos to see how easy the iCAP™ Q is to use
- Navigate through ground-breaking ICP-MS technology

Free safety glasses for every visitor who registers!

• thermoscientific.com/dramatic • Experience the difference!

Read our application note:
"IC-ICP-MS speciation analysis of As in apple juice"
in the February Application Notebook.

Volume 27 Number 2

Spectroscopy®

Solutions for Materials Analysis

February 2012 Volume 27 Number 2 www.spectroscopyonline.com

FT-IR Analysis of the Color Components of Red Wine

Atomic Force Microscopy–Infrared for Nanoscale Analyses

Contact Lens Manufacturing Quality Control Using Confocal Raman Microscopy

Raman Spectroscopy and Nanomaterials

ADVANSTAR SCIENCE

SPECTROSCOPY

February 2012

MB-*Rx*. Reaction Monitoring Made Easy

See our latest analyzer, the MB-*Rx* Reaction Monitor, at PITTCON 2012. The MB-*Rx* is a plug-and-play solution designed for research laboratories and pilot plants. It provides chemists with direct access to real-time experiment data via a rugged insertion probe and an intuitive software interface. The MB-*Rx* is maintenance-free and offers analytical performance, reliability and simplicity. **www.abb.com/analytical**

Visit us at PITTCON in booth #2559

PITTCON CONFERENCE & EXPO 2012
ORLANDO · MARCH 11-16

ABB Inc.
Analytical Measurement
Phone: +1 418-877-2944
1 800 858-3847 (North America)
Email: ftir@ca.abb.com

Power and productivity
for a better world™

ABB

REMARKABLY BETTER

experience
commitment
support
quality
investment
security
confidence
durability
accuracy
atomic
spectroscopy
data
reliability
results

THE ATOMIC SPECTROSCOPY LEADER

Making an investment in atomic spectroscopy comes down to one word: Trust. Trust in an instrument's performance. Trust in a provider's support and commitment to development. Trust in getting the best product and best results. When it comes to AA, ICP-OES, ICP-MS and the latest MP-AES solutions, you can trust Agilent – the atomic spectroscopy leader.

Learn what makes Agilent's Atomic Spectroscopy portfolio Remarkably Better.

www.agilent.com/chem/atomicspec

The Measure of Confidence

Agilent Technologies

Spectroscopy®

ADVANSTAR SCIENCE

MANUSCRIPTS: To discuss possible article topics or obtain manuscript preparation guidelines, contact the editorial director at: (732) 346-3020, e-mail: lbush@advanstar.com. Publishers assume no responsibility for safety of artwork, photographs, or manuscripts. Every caution is taken to ensure accuracy, but publishers cannot accept responsibility for the information supplied herein or for any opinion expressed.

SUBSCRIPTIONS: For subscription information: *Spectroscopy,* P.O. Box 6196, Duluth, MN 55806-6196; (877) 527-7008, 7:00 a.m. to 6:00 p.m. CST. Outside the U.S., +1-218-740-6477. Delivery of *Spectroscopy* outside the U.S. is 3–14 days after printing. Single-copy price: U.S., $10.00 + $7.00 postage and handling ($17.00 total); Canada and Mexico, $12.00 + $7.00 postage and handling ($19.00 total); Other international, $15.00 + $7.00 postage and handling ($22.00 total).

CHANGE OF ADDRESS: Send change of address to *Spectroscopy,* P.O. Box 6196, Duluth, MN 55806-6196; provide old mailing label as well as new address; include ZIP or postal code. Allow 4–6 weeks for change. Alternately, go to the following URL for address changes or subscription renewal: https://advanstar.replycentral.com/?PID=581

RETURN ALL UNDELIVERABLE CANADIAN ADDRESSES TO: Pitney Bowes, P.O. Box 25542, London, ON N6C 6B2, CANADA. PUBLICATIONS MAIL AGREEMENT No.40612608.

REPRINTS: Reprints of all articles in this issue and past issues are available (500 minimum). Call 800-290-5460, x100 or e-mail AdvanstarReprints@theYGSgroup.com.

DIRECT LIST RENTAL: Contact Tamara Phillips, (440) 891-2773; e-mail: tphillips@advanstar.com

INTERNATIONAL LICENSING: Maureen Cannon, (440) 891-2742, fax: (440) 891-2650; e-mail: mcannon@advanstar.com.

50% Recycled Paper, 10-20% Post Consumer Waste

BPA WORLDWIDE BUSINESS

american business media
The Association of Business Information Companies

HUMAN HEALTH

ENVIRONMENTAL HEALTH

Discover the PinAAcle of Performance in AA. Engineered around cutting-edge fiber-optic technology for enhanced light throughput and superior detection limits, the new PinAAcle™ series is the latest innovation from the world leader in atomic absorption. Available in flame, furnace, or combination models, PinAAcle instruments offer exactly the level of performance you need with the smallest footprint of any combined flame/graphite furnace AA system on the market. Experience peak performance and unmatched productivity. Step up to the PinAAcle series from PerkinElmer.

Request your PinAAcle welcome pack – www.perkinelmer.com/pinaaclewelcome

PerkinElmer®
For the Better

Spectroscopy®

PUBLISHING & SALES
485F US Highway One South, Suite 100, Iselin, NJ 08830
(732) 596-0276, Fax: (732) 647-1235

Michael J. Tessalone
Science Group Publisher, mtessalone@advanstar.com
Edward Fantuzzi
Publisher, efantuzzi@advanstar.com
Stephanie Shaffer
East Coast Sales Manager, sshaffer@advanstar.com
(508) 481-5885

EDITORIAL
Laura Bush
Editorial Director, lbush@advanstar.com
Megan Evans
Managing Editor, mevans@advanstar.com
Stephen A. Brown
Group Technical Editor, sbrown@advanstar.com
Cindy Delonas
Associate Editor, cdelonas@advanstar.com
Dan Ward
Art Director, dward@media.advanstar.com

MARKETING
Anne Young
Marketing Manager, ayoung@advanstar.com

MARKET DEVELOPMENT
Tamara Phillips
Direct List Rentals, tphillips@advanstar.com
YGS Group
Reprints, advanstarreprints@theYGSgroup.com
Maureen Cannon
Permissions, mcannon@advanstar.com

PRODUCTION AND AUDIENCE DEVELOPMENT
David Erickson
Production Manager, derickson@media.advanstar.com
Peggy Olson
Audience Development Manager, polson@advanstar.com
Gail Mantay
Audience Development Assistant Manager, gmantay@advanstar.com

ADVANSTAR SCIENCE

Joseph Loggia
President, Chief Executive Officer
Theodore S. Alpert
Executive Vice-President, Finance & Chief Financial Officer
Tony Calanca
Executive Vice-President, Exhibitions
Georgiann DeCenzo
Executive Vice-President, Licensing, Market Development & Europe
Chris DeMoulin
Executive Vice-President, Fashion & President MAGIC International
Thomas Ehardt
Executive Vice-President, Chief Administrative Officer
Eric I. Lisman
Executive Vice-President, Corporate Development
Daniel Phillips
Executive Vice-President, Powersports, Dental & Veterinary
Andrew Pollard
Executive Vice-President, Fashion & President, PROJECT
Steve Sturm
Executive Vice-President, Chief Marketing Officer
Ron Wall
Executive Vice-President, Pharmaceutical/Science & CBI
Francis Heid
Vice-President, Media Operations
J Vaughn
Vice-President, Information Technology
Mike Alic
Vice-President, Electronic Media Group
Nancy Nugent
Vice-President, Human Resources
Ward D. Hewins
Vice-President, General Counsel
Russell Pratt
Vice President Sales/Group Publisher of Pharmaceutical/Science Group
Peter Houston
Director of Content

What makes Glass Expansion different?

We are the world leader in the design of ICP sample introduction systems. The ICP that you are using now almost certainly incorporates sample introduction components based on original Glass Expansion designs.

We provide a unique no-risk guarantee. If you find one of our products unsuitable in any way, you can return it for a credit or refund.

We have a full staff of technical people to assist you. We have our own laboratory with four ICP spectrometers (ICP-OES and ICP-MS) and you can count on expert advice on your application from our experienced technical staff.

We provide rapid delivery. Most items are held in stock and we ship immediately after receiving your order.

To request a copy of our catalog, or sign up for our newsletter, please vist our website:

Glass Expansion
4 Barlows Landing Road
Unit 2A • Pocasset • MA 02559, USA
Toll Free Phone: 800 208 0097
Telephone: 508 563 1800
Facsimile: 508 563 1802
Email: geusa@geicp.com
Web: www.geicp.com

GE **GLASS EXPANSION**
Quality By Design

Spectroscopy
February 2012
Volume 27 Number 2

Cover image courtesy of Andreas Levers/Getty Images.

ON THE WEB

WEB SEMINARS

Introduction to and Instrumentation for Inductively Coupled Plasma–Mass Spectrometry (ICP-MS)
R. Samuel Houk, Professor of Chemistry, Iowa State University and Scientist in the Ames Laboratory, United States Department of Energy

Quantitative Raman Analysis of Polymers and Additives
Travis Thompson, Raman Spectroscopy Product Specialist at B&W Tek, and Henryk Herman, Chemical Physicist and Laser Specialist at GnoSys Global Ltd.

Register free for live or on demand events:

spectroscopyonline.com/webseminars

ICP-MS

Inductively coupled plasma–mass spectrometry (ICP-MS) is a primary technique for trace elemental analysis. In a new roundtable, experts discuss the effects of carbon in samples and the use of correction equations to account for interferences.

spectroscopyonline.com/TechForum

LinkedIn Join the Spectroscopy Group on LinkedIn

CONTENTS

VOLUME 27 NUMBER 2
FEBRUARY 2012

Columns

Articles

DEPARTMENTS

Spectroscopy (ISSN 0887-6703 [print], ISSN 1939-1900 [digital]) is published monthly by Advanstar Communications, Inc., 131 West First Street, Duluth, MN 55802-2065. Spectroscopy is distributed free of charge to users and specifiers of spectroscopic equipment in the United States. *Spectroscopy* is available on a paid subscription basis to nonqualified readers at the rate of: U.S. and possessions: 1 year (12 issues), $74.95; 2 years (24 issues), $134.50. Canada/Mexico: 1 year, $95; 2 years, $150. International: 1 year (12 issues), $140; 2 years (24 issues), $250. Periodicals postage paid at Duluth, MN 55806 and at additional mailing offices. POSTMASTER: Send address changes to *Spectroscopy*, P.O. Box 6196, Duluth, MN 55806-6196. PUBLICATIONS MAIL AGREEMENT NO. 40612608, Return Undeliverable Canadian Addresses to: Pitney Bowes, P. O. Box 25542, London, ON N6C 6B2, CANADA. Canadian GST number: R-124213133RT001. Printed in the U.S.A.

SHIMADZU

Elevating Excellence in UV-Vis Analyses

From Performance to Price, New Compact, Research-Grade UV-Vis Spectrophotometers Outclass the Competition

With advanced optical systems engineered to substantially reduce stray light, Shimadzu's new ultra-compact single-monochromator UV-2600 and double monochromator UV-2700 spectrophotometers offer a number of high-performance and productivity-enhancing features to enable confident and convenient use for routine analysis as well as demanding research applications.
At prices that can't be beat.

Learn more about Shimadzu's UV-2600/2700.
Call (800) 477-1227 or visit us online at
www.ssi.shimadzu.com/262700

Shimadzu's UV-2600/2700 spectrophotometers feature:

- High absorbance level to 8 Abs
- Wide measurement range to 1400 nm
- Ultra low stray light (0.00005 %T at 220 nm)
- Smallest footprint in their class
- USB connection
- Wide range of accessories and software packages
- Unbelievable performance/price ratio

For pharmaceutical and other applications requiring that hardware be validated, the UV-2600/2700 Series provides validation software as standard.

IR 55th 2011 60th 2012 UV ANNIVERSARY

Order consumables and accessories on-line at http://store.shimadzu.com
Shimadzu Scientific Instruments Inc., 7102 Riverwood Dr., Columbia, MD 21046, USA

Editorial Advisory Board

Spectroscopy's Editorial Advisory Board is a group of distinguished individuals assembled to help the publication fulfill its editorial mission to promote the effective use of spectroscopic technology as a practical research and measurement tool. With recognized expertise in a wide range of technique and application areas, board members perform a range of functions, such as reviewing manuscripts, suggesting authors and topics for coverage, and providing the editor with general direction and feedback. We are indebted to these scientists for their contributions to the publication and to the spectroscopy community as a whole.

Inorganic Certified Reference Materials

Inorganic product applications include:

- Single and multi-element standards for AA and ICP
- Single and multi-element standards for ICP and ICP-MS
- Standards for Ion Chromatography
- Environmental testing standards
- Organometallic oil standards
- Consumer safety compliance standards
- Contamination control products
- Custom standards for use with any application

For over 55 years, SPEX CertiPrep has offered a powerful combination of quality and unparalleled service to support scientific development around the world. You can rely on us to provide superior Certified Reference Materials (CRMs) when, where, and how you need them.

Visit us at PITTCON CONFERENCE & EXPO 2012 ORLANDO · MARCH 11-15

Booths # 2330 & 2333

SPEX CertiPrep®

Your Science is Our Passion.®

203 Norcross Ave.
Metuchen, NJ 08840
Phone: 1-800-LAB-SPEX
Fax: 1-732-603-9647
E-mail: crmsales@spexcsp.com
www.spexcertiprep.com

Follow SPEXCertiPrep on:

Your Science is Our Passion.®

Accredited by A2LA for ISO 17025 and Guide 34, and by Certified by UL-DQS for ISO 9001.

From the Editor

Laura Bush is the editorial director of *Spectroscopy* and *LCGC North America,* lbush@advanstar.com.

The Next Generation

A lively exchange of perspectives emerged recently on the LinkedIn group for *Spectroscopy,* as well as on the group for our sister magazine, *LCGC.* The conversation, sparked by a *New York Times* article, was about what it takes to become a scientist and why so many students, particularly in the United States, become discouraged along the way. The article noted that about 40% of students planning to major in science or engineering end up switching to other subjects or even failing to get a degree. When premedical students are included, the number increases to as high as 60%. That is twice the attrition rate of all other majors combined.

A number of participants in the LinkedIn communities said this phenomenon is not new. Science is challenging, and it requires hard work to obtain even an undergraduate degree. One noted that her roommate thought she was a graduate student, because she spent so much time in the laboratory and studying instead of socializing like the students majoring in business and liberal arts. If you don't have what it takes, or the love of it, many say, it's fine to move on.

That may be. But another important factor is the preparation students receive in these areas earlier in their education. There are too many American students who finish high school poorly prepared in math and science. And that's not just a problem for those who want to go on to earn a PhD in chemistry. In the current national conversation about the economy, and particularly over the question of which sectors can provide middle-class jobs for the future, many companies say they have difficulty finding people with the right education and skill sets in the United States. To cite just one example, the factories that remain in this country will produce high-end products that must be made with complex robotics rather than with large staffs of uneducated laborers. That means that even on factory floors, employees will need a stronger background in math and science than previous generations of American workers.

Improving the U.S. educational system is not easy. But student motivation is an important factor that should not be dismissed. As many people pointed out in the forum, our culture worships actors and athletes, not scientists or other intellectuals. (Just think of how scientists are portrayed in the television series, "The Big Bang Theory.")

Yet I have always believed the microculture trumps macroculture. We live in a larger society, but the greatest influence on our lives comes from the environment immediately surrounding us — the people we interact with every day. So even in an educational system with many gaps, an individual chemistry teacher can motivate students to continue with studies that may at first seem dry or difficult. One participant in the forum is a teacher who understands this well. In particular, he knows the value of paying attention to the average students, not just to the best and brightest. He writes:

"I once sat in front of a GC–MS system with a bunch of 'problem students' — the back-row gang. I talked of gasoline, additives, and octane. You could hear a pin drop. One of those went on to get a BS in chemistry because he saw what he could do. Little things matter."

Moving, isn't it? The good news is that it's not necessary to be employed as a teacher to contribute to this cause. Any scientist can visit a school and serve as a role model. You don't have to be famous, or a Nobel prize winner. You can just share what you do, what it took to get there, and why it was worth it.

In this online discussion, many participants expressed pride and satisfaction in their choice of profession. If some small percentage of today's generation of scientists visited a school this year to talk about why their work is rewarding, that could lead to countless students making the decision to stick with their preparation for future employment in the field.

Think about it. You, too, can make a difference. Would you like to be an ambassador for science?

B&W TEK INC.

Your Photonics Partner

SPECTROMETERS | LASERS | TOTAL SOLUTIONS

Sample Holders

Integrating Spheres

Fiber Probes

Light Sources

All you need, *and then some.*

B&W Tek has the most comprehensive line of UV, Vis & NIR spectrometers and accessories, with nearly limitless configurations.

- ***Reflectance***
- ***Absorption***
- ***Raman***
- ***Transmission***
- ***Emission***
- ***Fluorescence***

...And countless other applications.

Fiber Optic Spectrometers

Learn more!

Contact our applications specialists at 1-302-368-7824
or visit us at www.bwtek.com

News Spectrum

Jim Rydzak Joins *Spectroscopy*'s Editorial Advisory Board

Spectroscopy magazine is pleased to announce the addition of Jim Rydzak to its editorial advisory board.

Jim Rydzak is a practitioner of process analytical chemistry and chemometrics with experience primarily in active pharmaceutical ingredient development at GlaxoSmithKline (GSK), near Philadelphia, Pennsylvania, where he has worked for the past 12 years. Jim was a key person in starting the process analytical technology (PAT) group at GSK and Colgate-Palmolive. Jim was at Colgate-Palmolive for 16 years before joining GSK, first as a molecular spectroscopist. He then started the process analytical group in 1989, and later became a group leader and analytical and testing lab supervisor.

Jim's background in Fourier-transform infrared (FT-IR), Raman, and near-infrared (NIR) spectroscopy led him into the process analytical field in the early 1980s. During his time at Colgate, he was a member of the Directors of Industrial Research Process Analytical roundtable. More recently, Jim was one of the founding members of the ASTM E55 committee on the "Manufacture of Pharmaceutical Products" and is a member of the ASTM E13 committee on "Analytical Instrumentation."

Jim received his BS in Chemistry from Mount Union College in Alliance, Ohio, and his MS in Analytical Chemistry working for Peter Griffiths at Ohio University (Athens, Ohio). Jim taught short courses in molecular spectroscopy with for the Center for Professional Advancement for eight years in Amsterdam and New Jersey in the 1990s. Jim also has teamed with Chris Hassell to run the "Process Analytical Chemistry: Out of the Lab and into the Pipes" course on PAT at the Federation of Applied Chemistry and Spectroscopy Societies (FACSS) conference for several years.

Jim Rydzak

Jim has been active on the FACSS governing board and has held the offices of governing board, program, long-range planning, site selection, and workshop and employment bureau chair positions in the FACSS organization since 1996. He also is active in the Coblentz

Market Profile: Terahertz Spectroscopy

One of the newest and fastest-growing subsegments of the molecular spectroscopy market is terahertz spectroscopy. It makes use of a previously underused segment of the electromagnetic spectrum and is already seeing demand from a variety of industries. Although it remains unclear which industries will become major adopters of the technology, it looks certain that terahertz spectroscopy will develop into a major segment of the molecular spectroscopy market.

The terahertz region of the electromagnetic spectrum lies between the far-infrared region and the microwave region, and it includes wavelengths of about 0.1–1.0 mm. Terahertz spectroscopy is complementary to other spectroscopy techniques, as a number of compounds have unique fingerprints in the terahertz region, including some narcotics, explosives, and various polymorphic forms of active pharmaceutical ingredients. A variety of common materials, as well as human tissue, are semitransparent to terahertz radiation, and it is non-ionizing, making it safe for human exposure. A wide variety of commercial terahertz spectrometers are already on the market, including, conventional frequency-domain systems, time-domain systems, imaging systems, and portable instruments.

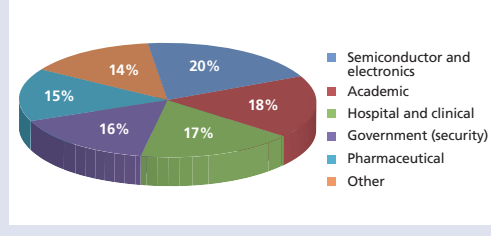

Terahertz spectroscopy demand by industry for 2011.

Although there is not yet widespread adoption of terahertz spectroscopy in any one industry, there is considerable potential and interest from several sectors. Some vendors have developed terahertz-based systems for oncology applications and are pursuing regulatory approvals. Most vendors are targeting industries as diverse as pharmaceuticals, semiconductors and electronics, and aerospace materials.

The first commercial terahertz spectrometers were introduced less than a decade ago, and since then, the market has grown to more than $10 million in annual sales. There are now more than half a dozen vendors of terahertz spectrometers, and, as with most new markets, most of the competitors are fairly recent start-ups. None of the major spectroscopy vendors are producing their own terahertz spectrometers yet.

The foregoing data were based on SDi's market analysis and perspectives report entitled *Global Assessment Report, 11th Edition: The Laboratory Life Science and Analytical Instrument Industry, October 2010.* For more information, contact Stuart Press, Vice President – Strategic Analysis, Strategic Directions International, Inc., 6242 Westchester Parkway, Suite 100, Los Angeles, CA 90045, (310) 641-4982, fax: (310) 641-8851, www.strategic-directions.com.

Society (President elect 2012) and the Society of Applied Spectroscopy organizations and was active at the Eastern Analytical Symposium (EAS) as a Coblentz representative or alternate from 1999–2007.

FACSS Innovation Awards Winners Announced

The Federation of Analytical Chemistry and Spectroscopy Societies (FACSS) announced the winners of the 2011 FACSS Innovation Awards, which showcase the newest and most creative science debuted orally at a FACSS-organized conference. Shortlisted finalists competed in front of expert panels for the top prizes at the 2011 FACSS conference in Reno, Nevada (October 2–7, 2011).

After commending the high quality of the entries, the panel selected four equal awardees. These are:

Ultrasound Enhanced ATR Mid-IR Fiber Optic Probe for Spectroscopy of Particles in Suspensions, Cosima Koch, Markus Brandstetter, Stefan Radel, and Bernhard Lendl, Vienna University of Technology (Vienna, Austria).

Large-Area Standoff Planetary Raman Measurements Using a Novel Spatial Heterodyne Fourier Transform Raman Spectrometer, S. Michael Angel and Nathaniel R. Gomer of the University of South Carolina (Columbia, South Carolina); Shiv K. Sharma of the University of Hawaii, (Honolulu, Hawaii); and J. Chance Carter and Lawrence Livermore of the National Laboratory (Livermore, California).

Single Molecule Fluorescence Imaging Studies of Dynamic Processes in Reversed Phase Chromatographic Materials, Justin Cooper, Eric Peterson, and Joel Harris, University of Utah (Salt Lake City, Utah).

Laser Ablation Molecular Isotopic Spectrometry — New Dimension of LIBS, Alexander Bol'shakov of Applied Spectra, Inc., (Fremont, California); Richard Russo of Applied Spectra, Inc., and Lawrence Berkeley National Laboratory (LBNL) in Berkeley, California; Xianglei Mao, Dale Perry, and Osman Sorkhabi of LBNL; and Chris McKay from the NASA-Ames Research Center (Moffett Field, California).

Each awardee will be presented with a cash prize and commemorative plaque, and are invited to return to the conference in 2012 to become a point of emphasis in the scientific program. The awards will be formally presented at FACSS' SCIX conference, which will be held in Kansas City from September 30 to October 4, 2012.

Because of the exceptional quality of this year's submissions, the FACSS Governing Board has decided to make the FACSS Innovation Awards an integral part of the annual conference presented by FACSS, and as a result, the 2012 FACSS Innovation Awards will be presented at the SCIX conference in Kansas City. Entries for the 2012 FACSS Innovation Awards may be made during the abstract submission period for the SCIX 2012 conference. Authors may opt in for award consideration by marking a single check-box during abstract submission. All attendees are eligible for the award irrespective of educational level or professional vocation.

University Develops Alternative Materials to Silicone Breast Implants Using MALS and QELS Technology

Researchers at the University of Akron's (Akron, Ohio) Department of Chemical and Biomolecular Engineering are using macromolecular engineering to precision-synthesize biocompatible polymers to produce bionanocomposites for use as silicone alternatives in breast implants. Led by Professor Judit E. Puskas, the group is using viscometers, refractive-index detectors, multiangle (18-angle) light scattering (MALS) detectors, and quasi-elastic light scattering (QELS) detectors from Wyatt Technology Corporation (Santa Barbara, California) in their study.

Traditionally, a simpler system would have been used that is commonly used with column calibration to polymer standards, or three-angle light scattering. The system the researchers are using instead reportedly delivers the accurate and reproducible results needed when performing these cutting-edge polymer studies.

The research group is part of an interdisciplinary group that is pursuing research aimed at reducing or eliminating capsular contracture associated with breast implants to help women in need.

European Airports to Test New Bottle Scanner that Uses Raman Spectroscopy

The European Civil Aviation Conference (ECAC, Neuilly sur Seine, France) has approved initial trials at several major airports of a bottle scanner that uses a proprietary technology called spatially offset Raman spectroscopy (SORS). The scanner potentially can enable aircraft passengers to carry liquid items larger than 100 mL, such as water, cosmetics, perfumes, and duty free items, through airport security. The scanner exceeded the ECAC standard for use with an almost perfect detection capability and a negligible false-alarm rate in unopened containers, ensuring maximum safety for the traveling public and a minimum of delays. The scanner is reportedly capable of identifying explosives unambiguously inside opaque bottles such as colored plastic shampoo containers or green glass wine bottles. Other systems do not precisely identify the threat reliably and may lead to large numbers of false alarms or missing genuine threats.

The SORS technique was developed by the Science & Technology Facilities Council (STFC) Central Laser Facility at its Rutherford Appleton Laboratory (Oxfordshire, UK), and led to the creation of Cobalt Light Systems as a spin out of STFC. ■

Molecular Spectroscopy Workbench

The Contribution of Raman Microscopy to the Characterization of Nanomaterials

Raman is usually thought of as a tool for studying molecular and crystalline structure; in this context it also can differentiate the amorphous phase from any number of crystalline phases. However, it is also known that Raman spectra of a crystalline phase can be acquired under conditions where X-ray crystallography indicates that the sample is amorphous. With the development of nanophase materials, Raman is exhibiting a unique capability for characterizing materials that are between crystalline and amorphous.

Fran Adar

I heard recently that the concept of nanoscience lies with Richard Feynman, one of the boy geniuses of the Manhattan Project. If you do not know who he was, you can do a Google search on Feynman's name that will bring you to a web site (feynmanonline.com) with this interesting summary of who he was: "This web site is dedicated to Richard P. Feynman (1918–1988), scientist, teacher, raconteur, and musician. He assisted in the development of the atomic bomb, expanded the understanding of quantum electrodynamics, translated Mayan hieroglyphics, and cut to the heart of the Challenger disaster. But beyond all of that, Richard Feynman was a unique and multifaceted individual." To get to the point, Feynman delivered a lecture on December 29, 1959, entitled "There's Plenty of Room at the Bottom" (1), which is cited as the origin of nanoscience. Several points are of interest. First, the transcript of the lecture has no term with "nano" in front of it, even though he describes things on the nanoscale level. Second, he describes many technologies that were far from development in 1959, but have since appeared. For example, he described nanolithography for storing all the information accumulated by man in something small enough to carry around, and miniaturizing computers, using germanium as the active substrate! But for us, what may be most interesting is a comment that he makes in the section entitled "Better Electron Microscopes"; he talks about using a better electron microscope that would enable one to visualize where the atoms are for chemical analysis. Maybe such a microscope has come close to realization, but we also should note that spectroscopy has been developed for indirect chemical analysis and is being done during reactions, which would be difficult to do in an electron microscope.

The goal of this column is to discuss the use of spectroscopy in studying nanomaterials, in particular, how Raman spectroscopy is being used to study nanomaterials. However, we are not going to include a discussion of microcrystalline and disordered carbon, carbon nanotubes, or graphene because we have dealt with them in earlier columns, and they actually are special cases.

Phonon Confinement

The essential point to understanding Raman spectra of solid-phase nanomaterials is to recognize the effect

of the crystallite size on the optical phonons that we detect. That means reviewing a bit of solid state physics. The reader is directed to the August 2007 issue of the *Journal of Raman Spectroscopy,* which was devoted to review papers on nanomaterials. In particular, the article by Arora and colleagues (2) discusses the role of phonon confinement in solids. Because this concept is key to understanding how Raman can contribute to the analysis of nanomaterials, we will attempt to summarize the theory here.

In a crystal of essentially infinite dimensions, there is translational symmetry that is reflected in the conservation of momentum selection rule. The phonons in such crystals are described by both their energy (ω) and wavevector (**q**). The wavevector describes how the phonon propagates in the crystal and is consequently a vector quantity — it has direction and magnitude. The wavevector can vary between 0 and $\pi/2a_i$, where a_i is the lattice constant along the ith axis. In a Raman scattering event the laser light enters a crystal along an axis, for instance the Z direction (for example, a (001) face) and the scattered light can be collected in the back-scattering geometry (-Z); to conserve momentum, for this geometry the scattering wavevector is $\mathbf{k}_l - \mathbf{k}_s = \mathbf{k}_l - (-\mathbf{k}_l) = 2\mathbf{k}_l = \mathbf{q}_{ph}$ where $\mathbf{k}_l$ is the wavevector of the laser photon in the crystal, $\mathbf{k}_s$ is the wavevector of the scattered light in the crystal, and $\mathbf{q}_{ph}$ describes the

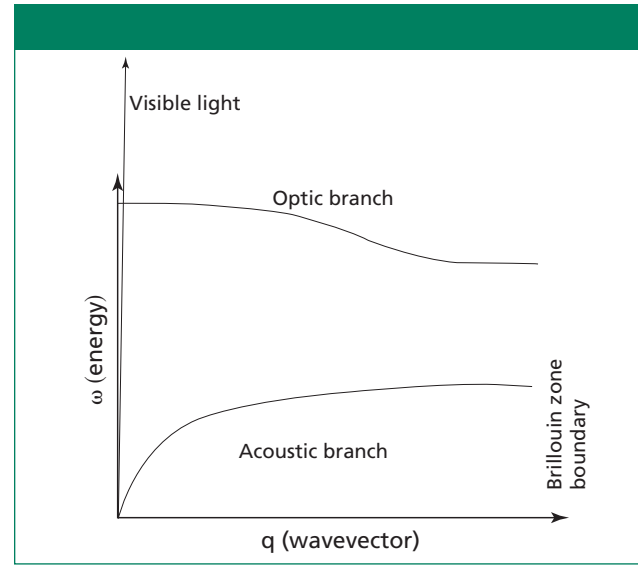

Figure 1: Typical dispersion curves for phonons in a crystal with 2 atoms/unit cell (for example, Si, Ge, and diamond). The *x* axis describes the momentum in a crystal, and the *y* axis describes the phonon energy. In the acoustic mode the atoms move in phase; in the optic mode they move out of phase. If the two atoms are dissimilar the phonon will support a dipole moment, will be IR-active, and there will be a splitting between the TO (transverse optical) and LO (longitudinal optical) modes. In longitudinal mode, atomic motion is parallel to the direction of propagation.

phonon scattering wavevector. The wavevectors in crystals of all visible photons are so close to zero in the reciprocal lattice that it is said that first order Raman scattering always occurs at the "Brillouin zone center" which means $\mathbf{q} = 0$. It is this approximation that breaks down in nanocrystals.

All states of a crystal (electronic and vibrational or phonons) are described in terms of energy and momentum. Electronic and phonon states cannot assume arbitrary energies and momenta in crystals. These states have to fit the properties of the crystal. The relationship between energy and momentum, called *dispersion,* is described in Figure 1, which shows the dispersion curves for the acoustic and optical phonon modes in a crystal with two atoms in the unit cell such as silicon, germanium, or diamond. If the crystal is small, the phonons are not free to drift over large distances. There will be scattering at the crystal boundaries which will change the phonon wavevector, effectively introducing uncertainty to its value.

The uncertainty in the phonon momentum means that scattering occurs not only at $\Delta\mathbf{k} = \mathbf{q} = 0$, but for some values of $\mathbf{q}$ greater than 0; the uncertainty in $\mathbf{q}$ is estimated to be equal to π/d, where d is the size of the grain. Clearly the smaller the value of d, the more the contributions from farther along the dispersion curve. In an early publication dealing with Raman scattering from such small crystals (3), a Gaussian confinement model was developed.

For isolated nanocrystals, the phonon cannot extend beyond the crystal boundary so its wavefunction is to be multiplied by a Gaussian confinement function, $W(r)$, which is sometimes expressed as

$$W(r) = \exp(-\alpha r^2/d^2) \qquad [1]$$

where d is the dimension of a "spherical crystal" and α describes how rapidly the phonon amplitude decays close to the surface. The scattering intensity is predicted to follow

$$I(\omega) = \int \frac{|C(q)|^2}{[\omega - \omega(q)]^2 + (\Gamma_o/2)^2}\, dq \qquad [2]$$

where $C(q)$ is a q-dependent weighting function that depends on the confinement model and Γ_o is the natural width of the zone-center optical phonon. This equation for $I(\omega)$ is compared to the measured spectrum to account for the shift and asymmetric broadening of the peaks. Usually, the dispersion of the optical phonon slopes downward around the center of the Brillouin zone (Figure 1), so the observed Raman signal becomes asymmetric with a tail on the low energy side. In cases where the phonon dispersion curve goes up before it goes down, the asymmetric tail will appear on the high frequency side; this has been observed in TiO_2 (4).

It is sometimes the case that more broadening and asymmetry are recorded than can be accounted for by the model. In this case, it is possible to invoke defect-induced scattering that shorten the lifetime and add to the broadening (Lorentzian function). In summary, the asymmetry can be attributed to a number of factors such as particle size distribution and irregularity in the particle shape (Gaussian function), as well as confinement. Arora and colleagues (2) surveyed the Raman scattering in many materials. One of the more interesting examples is porous silicon, which is of technological interest because of its efficient photo- and electroluminescence, despite the fact that the parent silicon is an indirect gap material (which means that it will only luminesce weakly as a phonon is created or absorbed during the electronic transition to take up the difference in wavevector of the electron in the conduction band and the hole in the valence band). In fact, it has been shown that the strong photoluminescence caused by a radiative recombination of carriers across the indirect gap in porous silicon is mediated by the confined phonons (5).

Applications

Since the development of chemical vapor deposition (CVD) methods to synthesize diamond films in the 1980s, Raman spectroscopy has been seen as a valuable tool for characterizing these materials. The size of the diamond crystals, the presence of twinning, and the amount and character of the nondiamond component has been correlated with conditions of deposition. While it was presumed that there could be nanocrystalline diamond present, its Raman spectrum was only identified in the year 2000 with the use of 244-nm excitation (6); the requirement for UV excitation is based on the need to reduce the relative contributions from the nondiamond species, and to detect the Raman signal in the absence of luminescence (which would occur at longer wavelengths). (In fact, the 244-nm-excited spectrum of CVD diamond was recorded in 1995, and the dependence of the peak position and width as a function of deposition conditions was noted, but not identified as evidence for nanodiamond [7].) If the Raman spectra of CVD diamond films are recorded with visible excitation wavelengths, one finds that a broad band at 1150 cm^{-1} often occurs, and it has often been attributed to nanodiamond. However, the band always occurs with a second band at 1450 cm^{-1}, and the excitation-wavelength dependence of the vibrational energies indicated that it could be more accurately assigned to resonance-enhanced transpolyacetylene segments at grain boundaries (8).

Raman scattering in nanoporous semiconductors also has been reviewed in the 2007 issue of the *Journal of Raman Spectroscopy* (9). In addition to a discussion of porous silicon and germanium, this review article considers scattering by polar semiconductors in which surface phonons with energy between that of the TO and LO phonons of the

bulk material appear. Because the surface phonons couple to the free-carrier plasmons, carrier depletion can be studied.

In their review article, Gouadec and Colomban (10) consider the role of interactions between nanophases in crystal growth and in composite structure and properties. In composites, one needs to be concerned with what happens at grain boundaries as well as in the grains themselves. When the composite is made of nanomaterials, the concentration of the boundaries relative to the bulk is quite high. Reactions at the grain boundaries include lattice reconstruction, passivation or corrosion, and contamination. In addition, large thermal-chemical gradients during processing result in further changes including the production of new phases. An interesting observation that the authors cite is the conversion of gas phase–deposited TiO_2 particles from rutile to the anatase structure at 5 nm diameter because of differences in surface energy (11).

Gouadec and Colomban consider the morphology (following crystallization and amorphization processes) of covalently bonded materials, especially inorganic and organic polymers. They point out that the long range order is directly reflected in the lattice and librational modes that occur in the low frequency range of the spectrum (<100 cm^{-1}) and Raman bands of molecular motions broaden in the amorphous phase in an analogous fashion to what is observed in X-ray diffraction (XRD). Thus the vibrations of the molecular motion are sensitive to short range order and the librational and lattice modes are sensitive to long range order required for crystallinity. They point out that it is possible to estimate the relative amounts of crystalline vs. amorphous phase by band-fitting the low frequency part of the spectrum to a Rayleigh background, an amorphous mode, and a crystalline lattice mode. As an example they reproduce the polarized spectra of a polyamide 6.6 fiber. The polarization behavior is observed for both the amorphous and the crystalline components. From these measurements it was possible to understand that the mechanical fatigue of the fiber follows from the transformation of the amorphous phase (12).

At this point, I want to diverge a bit. Since 1990, when Raman instruments were built on a single monochromator platform used in conjunction with some type of Rayleigh filter, the low frequency cutoff has been about 100 cm^{-1}. Until recently, if one wanted to measure spectral features much lower than 100 cm^{-1}, the only recourse was to use a triple spectrograph, which is a more complicated, more expensive instrument with less throughput. Within the past year or two Bragg filters have become available that allow measurement of Raman bands down to

10 cm^{-1} on specially designed single grating spectrographs (13).

Gouadec and Colomban also described the vibrational motion in nanoparticles. The elastic sphere model employed molecular dynamics simulations to calculate the vibrational density of states (14). The results of these calculations were the description of spheroidal modes (involving radial displacements) and torsional modes (involving tangential displacements with no volume change). Calculations show that the frequency is proportional to the particle diameter, and this finding has been confirmed in some systems.

Gouadec and Colomban also considered in what size domains the two models (phonon confinement vs. elastic sphere models) were most appropriate. They estimated that bulk properties should be adequate for crystals larger than ~50 nm. Between ~5 and 10 nm the elastic sphere model should be used. The phonon confinement model will be valid for crystals in the ~15–50 nm size range. Between ~10 and 15 nm, the elastic sphere and phonon confinement models overlap. Note that when these particles are embedded in a matrix there are additional possibilities for internal stress and other physical phenomena that can affect the spectra.

Ceramics and glass-ceramics are a class of composite materials whose properties can potentially be followed by analyzing their Raman spectra in the framework of nanomaterials. Transformations between various crystalline and amorphous phases during processing through the mesoporous and gel phases can be followed. Because the spectra of both tetrahedral and octahedral species in amorphous metal oxide structures have been assigned, one can infer details of the connectivity and distortions of these glasses as a function of sample history (that is, processing).

One of the more important types of composite is the reinforcement of ceramics with fibers because the final product is refractory, with low density and high damage tolerance. The goal is to incorporate fibers in the amorphous phase and prevent the onset of crystallization and grain growth. The shear stress between a fiber and its matrix can be studied by following the Raman shift as a function of position of the fiber relative to its exposure at the end of the part. (This is only possible when the matrix is optically transparent).

The behavior of glasses was mentioned in some of the examples above. In fact, the study of glass is a field in its own right, and by its very nature it can be aided by the concepts of nanomaterials. The goal of the analysis of glasses is to determine where in the phase space of composition good glasses with low quench rates will form. Experiments are confirming theoretical predictions that the sweet spots occur when there are "rigid but stress-free networks." According to Boolchand and colleagues (15), Raman scattering has been important in determining the "intermediate phases" in which "local and medium range molecular structures . . . form isostatically rigid networks . . . that do not age."

Summary

In this column installment, I tried to indicate how Raman spectroscopy has been contributing to the characterization of nanomaterials that are of intellectual and technological interest. To understand the concepts used to study these materials, interested readers will have to get a crash course in some areas of solid-state science if they have not been exposed to these concepts. The goal in this installment is to indicate what would be of interest in using Raman spectroscopy to study these materials and to provide an entry guide to the literature.

Next Installment

Before we wrap up, I would like to welcome David Tuschel as my collaborator on this column. The

feedback that I have been getting on the column is quite good, and consequently the two of us will be publishing five installments a year, instead of the three that I have been publishing until now. David's first column will appear in the March issue. I want to thank all of you that have shared your comments with me. Keep them coming, and be sure to read David's installment next month.

References

(1) http://www.feynmanonline.com/; published by CalTech's Engineering and Science, February 1960.

(2) A.K. Arora, M. Rajalakshmi, T.R. Ravindran, and V. Sivasubramanian, *J. Raman Spectros.* **38,** 604–607 (2007).

(3) H. Richter, Z.P. Wang, and L. Ley, *Solid State Commun.* **39,** 625 (1981).

(4) A.L. Bassi, D. Cattaneo, V. Russo, C.E. Bottani, E., Barborini, T. Mazza, P. Piseri, P. Milani, F.O. Ernst, K. Wegner, and S.E.J. Pratsinis, *Appl. Phys.* **98,** 074305 (2005).

(5) G.W.T. Hooft, Y.A.R.R. Kessenev, G.L.J.A. Rikkin, and A.H.J. Venhuizen, *Appl. Phys. Lett.* **61**, 2344 (1992).

(6) Z.Sun, J.R. Shi, B.K. Tay, and S.P. Lau, *Diamond Relat. Mater.* **9,** 1979 (2000).

(7) R.W. Bormett, S.A. Asher, R.D. Witowski, W.D. Partlow, R. Lizerski, and F. Pettit, *J. Appl. Phys.* **77**(11), 5916- 5923 (1995).

(8) A.C. Ferrari and J. Robertson, *Phys. Rev. B.* **63,** 121405 (2001).

(9) G. Irmer, *J. Raman Spectrosc. B* **38,** 634–646 (2007).

(10) G. Gouadec and P. Colomban, *Progress in Crystal Growth and Char. of Mater.* **53,** 1–56 (2007).

(11) E. Barborini, I.N. Kholmanov, P. Piseri, C. Ducati, C.E. Bottani, and P. Milani, *Appl. Phys. Lett.* **81**(16), 3052 (2002).

(12) J.M. Herrera-Ramirez, P. Colomban, and A. Bunsell, *J. Raman Spectrosc.* **35**(12), 1063 (2004).

(13) A.Rapaport, B. Roussel, H.J. Reich, F. Adar, A. Glebov, O. Mokhun, V. Smirnov, and L. Glebov, "Very Low Frequency Stokes and Anti-Stokes Raman Spectra Accessible with a Single Multi-Channel Spectrograph and Volume Bragg Grating Optical Filters", presented at the International Conference on Raman Spectroscopy (ICORS), Boston, Massachusetts, 2010.

(14) R. Meyer, L.J. Lewis, S. Prakash, and P. Entel, *Phys. Rev. B.* **68,** 104303 (2003)

(15) P. Boolchand, M. Jin, D.I. Novita, and S. Chakravarty, *Raman Spectrosc.* **38,** 660–672 (2007).

Fran Adar is the Worldwide Raman Applications Manager for Horiba Jobin Yvon (Edison, New Jersey). She can be reached by e-mail at fran.adar@horiba.com.

For more information on this topic, please visit: www.spectroscopyonline.com/adar

Chemometrics in Spectroscopy

Classical Least Squares, Part VIII: Comparison of CLS Values with Known Values

A comparison of the experimental results to the theoretical expectations showed appreciable discrepancies. We consider possible problems in the execution of the experiment as the cause of these discrepancies.

Howard Mark and Jerome Workman, Jr.

This column is an installment in a series of our discussion of the classical least squares (CLS) approach to calibration (1–7). Where do we stand as of now? At this point, we have developed the theory of the CLS approach to calibration (1,2), described the measurement procedures and the data (3,4), and shown that when we apply the mathematical theory to the data we can reconstruct the spectra of the mixtures (5).

However, the theory of CLS only considers the relationship of the spectrum of a mixture to the spectra of the components of that mixture; the theory tells us nothing about the relationship of the spectrum to other properties of the mixture. In particular, it is silent on the question of the concentrations of the various mixture components. The numerical results of the CLS calculations are fractions, each representing the fraction that each mixture component contributes to the total mixture spectrum.

Therefore, the remaining task is to verify whether the coefficients calculated for the spectra in fact represent the concentrations of the various components in the different mixtures. We begin this task by presenting the actual concentrations in the experimental mixtures made. The values in the experimental design, as we presented them in our May 2011 installment as Figure 5 (5), are the target values for the various mixtures comprising the design. The actual mixtures were made up gravimetrically to be close to the target values, but the true weight percentages were calculated from the actual weights of the various components added to the mixtures. Table I presents those actual values.

In our previous columns (5,6), we found that by computing the regression coefficients for the spectra of the pure components using the CLS algorithm and then applying those coefficients to those same pure component spectra, we were able to reproduce the spectra of mixtures of those materials very well. Our interest now is to ascertain whether the coefficients we calculated do, in fact, represent the concentrations of the corresponding materials.

Theoretically, any of the spectral regions having the absorbance bands that we previously noted should give equivalent results, the same results, and the correct results. It therefore makes sense to use both the entire spectral region we measured and each of the individual spectral regions that we previously separated out and plotted.

Table II presents the coefficients calculated from the various spectral regions for one of the ternary mixtures (25% toluene, 25% dichloromethane, and 50% *n*-heptane). We see that there is some variation in the percentage of each component calculated at the different wavelength ranges. Thus, we also calculated the mean percentage of each mixture component and include that as an entry in the table.

By "splitting the difference" this way, we expect that the mean composition we calculate will be a better estimate of the "true" calculated value in any of the individual calculated values. We are now ready to present the results for

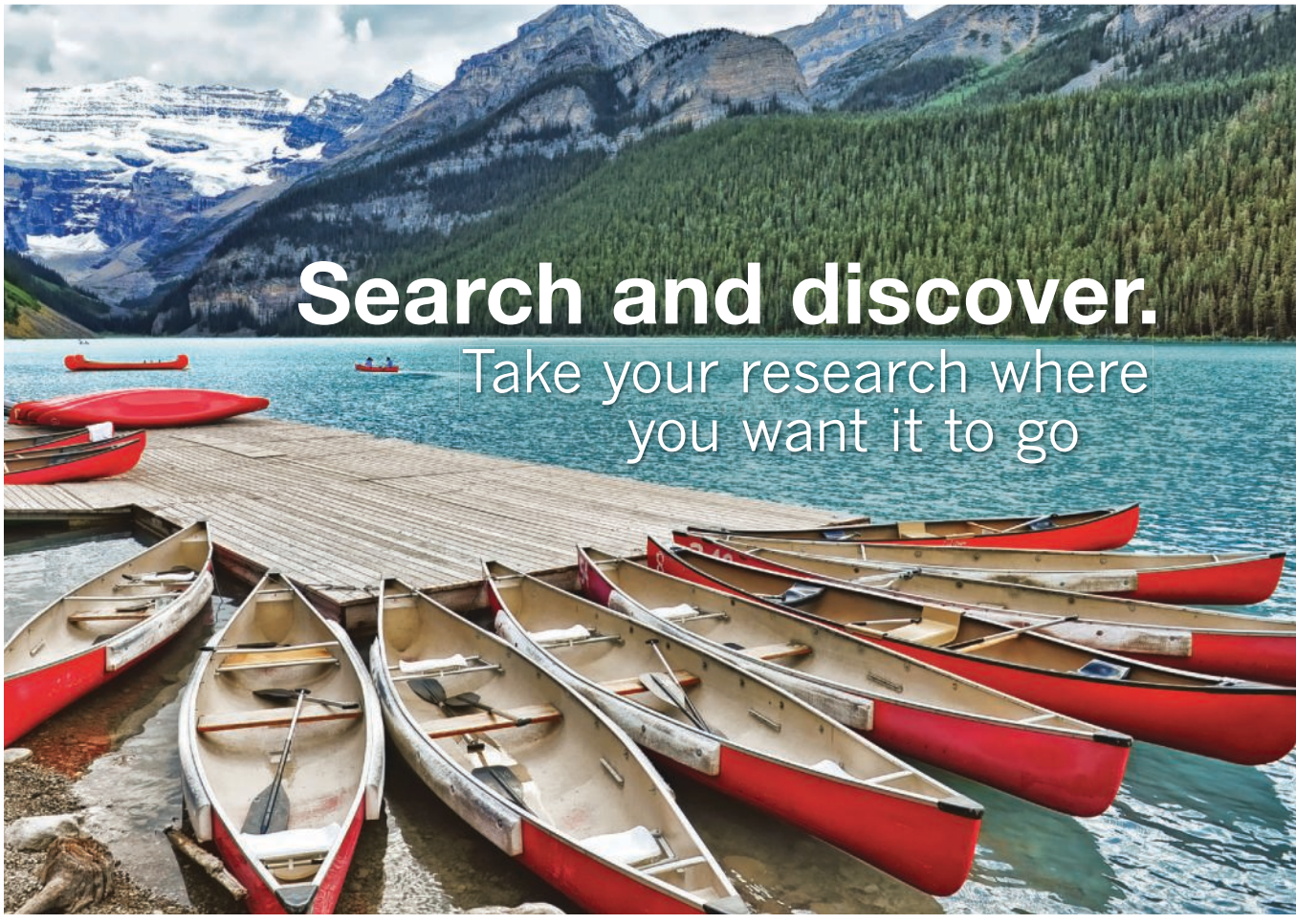

Introducing the new website from Harrick Scientific, pioneer of IR and UV-Vis sampling techniques, industry innovator for over 40 years. **www.harricksci.com**

Our new website was designed to assist you through any spectroscopy challenge. Harrick Scientific offers a comprehensive array of sampling tools for a wide range of applications, from routine quality control to advanced research investigations. **Harrick accessories extend the capabilities of FTIR and UV-Vis spectrometers to perform analyses that would otherwise be difficult or impossible.**

Through our site you'll gain guided access to application solutions, plus technical information, application notes and references. We also offer a full range of consumables and optics for online purchase. Our site is backed by a team of scientists, engineers, and industry experts. **In other words, the perfect place to turn to when embarking on your next endeavor.**

Visit our website for details about our newest addition, the Video MVP.
www.harricksci.com/Introducing-VideoMVP

Please visit us at PITTCON booth #2681

HARRICK **Scientific Products**

141 TOMPKINS AVE P.O. BOX 277 PLEASANTVILLE, NEW YORK 10570 T 914-747-7202 F 914-747-7209 INFO@HARRICKSCI.COM

Thermo SCIENTIFIC

Dramatically different ICP-MS

Experience dramatic differences in performance and ease-of-use with the all-new **Thermo Scientific iCAP Q ICP-MS**. For any application, class-leading sensitivity is achieved with revolutionary QCell flatapole technology, while single mode analysis and enhanced throughput can slash up to 50% off your total analysis time. One click set-up makes any user feel like an expert and a radical space-saving, easy-access design makes the iCAP Q extremely efficient to install and maintain in any laboratory. Another innovation in ICP-MS, ICP-OES and AA solutions.

for trace elemental analysis

• experience the difference • thermoscientific.com/dramatic

iCE 3000 Series AA
Innovative design for ease of use with flame and furnace AA technology

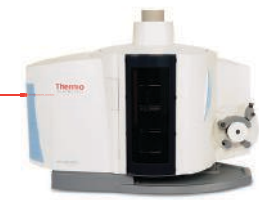

iCAP 6000 Series ICP-OES
Reliable, routine multi-element analysis with the best performing ICP-OES

iCAP Q ICP-MS
Delivering performance, productivity and reliability through advanced design

ELEMENT 2 HR-ICP-MS
High resolution ICP-MS for the most demanding of applications

Thermo SCIENTIFIC

Introducing Thermo Scientific iCAP Q ICP-MS
Simplified Operation. Advanced Performance.

Experience application flexibility with expanded capabilities for powerful elemental detection in established and emerging applications

Multi-element determination in food using ICP-MS

The elemental and dynamic range of ICP-MS makes it particularly suited to the analysis of food, simultaneously determining trace level contaminants and macro level nutrients.

The Thermo Scientific iCAP Qc ICP-MS is an excellent tool for multi-elemental determination in complex food samples. With its high sensitivity and analytical robustness, the iCAP Qc ICP-MS is capable of routinely measuring major and minor analyte concentrations in food in a single KED analysis mode, following a simple sample digestion step. Using the iCAP Q ICP-MS collision cell technology, interference-free, simultaneous determination of all elements of interest in a wide range of food sample types can be efficiently and rapidly carried out.

Multi-element determination in pharmaceutical preparations using ICP-MS

This application report demonstrates why the Thermo Scientific iCAP Q ICP-MS is the perfect solution for elemental determination in pharmaceutical preparations. With its high sensitivity and robustness, the instrument is easily capable of accurately and precisely measuring all 16 of the specified elements at the target limits currently listed in the US Pharmacopeia 232 method (USP 232) and in accordance with the analytical performance criteria described in USP 233. The range of security features, data management and audit trailing tools included in the advanced and flexible Thermo Scientific Qtegra software provide the necessary support to meet the demands of 21 CFR Part 11 compliance for the highly regulated pharmaceutical industry environment.

Speciation analysis of Cr (III) and Cr (VI) in drinking waters using anion exchange chromatography coupled with ICP-MS

Through the combination of the Thermo Scientific Dionex ICS-5000 ion chromatography system and the Thermo Scientific iCAP Q ICP-MS inductively coupled plasma-mass spectrometer, a sensitive, robust method for the speciation of Cr (III) and Cr (VI) in natural waters has been developed. The method developed enables fast and reliable speciation analysis of both Cr (III) and Cr (VI) species in water samples without prior incubation steps and with high purity nitric acid as mobile phase. The short, but highly efficient Thermo Scientific Dionex AG7 column provides complete separation of both species in under 150 seconds, allowing high sample throughput in the routine analysis of water samples. The new flatapole cell technology introduced in the iCAP Q ICP-MS provides interference-free detection of the ^{52}Cr and ^{53}Cr ions. Subppt detection limits are achievable due to the completely metal free pathway of the ICS-5000 and the powerful elemental detection capabilities of the iCAP Q ICP-MS operated in He KED mode.

Download these application notes, watch videos and navigate through the technology at www.thermoscientific.com/dramatic

Table I: Actual values for the various mixtures in the experimental design

Sample	Toluene	Dichloromethane	*n*-Heptane
1	100	0	0
2	76.40	23.60	0
3	74.10	0	25.90
4	50.30	49.70	0
5	48.90	25.11	25.99
6	49.94	0	50.06
7	25.30	75.77	0
8	25.33	49.65	25.02
9	23.86	26.45	49.68
10	25.19	0	74.81
11	0	100	0
12	0	75.04	24.95
13	0	49.54	50.46
14	0	24.34	75.66
15	0	0	100

all of the different mixtures that our experimental design specified. These are given in Table III, which also contains the actual gravimetric values for the composition. We use the term "actual" because even though the experimental design illustrated in Figure 5 of the May 2011 installment (5) specified the design points to use, the individual samples were made up according to the "dispense approximately and measure exactly" paradigm for preparing samples.

What do we observe in the results of Table III?

Although sporadic readings (such as toluene in sample 9) showed good agreement between the gravimetric and spectrally calculated values, for the most part the two readings disagreed markedly, often by several percent or more. We therefore have to conclude that this isn't working very well.

Troubleshooting

Why isn't the CLS method working? The first call to action is to suspect the experimental procedures. The two obvious potential causes for the disagreement are problems with the model or spectral data and problems with the composition values (that is, what we normally attribute to "reference laboratory error").

Let us examine these potential causes: Is the problem with the model?

- The reconstruction of the spectra is nearly perfect (for the whole spectrum and at all subranges).
- The results from the whole spectrum and from all subranges are consistent.
- The results for samples with similar compositions are consistent. Some spectra were measured more than once; those gave virtually identical results.
- Closure: the spectrally computed compositions add to 100%.
- B_0 => 0 (not shown in the tables, but the constant term of each CLS calibration approximates zero very well).

The conclusion we drew from this evidence was that the spectral values were correct, and there is no problem with the spectra or with the model.

Is the problem with the composition values (that is, "reference value" error)?

- Proper care was taken to avoid changes because of evaporation. Checks performed (such as loss of weight on standing) showed no effect.
- The samples were made up gravimetrically, so their compositions are precisely and accurately known.
- The laboratory technique of mixing was excellent. Ron Rubinovitz, who did the experimental work, is an experienced and careful worker.
- The possibility of evaporation was further considered:
  (a) *n*-Heptane has a lower boiling point than toluene, therefore evaporation should cause the *n*-heptane to decrease faster than toluene and thus show a decrease in relative percent. However, it showed a relative increase.
  (b) Proper care was taken to avoid changes caused by evaporation.
  (c) Multiple measurements of spectra showed no changes in spectra with time
  (d) Dichloromethane is the lowest-boiling material in the samples. Thus, samples with zero dichloromethane should have shown no effect from this cause, but despite this, there were differences between samples, counter to what we expected from evaporation.
  (e) Evaporation should have caused ternary samples to show an effect proportional to the concentration of dichloromethane, (again because that is the lowest-boiling component), but this was not observed.

Conclusions from this evidence:

- The samples were made up correctly.
- Evaporation was not a cause of the variations.
- The component values were correct, there was no problem with the sample compositions.

Thus, we see that there is no reason to suspect problems with any of the experimental data, neither the gravimetric values nor the spectral values. So, what is the cause of the discrepancy?

After considering the potentials for error in the measurements (both in the spectra and in the reference values) we concluded that those were both correct, and therefore the discrepancy is because of a fundamental problem in the interpretation: When we measure spectra and when we measure weight percentages we are measuring different things. Normally when we do spectroscopic calibration, the calibration calculations connect the different types of measurements and implicitly make the appropri-

Table II: Results from sample with nominal composition: 25% toluene, 25% dichloromethane, 50% *n*-heptane. All tabled values are wt %.

Component	Actual wt %	Using All Wavelengths	4500–5000 cm^{-1}	5000–6500 cm^{-1}	6500–7500 cm^{-1}	7500–9000 cm^{-1}	Mean Spectral Value
Toluene	23.86	23.67	22.66	26.42	19.82	21.66	23.01
Dichloromethane	26.45	15.54	17.79	14.15	14.08	16.90	17.48
n-Heptane	49.68	61.30	46.75	60.72	62.06	61.03	56.92

Table III: Gravimetric and spectrally calculated compositions for all samples

Sample	Gravimetric Values			Spectroscopic Values		
	Toluene	Dichloromethane	*n*-Heptane	Toluene	Dichloromethane	*n*-Heptane
1	100.00	0	0	100.00	-0.00	0.00
2	76.40	23.60	0	83.06	14.39	1.58
3	74.10	0	25.90	70.45	0.72	29.21
4	50.30	49.70	0	61.04	35.35	3.03
5	48.90	25.11	25.99	50.76	15.84	33.79
6	49.94	0	50.06	45.57	0.76	54.33
7	25.30	74.77	0	34.78	62.43	2.68
8	25.33	49.65	25.02	28.82	35.17	36.53
9	23.86	26.45	49.68	23.67	15.54	61.30
10	25.19	0	74.81	21.98	0.47	77.85
11	0	100.00	0	-0.00	100.00	0.00
12	0	75.04	24.96	-0.47	61.19	40.87
13	0	49.54	50.46	0.50	34.76	67.21
14	0	24.34	75.66	0.33	14.72	86.47
15	0	0	100.00	0.00	-0.00	100.00

ate corrections for the differences in the units used as well. There is an implicit and unstated assumption that except for scaling factors, all measures of concentration are equivalent.

Our conclusion here is that the problem is in the interpretation of the meaning of "concentration". There is a fundamental difficulty: What is it that we are measuring? The mathematics of CLS calculations ensure that the calibration calculations allow us to determine the fraction of the spectral information from each component in the various mixtures, but because there is no connection with the physical properties of the mixtures, there is no *a priori* reason to expect that the weight percentage is the correct physical property to use.

Table IV: Converting the weight % values to mole %

Component	Known Weight %	Molecular Weight	Number of Moles	Mole %	Spectral Value
Toluene	23.86	92.13	0.2590	24.29	23.01
Dichloromethane	26.45	84.94	0.3114	29.21	17.48
n-Heptane	49.68	100.2	0.4958	46.50	56.92

Because we so often use weight percent as the operative composition variable when performing near-infrared (NIR) calibrations, we normally assume that the spectrally active molecules are present in proportion to their weights. However, upon reflection on the subject, it is clear that this cannot be true. Molecules with the same number of, say, methyl groups, could have considerably different molecular weights. Thus, a calibration model that happened to key in on the absorbance of methyl groups might have the same coefficients for the spectral absorbances of the methyl groups, but this clearly could not correctly translate into the same weight percentage for the two different molecules. When we do "ordinary" types of NIR calibrations the weight percent of the analyte is generally given as one of the pieces of the input data.

Therefore, coefficients that are calculated for multiple linear regression (MLR), principal components

regression (PCR), or partial least squares (PLS) calibrations implicitly incorporate into themselves whatever conversion factors are needed to convert the spectral changes into the weight percent compositions of the samples. In the current experiment, we don't have that information to put into the calibration calculations. We have seen that the model we developed does, in fact, accurately predict the spectrum of the mixture, if not the weight percent. It is clear that the coefficients of the pure materials that were calculated are solely functions of the spectral behavior of the materials, whereas the composition information we are trying to relate that to is defined in terms of the weight percent, and we have nothing to draw a connection with between the two disparate types of units.

A dimensional analysis can show this, also:

Units for spectra:
$A_T + A_D + A_H = A_{mix}$

Units for reference values:
$Wt\%_T + Wt\%_D + Wt\%_H = Wt\%_{mix}$

Even worse, although each set of units is self-consistent, not only are the nominal units for the two types of measurement different, they are incompatible. When we use CLS to calibrate the spectra for the mixture composition, that has nothing to do with the weight percentages of the mixture components, and nothing in the calibration process creates that connection.

Therefore, we see that although the CLS algorithm gives us the contribution of each pure component to the *spectral* mixture, as noted above it does not create a connection to the *physical* mixtures that are being measured. The experimenter has to create, or find, the connection between the weight percentages that were used to specify the mixtures and the spectral results obtained from those mixtures. The reference results, therefore, need to be converted into units that relate to the fundamental composition of the samples as measured by the spectroscopy, not their weight percentages.

The Search for Composition

It's clear that the spectral results must be reflecting *some* physical characteristic of the samples. Although we don't know yet what that characteristic is, from the data it's also clear that it's *not* weight percentages. This actually shouldn't be too surprising. The weight of a molecule is determined mainly by the nuclei of the atoms in the molecule and, those do, after all affect the vibrational frequencies. On the other hand, there is no direct connection between what happens in the atomic nuclei and the interactions of the electromagnetic radiation with the atoms, because those interactions involve the electron clouds surrounding the atoms and molecules, but not the nuclei.

After some thought, it also becomes almost intuitively obvious that at this fundamental level, there's no reason to expect a relationship between the spectroscopy and the weights of the materials. The weight of a substance, after all,

comes from the nuclei of the atoms in that substance. The nuclei, however, at most play an indirect role in the interactions between electromagnetic radiation and the electron clouds of the materials that give rise to the absorbance. The conclusion here is that there is no reason to expect a relationship between the nuclei and the spectroscopy.

First Alternate Unit Considered

Our initial guess in this direction was that absorbance is proportional to the number of molecules absorbing. Ordinarily, weight percent is a surrogate for that, with unit conversions implicit in the standard calibration algorithms "filling in the holes."

Therefore, in the absence of that mathematical connection and to connect the spectroscopy to the gravimetry, our initial approach is to convert the weight percent into a measure of the relative number of molecules (that is, mole percent). This is a fairly straightforward calculation. Knowing the molecular weights of the pure materials we are using, we can perform our calculations; for example, by assuming 100 g of mixture so that the weight percent of each material in the mixture equals the actual weight (strictly speaking, mass) of each material, which is known. Dividing the weight of each material by its molecular weight gives us the number of moles of each material, and then the mole percent of each material can be calculated. For our example, we will use the mixture 25% toluene, 25% dichloromethane, and 50% *n*-heptane (sample 9 in Table III) as our benchmark mixture. This is convenient because we already used the results from that mixture in Table II, and that can serve as a comparison value for us. Table IV shows, step-by-step, the results of converting the weight percent values to mole percent values, as described above. We also include the spectral (CLS) value on the right hand side of the table, for comparison.

We can similarly compute the values for all the samples in the study, as we did in Table III for the gravimetric results. Those data are presented in Table V.

Comparing the mole percent values with the weight percent values (from Table II) we see that while the value for toluene is almost unchanged, the values for the other two components differ even more from the spectrally computed values than they previously did. This correction seems to have resulted in a degradation of the results, rather than an improvement. Thus, we see that the mole percent still doesn't adequately represent the spectroscopic results. We need to look further.

Second Alternate Unit Considered

After further cogitation, the realization dawned that when we measure spectra in the NIR region, we are not necessarily measuring the amount of different molecules. One of the first lessons learned by anyone doing NIR spectroscopy is that virtually all absorbance bands that are NIR-active are caused by the various vibrations of hydrogen atoms in the samples. Indeed, while we have not extensively discussed the point, we noted early on in this study that the absorbance bands of the different molecules are grouped together in some fairly

Table V: Mole % and spectrally calculated compositions for all samples

Sample	Mole % Values			Spectroscopic Values		
	Toluene	Dichloromethane	*n*-Heptane	Toluene	Dichloromethane	*n*-Heptane
1	100.00	0	0	100.00	-0.00	0.00
2	77.83	22.16	0	83.06	14.39	1.98
3	72.45	0	27.54	70.45	0.72	29.21
4	52.32	47.67	0	61.04	35.35	3.03
5	48.74	23.07	28.17	50.76	15.84	33.79
6	47.84	0	52.15	45.57	0.76	54.33
7	26.84	73.15	0	34.78	62.43	2.68
8	25.76	46.55	27.67	28.82	35.17	36.63
9	23.32	23.84	52.82	23.67	15.54	61.30
10	23.64	0	76.35	21.98	0.47	77.87
11	0	100.00	0	-0.00	100.00	0.00
12	0	71.81	28.18	-0.47	61.19	40.87
13	0	45.42	54.57	0.50	34.76	67.21
14	0	21.42	78.57	0.33	14.72	86.47
15	0	0	100.00	0.00	-0.00	100.00

well defined ranges (for example, 4500–5000 cm^{-1}). In fact, we even used those various ranges when we plotted the data, because all three materials' absorbance bands fell into the same ranges. Considering the various underlying molecular vibrations, we know, for example, that the 4500–5000 cm^{-1} range (corresponding to 2200–2000 nm), corresponds to the combination of the stretching and bending vibrations of $-CH_2$ and the 5000–6500 cm^{-1} range (which corresponds to 1530–2000 nm) is because of the second overtone of the various CH stretching vibration, and so forth.

From this we conclude that it is not necessarily the number of moles (or molecules) of each compound that are present that should matter, but the number of moles of hydrogen atoms from the various sources, because those are the atoms that are spectroscopically active. For the compounds used in this study, one molecule can have anywhere from two (dichloromethane) to 16 (*n*-heptane) hydrogen atoms. This difference needs to be taken into account. In Table VI we

Cutting-edge technology. Ultimate commitment.

The PANalytical Difference

Come see PANalytical at Pittcon booth 2019

The PANalytical Difference…it's more than just a statement about our committment to product quality and advancement of our technologies. It's about a team of people dedicated to serving our customers, so that they feel appreciated, informed and excited.

XRD

Empyrean - the only XRD platform with unique PIXcel^{3D} detector that does it all: powder, thin films, nanomaterials, solid objects

X-ray solutions

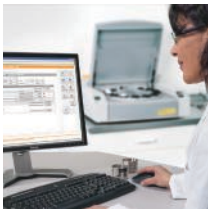

Omnian - standardless analysis software for Axios and Epsilon 3 spectrometers

HighScore - total X-ray powder pattern analysis software. Supports all reference databases

XRF

Axios range with Axios^{mAX} and Axios (1 kW)

Epsilon 3 range of cost-effective benchtop energy dispersive X-ray fluorescence systems

Expertise

Eagon 2 - beadmachine for safe, simple high-performance fusion

Global support

PANassist - keep your instrument in peak condition at all times. Always at work for you.

PANalytical Inc.
117 Flanders Road
Westborough, MA 01581
USA
T +1 508 647 1100
F +1 508 647 1115
Toll Free: +1 800 279 7297

info@panalytical.com
www.panalytical.com

The Analytical X-ray Company

PANalytical

Quantitative Raman Analysis of Polymers and Additives

LIVE WEBCAST: Wednesday, March 7, 2012 at 1:00 PM EST

Register free at http://www.spectroscopyonline.com/quantitativeraman

EVENT OVERVIEW:

Hot in recent years, Raman spectroscopy has gained acceptance in the area of plastics characterization, not only for qualitative analysis for materials identification, but also for more demanding applications requiring quantitative analysis.

With the growing regulatory complexities in the plastics industry, it is crucial for manufacturers to know the exact composition of their polymer matrices to ensure not only compliance but also the performance requirements to meet customer specifications. Raman provides a simple, non-destructive, and rapid tool for the analysis of polymer grade and additives, including flame retardants, antioxidants, impact modifiers, plasticisers, and others.

During this webinar, we will discuss the use of Raman in the plastics industry, reviewing both qualitative and quantitative analysis techniques. We will cover the numerous phases during the production cycle from initial research and development to final production QA/QC. We will focus on a number of key examples, including the analysis of Br and P flame retardants, degradation tracking and end of life cycle monitoring, and how Raman can be used to determine physical properties such as strength and density.

Key Learning Objectives:

- Understand the role of Raman spectroscopy in modern plastics engineering
- Understand how Raman can be applied to predictive modeling of lifetime and degradation
- Understand how Raman can be used for the analysis of physical properties such as viscosity, impact strength, and density

Who Should Attend:

- Analytical Chemists
- QA/QC Managers
- Plastics Engineers
- Materials Scientists
- Polymer Chemists
- Anyone interested in learning more about applications of Raman spectroscopy

Presenters:

Travis Thompson
Raman Spectroscopy
Product Specialist
B&W Tek

Dr. Henryk Herman
Chemical Physicist
and Laser Specialist
GnoSys Global Ltd

Moderator:

Meg Evans, Managing Editor, Spectroscopy

Presented by

Spectroscopy

Sponsored by

B&W TEK INC. Your Photonics Partner

For questions contact Jamie Carpenter at jcarpenter@advanstar.com

Table VI: Composition corrected for molecular weight and number of hydrogen atoms

	Known Weight %	Molecular Weight	Number Moles	Mole %	Number of H/Molecule	Moles of H	% H	Spectral Value
Toluene	23.86	92.13	0.2590	24.29	8	194.32	19.5	23.01
Dichloromethane	26.45	84.94	0.3114	29.21	2	58.42	5.86	17.48
n-Heptane	49.68	100.2	0.4958	46.50	16	744.0	74.64	56.92

Table VII: Hydrogen percentage corrected for density

Component	Weight (Weight %)	Molecular Weight	Density (g/mL)	Moles/ 100 mL (density/ MW)	Mixture Moles/mL (wt % × mol/mL)	% mol/mL	Moles Hydrogen Atoms	% Hydrogen Atom	Spectral Value (Reference)
Toluene	23.86	92.13	0.867	0.941	22.45	22.92	8	22.30	23
Dichloromethane	26.45	84.94	1.336	1.573	41.60	42.47	2	10.33	17
n-Heptane	49.68	100.2	.6837	0.682	33.90	34.61	16	67.36	56

copy the pertinent information from Tables IV and V, add the information about the number of hydrogen atoms per molecule, and then compute the percentage of hydrogen atoms from each material in the mixture.

We see in Table VI that the mole percent of hydrogen atoms still doesn't adequately represent the spectroscopic results. If anything, the correction went too far. The toluene value, which was in reasonably good agreement before, now also deviates wildly from the spectral value. The dichloromethane, whose weight percent and mole percent values were much higher than the spectral value is now far too low, and the *n*-heptane went from being too low to being too high.

Third Alternate Unit Considered

The next guess as to the nature of the physical characteristic that might conform to the spectroscopic behavior was

to correct the percentage of the number of hydrogen atoms for the volume they occupy by applying a correction for the density of each component. This volume density of hydrogen atoms was calculated as follows:

- First, we note that to correct for density we need to know the weight (mass) of each component. Therefore, for the purpose of this calculation we again make the assumption that we are working with 100 g of mixture, so that the weight of each component is the same as the weight percent in the mixture.
- The volume occupied by a mole of each pure component is calculated from its density and molecular weight.
- The volume occupied by the given concentration of a component in the mixture is calculated from the molar volume and the weight percentage in the mixture.
- From the results of those three steps, we calculate the fraction of volume occupied by each component.
- Multiply that by the number of hydrogen atoms in each component.
- Compute the fraction of hydrogen atoms from each component contributing to the spectrum.

As we can see in Table VII, this transformation did not make any appreciable improvement, either.

We continue in our next column with a report on the results of a repetition of the work.

References

(1) H. Mark and J. Workman, Jr., *Spectros.* **25**(5), 16–21 (2010).
(2) H. Mark and J. Workman, Jr., *Spectros.* **25**(6), 20–25 (2010).
(3) H. Mark and J. Workman, Jr., *Spectros.* **25**(10), 22–31 (2010).
(4) H. Mark and J. Workman, Jr., *Spectros.* **26**(2), 26–33 (2011).
(5) H. Mark and J. Workman, Jr., *Spectros.* **26**(5), 12–22 (2011).
(6) H. Mark and J. Workman, Jr., *Spectros.* **26**(6), 22–28 (2011).
(7) H. Mark and J. Workman, Jr., *Spectros.* **26(**10), 24–31 (2011).

Jerome Workman, Jr. serves on the Editorial Advisory Board of *Spectroscopy* and is the executive vice president of Engineering at Unity Scientific, LLC, (Brookfield, Connecticut). He is also an adjunct professor at U.S. National University (La Jolla, California), and Liberty University (Lynchburg, Virginia). His email address is JWorkman04@gsb.columbia.edu

Howard Mark serves on the Editorial Advisory Board of *Spectroscopy* and runs a consulting service, Mark Electronics (Suffern, New York). He can be reached via e-mail: hlmark@prodigy.net

For more information on this topic, please visit: www.spectroscopyonline.com

One Touch Can
Make All the Difference

Find out how CEM's new One Touch™ Technology can make a difference in your microwave sample preparation at

BOOTH #2569 at Pittcon.

CEM

Microwave-Enhanced Science

www.cem.com

Application of Infrared Spectroscopy for the Prediction of Color Components of Red Wines

The chemistry of red wine color is a complex topic that is of great interest for winemaking. Improved or innovative methods of analysis are required for research and quality control. Several techniques are currently available to analyze grape and wine color, including high performance liquid chromatography and ultraviolet, visible, near-infrared, and mid-infrared spectroscopy. In particular, Fourier-transform infrared spectroscopy combined with chemometrics is well suited for correlating the spectral response of a sample to its compositional profile, and represents a valid alternative to the standard UV–vis technique. This short review focuses on the application of spectroscopy for the analysis of grape and wine color components and the contribution of spectral preprocessing to improve the multivariate calibration.

Andrea Versari, Giuseppina Paola Parpinello, and Luca Laghi

The color of red wine is an important quality parameter for both scientific and commercial purposes. Although some color components contribute to the sensory profile of a wine (such as astringency and bitterness), the color itself affects the consumers' preference and sensory expectations. *Anthocyanins* are the pigments responsible for the color of red wine grape cultivars and the color of young red wine. The anthocyanins in grapes are glucosides of five anthocyanidins: malvidin, delphinidin, peonidin, cyanidin, and petunidin. These occur as -3-*O*-glucosides, -3-*O*-acetylglucosides, and 3-*O*-*p*-coumaroylglucosides (1). In young wines, the majority of color results from these monomeric anthocyanins, with up to 50% of color derived from copigmented forms (2). *Copigmentation* refers to the association of anthocyanins with certain phenolic acids, flavonols, and flavones, as well as self-association, which results in the hyperchromic and frequently bathochromic shift in the visible absorbance (2). As wines age, the monomeric anthocyanins react with tannins to form more stable molecules, known as pigmented polymers, that are responsible for the color of mature red wines. The polymeric pigments can be further classified into two categories: long polymeric pigments (LPPs) and short polymeric pigments (SPPs). LPPs consist of those chains with a polymer length greater than three, which can be precipitated with protein, and SPPs, those that do not precipitate with protein (3). The nature of these fractions has been the subject of recent research to determine their structures. In the case of the LPPs, these are likely anthocyanins covalently bound to tannin polymers; however, the reaction mechanism by which this process occurs in the wine and the factors that influence rates of pigmented polymer formation are not fully understood yet (4,5). SPPs include some compounds comprising anthocyanins bound to flavanol oligomers, but also include pigments resulting from a range of reactions to form new compounds such as vitisins, portisins, and pinotins (6–8) (Figure 1). Several techniques are currently used to analyze grape and wine color, including ultraviolet (UV), visible (vis), near-infrared (NIR) and mid-infrared (MIR) spectroscopy.

The UV–vis Measurement of Red Wine Color

The UV–vis portion of the electromagnetic spectrum contains much information regarding phenolic compounds. The anthocyanins have absorbance features at 267–275 nm and 475–545 nm; the benzoic acids show a single absorbance in the region of 235–305 nm; hydroxycinnamic acids have

absorbance maxima at 227–245 nm and 310–332 nm; flavonols typically have maxima in the 250–270 nm and 350–390 nm regions; and the flavan-3-ols (catechins) have a single absorbance band at about 280 nm (9,10). Inspection of second-derivative spectra revealed peaks at 440, 460, 480, 500, 550, 610, and 645 nm, representing the various chemical forms of anthocyanins depending on pH, concentration, and individual anthocyanin species (11). Figure 2 shows the absorbance spectra of aqueous methanolic solutions of several types of phenolic compounds. In a red grape extract or red wines, these signals overlap. Several UV–vis-based spectroscopic methods have been applied to measure the colored compounds in grapes and wines; these include the Somers (12), Boulton copigmentation (13), and Harbertson-Adams (3) assays.

The method of Somers (12) generates values for total phenols, total anthocyanins, colored anthocyanins, percentage of anthocyanins in the colored form, total red pigments, and total phenolics by direct measurement of wine sample absorbances at 280, 420, and 520 nm. The sample absorbance at 520 nm can be attributed to free anthocyanins, copigmented anthocyanins, and polymeric pigments. Absorbances are measured following pH adjustment or the addition of a bisulfite solution or acetaldehyde to separate total anthocyanin and polymeric pigment. Lowering the pH of the sample allows for the measurement of anthocyanin monomers and pigmented polymers; treatment with acetaldehyde removes the bleaching effects of any SO_2 present in the sample; and the addition of bisulfite to samples reveals the degree to which the color is in polymer forms. There is no consideration of wine pH on the 520-nm absorbance value and no accounting for copigmentation, which results in overestimation of anthocyanin content (2). In this assay, the total phenolics value is approximated by subtracting a constant value from the acidified, diluted sample absorbance value at 280 nm to account for interference from other compounds that also absorb at 280 nm. Even though these procedures are simple to perform,

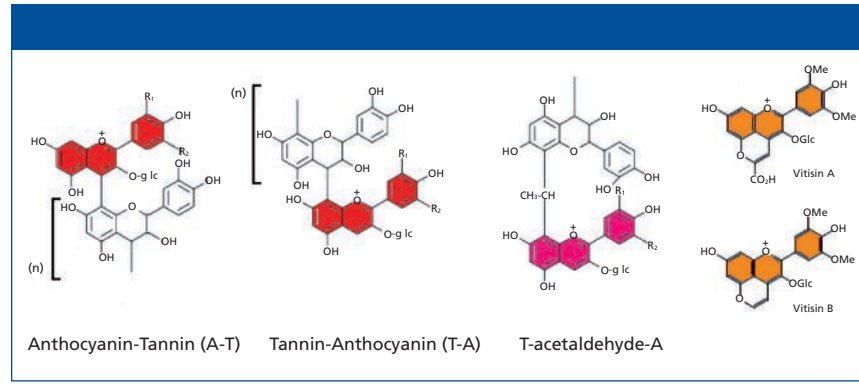

Figure 1: Example of anthocyanin-derived pigments of red wines.

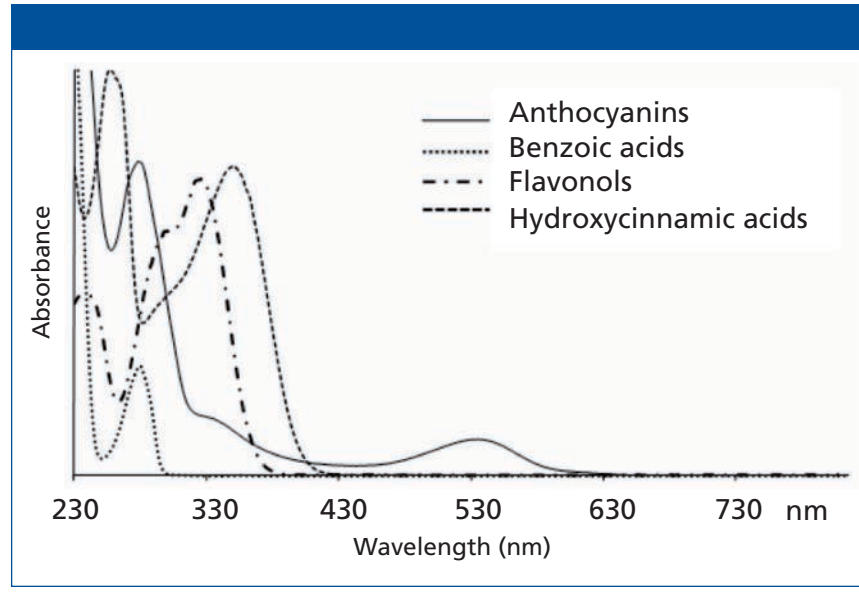

Figure 2: UV–vis absorbance spectra of selected classes of phenolic compounds.

the value of the numbers obtained is questionable. Nevertheless, these analytical techniques are widely practiced in wineries.

The copigmentation assay of Boulton and colleagues (13) addresses some of the shortcomings of the Somers method. This method distinguishes anthocyanin, copigmented, and polymeric forms of color in wines. Similarly to the Somers method, the absorbance value at 520 nm is read following the addition of either acetaldehyde or bisulfite solution; before these readings, however, the wine pH and ethanol content are adjusted to a constant level (3.6 and 12%, respectively) across wines. Color caused by copigmentation is calculated by subtracting the absorbance value for the 20-fold dilute wine from the acetaldehyde-treated sample. Color from polymeric pigments is measured from the bisulfite-treated sample and color from anthocyanins measured from the 20-fold dilute sample minus the bisulfite-treated sample. Thus, it suffers from the bleaching uncertainty of the Somers method.

The Harbertson-Adams assay allows for quantification of anthocyanins, protein-precipitable tannins, polymeric pigments, and iron-reactive phenols (3). Anthocyanin measures are based on absorbance differences at 520 nm after adjusting samples to pH 1.8 and 4.9; under those conditions free anthocyanins have their highest and lowest absorbances, respectively (14). Bisulfite bleaching (pH 4.9) of the monomeric anthocyanins in the sample distinguishes the polymeric pigments from total color. Iron-reactive phenols are measured by the change in absorbance because of reaction with iron chloride (15). Tannin and polymeric

Table I: Statistics for measurement of color components in red wines

Parameter	Technique	Preprocessing (Fitting)	Sample Type	Range	R^2_V	Error	RPD*	Reference
Anthocyanins (mg/g)	AOTF-NIR	Derivatives (PLS)	Intact red grapes	0.05–1.15	0.70	SEP = 0.14	—	63
Anthocyanins (mg/g)	NIR	None (PLS)	Intact red grapes	0.05–2.71	0.40–0.68	RMSEP = 0.18–0.31	0.49	64
Color (mg/g)	NIR	— (PLS)	Intact red grapes	—	0.50	SEP = 0.14	1.9	20
Anthocyanins (mg/g)	Vis–NIR reflectance	None (PLS)	Red grape homogenates	0.10–3.10	0.88	SEP = 0.18	2.94	11
Anthocyanins (mg/g)	Vis–NIR reflectance	None (LOCAL)	Red grape homogenates	0.10–3.10	0.94	SEP = 0.12	4.17	11
Color (mg/g)	Vis–NIR	— (PLS)	Red grape homogenates	0.38–1.72	0.92	RMSEC V=0.07	4.2	65
Malvidin-3-Glucoside (mg/L)	Vis–NIR	None (PLS)	Red wine fermentations	14–427	R^2_C=0.82–0.94	SECV= 17.5–31.5	2.5–4.3	22
Pigmented polymers (mg/L)	Vis–NIR	None (PLS)	Red wine fermentations	4–103	R^2_C=0.81–0.94	SECV= 3.2–26.8	2.1–5.8	22
Color (420 + 520 + 620 nm)	Vis–NIR	Scatter correction, Derivatives (PLS)	Red wines	3.8–21.4	0.70	SEP = 1.83	1.51	21
SPP (AU at 520 nm)	Vis–NIR	None (PLS)	Red wines	0.0–4.2	0.85	RMSEP = 0.31	2.58	Recalculated from 16
SPP (AU at 520 nm)	Vis–NIR	DOSC (PLS)	Red wines	0.0–4.2	0.89	RMSEP = 0.27	2.96	Recalculated from 16

*RPD: ratio of the standard deviation of the reference data to the standard error of prediction (SD_{ref}/SE_{pred})

pigments are measured in parallel by a bovine serum albumin (BSA) precipitation assay adapted from the method of Hagerman and Butler (15). The tannin is precipitated with BSA at pH 4.9. The tannin in the pellet is then resuspended

and measured by reaction with ferric chloride and reported as catechin equivalents. Polymeric pigments (PPs) can be subdivided into LPPs and SPPs based on their ability to precipitate with BSA. Because polymeric pigments with more than three catechin subunits precipitate with BSA (3), the supernatant above the tannin pellet can be assayed separately to measure SPP. LPP is calculated as the difference between PP and SPP.

These UV–vis-based methods commonly used in wineries and research settings require multistep sample processing and measurements. Spectroscopy-based predictive methods are an attractive alternative to the traditional methods because they require little or no sample preparation and generate instantaneous results. Predictive methods based on UV–vis spectra have been developed and demonstrated for wine samples. In the method by Skogerson and Boulton (16), the UV–vis spectrum of diluted wine is collected and used to populate a partial least squares (PLS) model. The model instantaneously generates values for the Harbertson-Adams assay parameters. The predictive ability of this model is strongest for anthocyanins, total phenolics, and tannin. Non-tannin phenols also were well predicted, but confident prediction of polymeric pigment remains elusive.

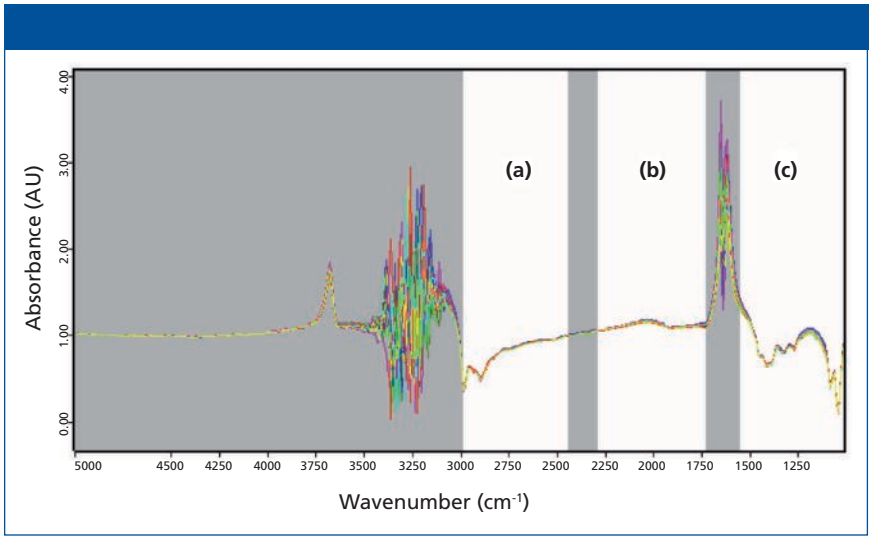

Figure 3: Example of FT-MIR spectra of red wines. The three white-shaded intervals show the frequency regions usually considered for calculation: (a) 2970–2435 cm^{-1}, (b) 2280–1715 cm^{-1}, and (c) 1545–965 cm^{-1} (fingerprint region).

The Infrared Approach

An indirect method of determining these color components in red grapes

Table II: Statistics for measurement of color components in red wines using FT technology

Parameter	Technique	Preprocessing (Fitting)	Sample Type	Range (mean ± SD)	R^2_V	Error	RPD*	Reference
Anthocyanins (mg/L)	FT-IR	Raw spectra (PLS)	Red wines different ages	73±58	0.62	RMSEP = 52	0.9	37
SPP (AU)	FT-IR	Raw spectra (PLS)	Red wines different ages	1.29–0.49	0.92	RMSEP = 0.23	2.2	37
LPP (AU)	FT-IR	Raw spectra (PLS)	Red wines different ages	1.07–0.49	0.76	RMSEP = 0.32	1.4	37
Anthocyanins (mg/L)	FT-IR	Raw spectra (PLS)	Red grape extracts	1219 (mean)	0.88	RMSEP = 263	2.1	37
Anthocyanins (mg/L)	FT-IR	Raw spectra (PLS)	Red young wines	380 (mean)	0.94	RMSEP = 52	2.9	37
Anthocyanins (g/kg)	FT-IR	First derivative (PLS)	Red grape extracts	1.34±0.17	0.73	RMSEP =0.08	2.1	38
Anthocyanins (mg/L)	FT-NIR	SNV-d^2 (PLS)	Red wine fermentations	9–228 (range)	0.86	RMSEC = **V**–27.5	2.8	40
Anthocyanins (mg/L)	FT-IR	SNV-d^2 (PLS)	Red wine fermentations	9–228 (range)	0.83	RMSEC = **V**–32.2	2.4	40
Malvidin-3-glucoside (mg/L)	FT-IR	Raw spectra (PLS)	Young red wines	128±59	0.82	SE**CV** = 22.28	2.6	43
Anthocyanins (mg/kg)	FT-IR	Raw spectra (PLS)	Red grape extracts	791±184	0.93	RMSEP = 5.9	3.5	33
Polymeric pigments (AU)	ATR-FT-IR	DOSC (PLS)	Red wines	2.07±0.84	0.82	RMSEP = 0.4	2.1	42

*RPD: ratio of the standard deviation of the reference data to the standard error of prediction (SD_{ref}/SE_{pred})

and wines using a fast, reproducible approach, with no or minimal sample preparation would be of great value for to the modern wine industry (17). Fourier-transform infrared (FT-IR) spectroscopy combined with multivariate data analysis, most notably PLS regression analysis (18), is well-suited for correlating the spectral response of a sample to its compositional profile and represents a valuable alternative to the classic UV–vis techniques (19). The suitability of both NIR and mid-IR spectroscopy — whether FT or dispersive — for the analysis of grape and wine color components has recently been demonstrated and the importance of spectral preprocessing to improve the multivariate calibration has been highlighted. In particular, FT-based instruments are considered faster and produce spectra with lower signal-to-noise ratios.

NIR Spectroscopy

The NIR spectral region corresponds to wavelengths in the 13,400–4000 cm^{-1} (750–2500 nm) region and is typical of stretching vibration including C–H high frequency combination bands and C–H complex overtones. The OHs also heavily contribute to NIR spectra, but they overlap heavily with alcohol and water OHs, so they are not useful. Because of its low absorptivity, NIR energy passes easily through the samples and allows the use of longer pathlengths (up to 10 cm) than those used for mid-IR analysis. Moreover, the low reflectivity of NIR permits the energy to penetrate beneath the surface of samples for the analysis of intact grape berries (20). The anthocyanin content of a berry gradually increases with grape maturity and usually shows a normal distribution, with slight skewing to the lower end of the scale, indicative of immature grapes (11).

NIR reflectance spectroscopy was used to develop predictive models for color intensity of red wines (R^2_V = 0.70; standard error of prediction [SEP] = 1.83; bias = – 0.91), yielding standard errors similar to the reference spectrophotometric method (1.48 AU) (21). In another study, researchers employed vis–NIR in transmission mode to develop predictive models of malvidin-3-glucoside (Mv-3-G) and polymeric pigments in red

wine fermentations, with $R^2 = 0.91$ for Mv-3-G (reference method: high performance liquid chromatography [HPLC]) (22). The visible and the NIR spectra explain 85% and 15% of the variation in the concentration of the color components, respectively; therefore, calibration for anthocyanins relied mainly on the visible wavelengths.

The PLS calibration for total anthocyanins in red grapes can be significantly affected by large data sets including vintage year, region, and grape cultivar, leading to nonlinearity of combined vis–NIR against the reference visible method. This situation can be partially corrected by using a calibration algorithm (11), a combined principal component analysis–artificial neural networks (PCA-ANN) approach (23), or by fitting calibrations using restricted sample sets into selected analyte ranges, irrespective of other classifying parameters such as region, vintage, and variety. In the latter case, the SEP values reported for total anthocyanins improved about threefold, from 0.18 to 0.05 mg/g (24,25). This advance is most probably caused by narrowing down the range of anthocyanins. The calibration algorithm regression approach selects a calibration subset with similar analyte concentration of the prediction samples and improves the prediction of anthocyanins in grape especially at low concentration. Anthocyanins can be among the possible source of nonlinearity from the Lambert-Beer law because of the enhancement of absorbance by copigmentation or eventually self-association that occurs at high concentrations (11).

Besides free anthocyanins, the polymeric pigments also contribute to the color of red wines and their prediction using visible and NIR spectroscopy has been explored (16). The original dataset was treated with two selected preprocessing procedures before PLS regression, namely direct orthogonal signal correction (DOSC) and a kernel function (66), that have improved the performance of the predictive model compared to the raw data (Table I).

FT-IR Spectroscopy

FT-IR spectrometers require minimum sample preparation and are currently used for routine analyses in enology laboratories for more than 20 parameters including sugars, pH, alcohol, several organic acids (tartaric, malic, acetic, and gluconic) and glycerol (26–29). However, advanced analysis functions are required to monitor the red wine color with a reliable calibration model.

As grape and wine samples are complex mixtures, the definite assignment of the spectral bands is challenging. Although the whole vibrational IR spectral range (4000–400 cm^{-1}) is usually stored for each sample, only the so-called fingerprint region (1600–900 cm^{-1}) is considered (Figure 3). Liquid samples, such as wine, show the presence of some IR regions that introduce noise to the calibration because of the absorbance caused by water (1717–1543 cm^{-1} and 3627–2971 cm^{-1}). Moreover, the 5012–3627 cm^{-1} region contains very little useful information.

The FT-IR spectra of anthocyanin extract reported by Mortensen (30) show numerous bands in the 1680–900 cm^{-1} region, typical of wine phenolic compounds (2,31). Anthocyanins and tannins are very similar chemically and therefore display similar IR absorption characteristics (33). For example, the bands at 1450–1510 cm^{-1} are assigned to C=C–C aromatic ring stretching, whereas several aromatic C–H out-of-plane and in-plane bending vibration are attributed to 670–900 cm^{-1} and 950–1225 cm^{-1}, respectively (34). In particular, the peak around 1285 cm^{-1} is characteristic for the flavonoid-based tannins (35) and was assigned to the ethereal C–O stretching vibration (36).

Jensen (37) has constructed FT-IR–based predictive models based on traditional visible assays to determine select red wine color components, including free anthocyanins, SPP and LPP (Table II). The initial unsatisfactory performance of the model for anthocyanins (residual predictive deviation [RPD] values < 2.2), was likely because of the large variation in the ages of the wines included in this study. With aging, the free anthocyanin content of wines rapidly decreases and interferences from the anthocyanin derivatives formed during aging (such as polymeric pigments) cannot be excluded. The subsequent analysis of selected young red wines confirmed that anthocyanins and polymeric pigments could be quantified to some extent with RPD values up to 2.9 (Table II). Similar results were obtained by Picque and colleagues (38) that used FT-IR spectroscopy of red grape extracts to build a predictive model that was able to quantify anthocyanins to some extent (RPD = 2.1) with a similar error to the analytical reference French Technical Institute for Viticulture and Oenology (ITV) method (accuracy: 0.06 g/kg). Anthocyanin prediction was improved if the regression was calculated from sample sets restricted to a single growing region. Consequently, a calibration model is required for each geographical region that the grapes originate from.

RPD is the ratio of the SEP to the standard deviation (SD) of the original data and provides a statistic basis for standardizing the SEP. For example, if the standard deviation of the original data is 1.83 and the SEP is 0.27, the RPD is given by 1.83/0.27 = 6.78. The RPD should be as high as possible: values of 5–10 are adequate for quality control, and 2.5 and over are satisfactory for screening. On the other hand, an RPD value of 1.0 means that the SEP and the SD are the same, and the instrument is not capable of predicting the parameter accurately, using that calibration (39).

To our knowledge, the best prediction for monitoring anthocyanins in red grapes using FT-IR spectroscopy was presented by Fragoso and colleagues (33); they obtained a valid PLS regression model for prediction of total anthocyanins (root mean standard error of prediction [RMSEP] = 4.8% and RPD = 4.8) working in the region of 979–2989 cm^{-1}. This parameter was determined with a reference method by measuring the absorbance at 520 nm of the grape extract previously diluted 25 times with 0.1 M HCl to get a pH close to 1.0. The variance of the measurement error in the reference values was 0.73%. The authors reported that there was no bias between the reference and the predicted values.

A recent investigation has compared the ability of FT-NIR (800–2778 nm, corresponding to 12,500–3600 cm^{-1}) with attenuated total reflectance (ATR)-FT-IR (4000–700 cm^{-1}) for the same sample set (40). Results show that the total anthocyanins content in red wine fermentations can be slightly better when determined from FT-NIR spectra (RPD = 2.8) compared to FT-IR (RPD = 2.4). In both cases, the spectra were treated with standard normal variate (SNV) in combination with second derivatives as preprocessing treatments before PLS.

A preliminary study on the ability of several preprocessing treatments to predict the color components of red wines based on FT-IR spectrometry was carried out in terms of root mean standard error of cross-validation (RMSECV) and R^2. For total anthocyanins and LPP, the best results were obtained using raw spectra whereas for SPP and copigmentation the best option was vector normalization (41). Later studies showed that DOSC preprocessing (R^2 = 0.82; RMSEP = 0.4) has improved the prediction of polymeric pigments in red wines (2.07 ± 0.84 AU) by FT-IR spectroscopy compared to the raw spectra (R^2 = 0.66; RMSEP = 0.6) (42).

The only study available in the literature showing the prediction of individual anthocyanins content in young red wines using FT-IR spectra showed values for R^2 between the range of 0.706 and 0.931 (43). In particular, malvidin-3-glucoside (validation set: 128 ± 59 mg/L) showed an SECV of 22.3 mg/L (FT-IR method) with a standard error of laboratory of 5.45 mg/L (HPLC method). Because of the presence of a systematic error (that is, the values were systematically higher as predicted by FT-IR than by HPLC because of the negative intercept) to improve the prediction for several anthocyanins, there is a need to use a correction factor.

The need for authenticity and classification of grape varieties and wines has led to considerable advances in the application of spectroscopic techniques. In this view, Edelmann and colleagues (31) used MIR spectroscopy of phenolic red wine extracts to build a discriminant model based on the soft independent modeling of class analogy (SIMCA) method to classify red wines based upon cultivar. Similarly, FT-IR spectrometry combined with PCA and linear discriminant analysis (LDA) also was found as a suitable technique for the classification of red wines, being able to predict the variety with greater than 95% success on an external dataset (44).

Besides their red color, the anthocyanins, as phenolic compounds, contribute to the antioxidant power of red wines. The first attempt to apply FT-IR spectroscopy for the prediction of ferric reducing ability of plasma (FRAP) in red wines showed an initial RPD value of 2.02 (45). Taking into account the importance of this parameter, further work is in progress to improve this performance.

More Capability—you've got it!
More Analysis Power—you bet!

Designed for materials identification, the Powder Diffraction File offers comprehensive, high-quality data. Independent of whether phase identification is performed by classic d,I pair analysis or by total pattern comparisons, the accuracy of the reference in comparison to an unknown is improved with higher quality reference data. Enhance your competitive analysis with more high-quality data, more capability and more analysis power—found only in the Powder Diffraction File!

Comprehensive: 747,650 unique data sets

Improve your ability to analyze minor and trace phases

Exploit a full suite of data simulation programs enabling the use of neutron, electron, synchrotron, and X-ray data

Tailor simulations for various instrumental and specimen characteristics

Utilize quantitative analysis methods:

- **Atomic parameters for Rietveld analysis**
- **I/I_c for Reference Intensity Ratio (RIR)**
- **Full digital patterns for total pattern analysis**

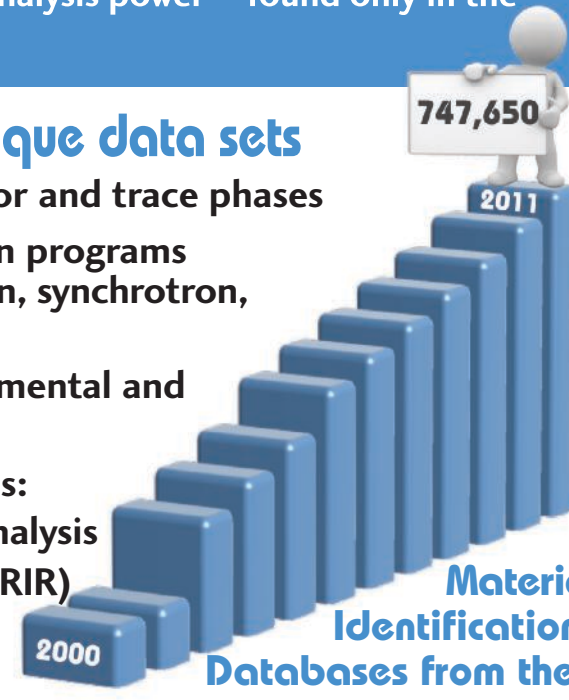

Material Identification Databases from the Database Experts

The Powder Diffraction File

PDF-2 Release 2011	243,911	material data sets
PDF-4+ 2011	316,291	material data sets
PDF-4/Minerals 2011	37,642	material data sets
PDF-4/Organics 2012	470,181	material data sets

The International Centre for Diffraction Data

ICDD® International Centre for Diffraction Data

marketing@icdd.com
www.icdd.com

ISO 9001:2008 QUALITY ASSURED COMPANY CERT.NR. 11409.1

610.325.9814 / Toll-free U.S. & Canada: 866.378.9331

Chemometrics

The IR spectrum of a wine sample contains information about a wide variety of molecules, including phenolic compounds, ethanol, organic acids, and sugars. This provides opportunities to develop mathematical models for the prediction of multiple wine compositional parameters from IR spectra. Unfortunately, both the wine and corresponding spectral complexity makes it impossible to find a single wavelength related to the characteristic of interest. For this reason, the relationship between IR data and the concentration of molecules is usually explored using multivariate calibration techniques. Because the relationship between the concentration of a molecule and its effect on the IR spectrum is considered linear, as stated in the Lambert-Beer law, the multivariate technique usually applied is the linear regression method called projection on latent structures regression (PLSR) (46).

Robustness and parsimony are critical characteristics for any predictive model of practical use. *Robustness* can be defined, according to Zeaiter and colleagues (47), as "the stability of its predictive capacity against perturbations centered on standard conditions". *Parsimony* is defined as the possibility of the model to be built on the minimum number of variables. This latter characteristic contributes to the robustness itself and allows a direct correlation between the found variables and specific physical characteristics of the studied system, making the model much more informative (48).

To reach the best compromise between robustness and parsimony of an IR data–based PLS regression model it is a common practice to mathematically transform the spectra before their use. Such preprocessing methods can be grouped into two categories (49). The first category consists of geometric transformation methods, such as multiplicative scatter correction (MSC) (50) and its extended version (EMSC) (51), standard normal variate transformation (SNV) (52), and first- and second-order derivatives, generally performed on the IR spectra and smoothed through the Norris-Williams (53) or the Savitzky-Golay (54) algorithms. The geometric transformation methods compensate for baseline shifts and distortions from the Lambert-Beer law induced by light scattering. Light scattering affects both reflectance and transmittance IR techniques, and is primarily caused by the particles present in biological samples with dimensions comparable with the IR wavelengths (49). The effect of the above mentioned methods on robustness and parsimony of the calibration models depends on the characteristics of the samples under investigation and of the employed IR instrument (47). Generally speaking, SNV is tailored to reduce scattering multiplicative effects, and consists in the centering of the spectra followed by a scaling for its standard deviation. MSC and derivatives correct for both multiplicative and additive effects.

A systematic study of the effects of geometric spectral preprocessing methods on the analysis of marzipan samples was described by Rinnan and colleagues (55). Moisture and sugar content were evaluated from IR spectra and collected with six spectrometers employing three different optical principles. The maximum improvement of any preprocessed model compared to the global model was 25% in RMSE, and each model based on pretreated spectra was more parsimonious. In another study, Zhang and colleagues (56) investigated the discrimination of red wines based on their sugar content from FT-MIR spectra and their second derivative, observing that the second derivative preprocessing step allowed the separation of overlapping peaks, thus enhancing minor differences among the studied wines.

The second category of preprocessing methods includes algorithms that select the wavelengths (x-values) that are better correlated with the compositional parameters of interest (y-values). The first such algorithm described is the orthogonal signal correction (OSC) algorithm (57). This algorithm and improvements or

modifications subsequently described split the *x* matrix of the IR data into two sub-matrices, one consisting of the information related to *y*, and the other with the information systematically orthogonal or unrelated to *y* (58). Such separation generally yields models characterized by lower RMSE and much higher parsimony than the raw spectra model counterparts. Laghi and colleagues (42) collected FT-MIR spectra on 145 red wines from 13 grape varieties to build predictive models for wine color, anthocyanin content, polymeric pigment content, and copigmentation index. They found the models built on the IR spectra pretreated with geometric transformations to perform similarly to those based on the raw spectra, while being slightly more parsimonious. In contrast, spectra preprocessed by the DOSC (48) algorithm yielded small improvements in the RMSEP (30% for polymeric pigments content) while dramatically increasing the parsimony of the model (from 6–10 latent variables when raw data were considered, to 1–3 variables with DOSC treated spectra). Versari and colleagues (45) compared mid- and near-FT-IR spectra to predict the colloidal stability of 111 white wines assessed through a heat stability test (59). The FT-NIR models based on DOSC pretreated spectra gave an R^2 of 0.8, even if only based on three latent variables, whereas similar models on raw spectra showed poor performances.

A second advantage of the separation of the IR data into *y*-predictive and *y*-orthogonal matrix is represented by the possibility offered by the latter method to better detect unexpected anomalies in the data, such as instrumental drift, batch differences, or unanticipated biological variation (58) This is possible because such pieces of information are cleared from the *y*-related information, which in many practical cases has the greatest influence on the collected data.

For a description of the algorithms described in 1998 to separate *y*-orthogonal from *y*-predictive information, readers should refer to Trygg and Wold (60). Among such methods the Kernel-OPLS (61) method seems particularly promising, even if it still has not been applied to wine. While retaining the goal of separating the *x* matrix into the now familiar two submatrixes, it is based on the application of the "kernel-trick" (62), which reduces the computation time, is able to model nonlinear structures in the data, and still offers optimal performances in cases where the number of variables is much higher than the number of observations (which is indeed typical on many experiments based on IR spectroscopy).

Conclusions

It has been shown that FT-IR and FT-NIR spectroscopy allow for the measurement of important color components in red grape and wine within a short period of time. The improved performance of predictions by visible spectroscopy is obviously related to

the strong absorptions of anthocyanins in the visible region. In the future, there is a need for more instruments for on-line measurements and more instrumentation with dedicated precalibration. Moreover, upgrading fiber-optic probes can further improve the ability of NIR techniques to monitor the winemaking process.

References

(1) G. Mazza, *Crit. Rev. Food Sci. Nutr.* **35,** 341–371 (1995).

(2) R. Boulton, *Am. J. Enol. Vitic.* **52,** 67–87 (2001).

(3) J.F. Harbertson, E.A. Picciotto, and D.O. Adams, *Am. J. Enol. Vitic.* **54,** 301–306 (2003).

(4) H. Fulcrand, V. Atanasova, E. Salas, and V. Cheynier, in *Red Wine Color: Revealing the Mysteries* (ACS Symp. Ser. Washington, DC, **886**, 2004), pp. 68–88.

(5) J.A. Kennedy and Y. Hayasaka, in *Red Wine Color: Revealing the Mysteries* (ACS Symp. Ser., Washington, DC, **886,** 2004), pp. 247–264.

(6) J. Bakker and C.F. Timberlake, *J. Agric. Food Chem.* **45,** 35–43 (1997).

(7) M. Schwarz, P. Quast, D. von Baer, and P. Winterhalter, *J. Agric. Food Chem.* **51,** 6261–6267 (2003).

(8) V. De Freitas and N. Mateus, in *Red Wine Color Exploring the Mysteries* (ACS Symp. Ser., Washington, DC, **886,** 2004), pp. 160–178.

(9) L. Jurd, in *The Chemistry of Flavonoid Compounds* (Pergamon Press, Oxford, England, 1962), pp. 107–155.

(10) J.B. Harborne, in *Plant Phenolics. Vol. 1. Methods in Plant Biochemistry* (Academic Press, London, England, 1989), pp. 1–28.

(11) R.G. Dambergs, D. Cozzolino, W.U. Cynkar, L. Janik, and M. Gishen, *J. Near Infrared Spectrosc.* **14,** 71–79 (2006).

(12) T.C. Somers and M.E. Evans, *J. Sci. Food Agric.* **28,** 279–287 (1977).

(13) R. Boulton, R. Neri, J. Levengood, and M. Vaadia, in *Proceedings of the 6th Symposium International d'Œnologie. Tec. & Doc. Publ.,* Paris, France, p. 35 (1999).

(14) L. Cabrita, T. Fossen, and M. Andersen, *Food Chem.* **68,** 101–107 (2000).

(15) A.E. Hagerman and L.G. Butler, *J. Agric. Food Chem.* **26,** 809–812 (1978).

(16) K. Skogerson, M. Downey, M. Mazza, and R. Boulton, *Am. J. Enol. Vitic.* **58,** 318–325 (2007).

(17) J.H. Thorngate, *Am. J. Enol. Vitic.* **57,** 269–279 (2006).

(18) H. Martens and T. Næs, *Multivariate Calibration* (Wiley & Sons, New York, New York, 1992).

(19) J.F. Harbertson and S. Spayd, *Am. J. Enol. Vitic.* **57,** 280–288 (2006).

(20) R. Bauer, H. Nieuwoudt, F.F. Bauer, J. Kossman, K.R. Koch, and K.H. Esbensen, *Anal. Chem.* **80,** 1371–1379 (2008).

(21) M. Urbano-Cuadrado, M.D. Luque de Castro, P.M. Pérez-Juan, J. García-Olmo, and M.A. Gómez-Nieto, *Anal. Chim. Acta* **527,** 81–88 (2004).

(22) D. Cozzolino, M.J. Kwiatkowski, M. Parker, W.U. Cynkar, R.G. Dambergs, M. Gishen, and M.J. Herderich, *Anal. Chim. Acta* **513,** 73–80 (2004).

(23) L.J. Janik, D. Cozzolino, R. Dambergs, W. Cynkar, and M. Gishen, *Anal. Chim. Acta* **594,** 107–118 (2007).

(24) M.B. Esler, M. Gishen, I.L. Francis, R.G. Dambergs, A. Kambouris, W.U. Cynkar, and D.R. Boehm, in *Proc. 10th Int. NIR Conference* (NIR Publ. Chichester, UK, 2002), p. 249.

(25) R.G. Dambergs, D. Cozzolino, W.U. Cynkar, M.B. Esler, L.J. Janik, I.L. Francis, and M. Gishen, in *Proc. 11th Int. NIR Conference* (NIR Publ. Chichester, UK, 2003), p. 183.

(26) C.D. Patz, A. David, K. Thente, P. Kurbel, and H. Dietrich, *Wein-Wissen.* **5454,** 80–87 (1999).

(27) M. Dubernet and M. Dubernet, *Rev. Fr. Œnol.* **181,** 10–13 (2000).

(28) M. Gishen and M. Holdstock, *Aust. Grapegrower Winemaker Ann. Tech.* **75–81,** (2000).

(29) S.A. Kupina and A.J. Shrikhande, *Am. J. Enol. Vitic.* **54,** 131–143 (2003).

(30) R.R. Mortensen, "Prediction of Wine Color Based on Rapid Analyses on Red Grapes," PhD Thesis, The Technical University of Denmark, Lyngby, Denmark and the Royal Veterinary and Agricultural University, Copenhagen, Denmark, 2004.

(31) A. Edelmann, J. Diewok, K.C. Schuster, and B. Lendl, *J. Agric. Food Chem.* **49,** 1139–1145 (2001).

(32) K. Fernandez and E. Agosin, *J. Agric. Food Chem.* **55,** 7294–7300 (2007).

(33) S. Fragoso, L. Aceña, J. Guasch, O. Busto, and M. Mestres, *J. Agric. Food Chem.* **59,** 2175–2183 (2011).

(34) D. Picque, T. Cattenoz, and G. Corrieu, *J. Int. Sci. Vigne Vin.* **35,** 165–170 (2001).

(35) A. Edelmann and B. Lendl, *J. Am. Chem. Soc.* **124,** 14741–14747 (2002).

(36) G. Socrates, *Infrared and Raman Characteristic Group Frequencies: Tables and Charts* (John Wiley & Sons: Chichester, UK 2001).

(37) J.S. Jensen, "Prediction of Wine Color from Phenolic Profiles of Red Grapes," PhD thesis, FOSS and DTU Chemical and Biochemi-

cal Engineering. Printed by Frydenberg a/s, Copenhagen, Denmark, 2008.
(38) D. Picque, P. Lieben, Ph. Chrétien, J. Béguin, and L. Guérin, *J. Int. Sci. Vigne Vi.* **44,** 219–229 (2010).
(39) P.C. Williams and D.C. Sobering, *J. Near Infrared Spectrosc.* **1,** 25–32 (1993).
(40) V. Di Egidio, N. Sinelli, G. Giovanelli, A. Moles, and E. Casiraghi, *Eur. Food Res. Technol.* **230,** 947–955 (2010).
(41) A. Versari, R.B. Boulton, and G.P. Parpinello, *It. J. Food Sci.* **18,** 423–431 (2006).
(42) L. Laghi, A. Versari, G.P. Parpinello, Y.D. Nakaji, and R.B. Boulton, *Food Anal. Methods*, in press DOI 10.1007/s12161-011-9240-2 (2011).
(43) P.M. Soriano, A. Pérez-Juan, J.M. Vicario, and M.S. González Pérez-Coello, *Food Chem.* **104,** 1295–1303 (2007).
(44) C.J. Bevin, R.G. Dambergs, A.J. Fergusson, and D. Cozzolino, *Anal. Chim. Acta* **621,** 19–23 (2008).
(45) A. Versari, G.P. Parpinello, F. Spazzina, and D. Del Rio, *Food Control* **21,** 786–789 (2010).
(46) D. Perez-Marin, A. Garrido-Varo, and J.E. Guerriero, *Talanta* **72,** 28–42 (2007).
(47) M. Zeaiter, J.-M. Roger, V. Bellon-Maurel, and D.N. Rutledge, *Trends Anal. Chem.* **23,** 157–170 (2004).
(48) J.A. Westerhuis, S. de Jong, and A.K. Smilde, *Chemom. Intelligent Lab. Sys.* **56,** 13–25 (2001).
(49) J. Gabrielsson and J. Trygg, *Crit. Rev. Anal. Chem.* **36,** 243–255 (2006).
(50) P. Geladi, D. MacDougall, and H. Martens, *Appl. Spectrosc.* **39,** 491–500 (1985).
(51) H. Martens and E. Stark, *J. Pharmaceut. Biomed. Anal.* **9,** 625–635 (1991).
(52) R.J. Barnes, M.S. Dhanoa, and S.J. Lister, *Appl. Spectrosc.* **43,** 772–777 (1989).
(53) K.H. Norris and P.C. Williams, *Cereal Chem.* **61,** 158–165 (1984).
(54) A. Savitzky and J.E. Golay, *Anal. Chem.* **36,** 1627–1632 (1964).
(55) A. Rinnan, F. van den Berg, and S.B. Engelsen, *Trends Anal. Chem.* **28,** 1201–1222 (2009).
(56) Y. Zhang, J. Chen, Y. Lei, Q. Zhou, S. Sun, and I. Noda, *J. Mol. Struct.* **974,** 144–150 (2010).
(57) S. Wold, H. Antti, F. Lindgren, and J. Ohman, *Chemom. Intelligent Lab. Sys.* **44,** 175–185 (1998).
(58) M. Bylesjo, M. Rantalainen, J. Nicholson, E. Holmes, and J. Trygg, *BMC Bioinformat.* **9,** 106–112 (2008).
(59) R.B. Boulton, in *Proceedings of the Sixth Annual Wine Industry Technology Seminar of the Wine Institute* (San Francisco, California, 1980), pp. 46–58.
(60) J. Trygg and S. Wold, *J. Chemom.* **16,** 119–128 (2002).
(61) M. Rantalainen, M. Bylesjö, O. Cloarec, J.K. Nicholson, E. Holmes, and J. Trygg, *J. Chemom.* **21,** 376–385 (2007).
(62) M. Aizerman, E. Braverman, and L. Rozonoer, *Autom. Remote Control* **25,** 821–837 (1964).
(63) I. Nazarov, R.L. Wample, O. Kaye, A.O. Santos, and K. Goulart, *FRUTIC* **05,** 355–362 (2005).
(64) M. Larraín, A.R. Guesalaga, and E. Agosín, *IEEE Trans. Instrum. Meas.* **57,** 294–302 (2008).
(65) D. Cozzolino, M.B. Esler, R.G. Dambergs, W.U. Cynkar, D.R. Boehm, I.L. Francis, and M. Gishen, *J. Near Infrared Spectrosc.* **12,** 105–111 (2004).
(66) S. Rannar, F. Lindgren, P. Geladi, and D. Wold D, *J. Chemom.* **8,** 111–125 (1994).

Andrea Versari, Giuseppina Paola Parpinello, and **Luca Laghi** are with Dipartimento di Scienze degli Alimenti, Università di Bologna, Cesena, Italy. Please direct correspondence about this article to: andrea.versari@unibo.it. ■

For more information on this topic, please visit our homepage at: www.spectroscopyonline.com

Confocal Raman Microscopy in Forensic Pharmaceutical Investigations

Scanning electron microscopy with energy dispersive X-ray spectrometry (SEM-EDS) and Fourier-transform infrared microspectrophotometry (micro-FT-IR) have been widely demonstrated as complementary analytical tools for the identification of complex mixtures and unknown materials. However, there is a gap between the information provided by these two techniques. Even though elemental and morphological information is obtained on small single particles with SEM-EDS technology, no molecular or structural information is available. Likewise, although chemical information can be acquired using FT-IR, analysis of small single particles is significantly limited. We applied confocal Raman microscopy (CRM) in our laboratory to bridge the gap between FT-IR and SEM, and it provided chemical and vibrational information on a scale approaching the resolution of an SEM. In one application, monomer solutions used during a contact lens manufacturing process exhibited haze that was related to particulate contamination. The particles were isolated and analyzed by CRM, SEM, and micro-FT-IR. The particle size range was about 1–500 µm. Particles <50 µm were analyzed and identified by Raman spectroscopy and SEM. Particles >50 µm were analyzed and identified by micro-FT-IR and SEM. Numerous materials associated with the manufacturing process of the monomer were identified, as well as foreign materials. The identification of the particulate materials causing the haze of the monomer assisted the manufacturer in determining the sources of the contamination and improving the quality of the product.

Mary A. Miller, Michelle R. Cavaliere, Ming Zhou, and Pronda Few

Raman spectroscopy is an ideal technique for analyzing product contaminants. Many materials can be identified by their Raman spectra, including minerals, dyes and pigments, polymers, and drugs. Raman microscopy has high spatial resolution, excellent sensitivity, and can quickly obtain spectral data. The technique often requires little-to-no sample preparation, and it is possible to collect spectra of materials through glass, plastics, and aqueous solutions. The ability to acquire spectral data without sample preparation limits accidental contamination and loss of the particle or material of interest (1). The technique is nondestructive in most applications. Confocal Raman microscopy (CRM) is especially useful for obtaining depth profiles (*x–z* scans) without conventional cross-sectioning of the samples (2–4). The ability to obtain vibrational spectra of small particles (<1–50 µm) complements the data obtained by the more traditional techniques of micro Fourier-transform infrared (micro-FT-IR) and scanning electron microscopy with energy dispersive X-ray spectrometry (SEM-EDS) (5–7). Raman spectroscopy is a particularly useful method for applications in the pharmaceutical, biomedical device, and consumer health products industries.

Janet Woodcock's article "The Concept of Pharmaceutical Quality" describes the Food and Drug Administration's (FDA) perspective on the quality of pharmaceuticals and highlights the efforts and financial resources invested to protect the health and safety of consumers (8). Forensic investigations in the pharmaceutical industry began with examinations of counterfeit and adulterated

Figure 1: (a) Clear (least hazy) transparent monomer solution; (b) haziest monomer solution.

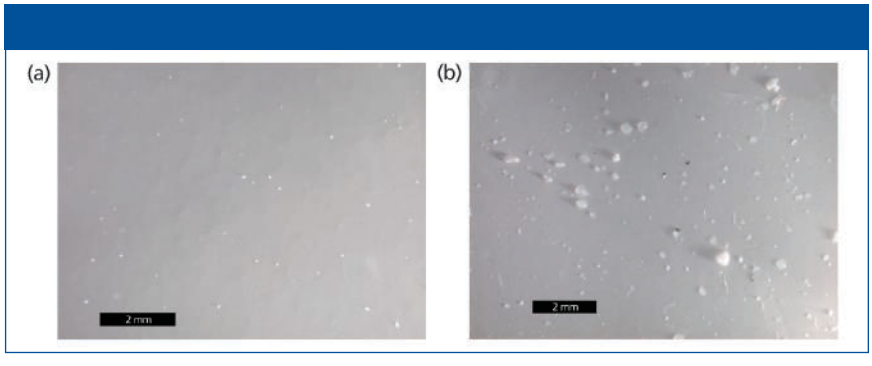

Figure 2: Photomicrographs showing isolated particulate materials on filter membranes from (a) least hazy solution and (b) haziest solution.

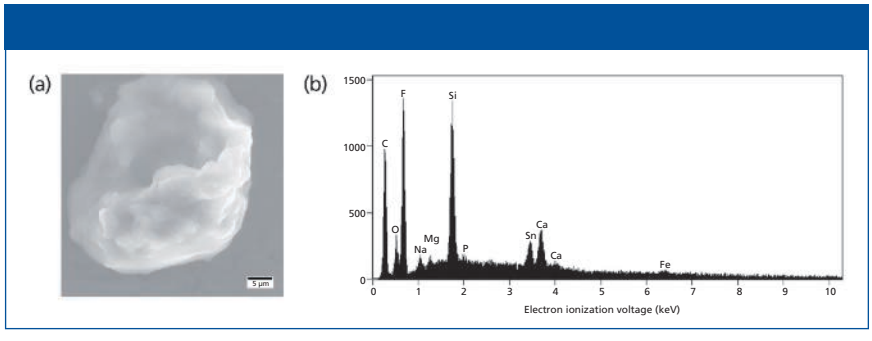

Figure 3: (a) SEM image of bumpy, textured particle isolated from least hazy monomer solution; (b) EDS spectrum from particle shown in (a).

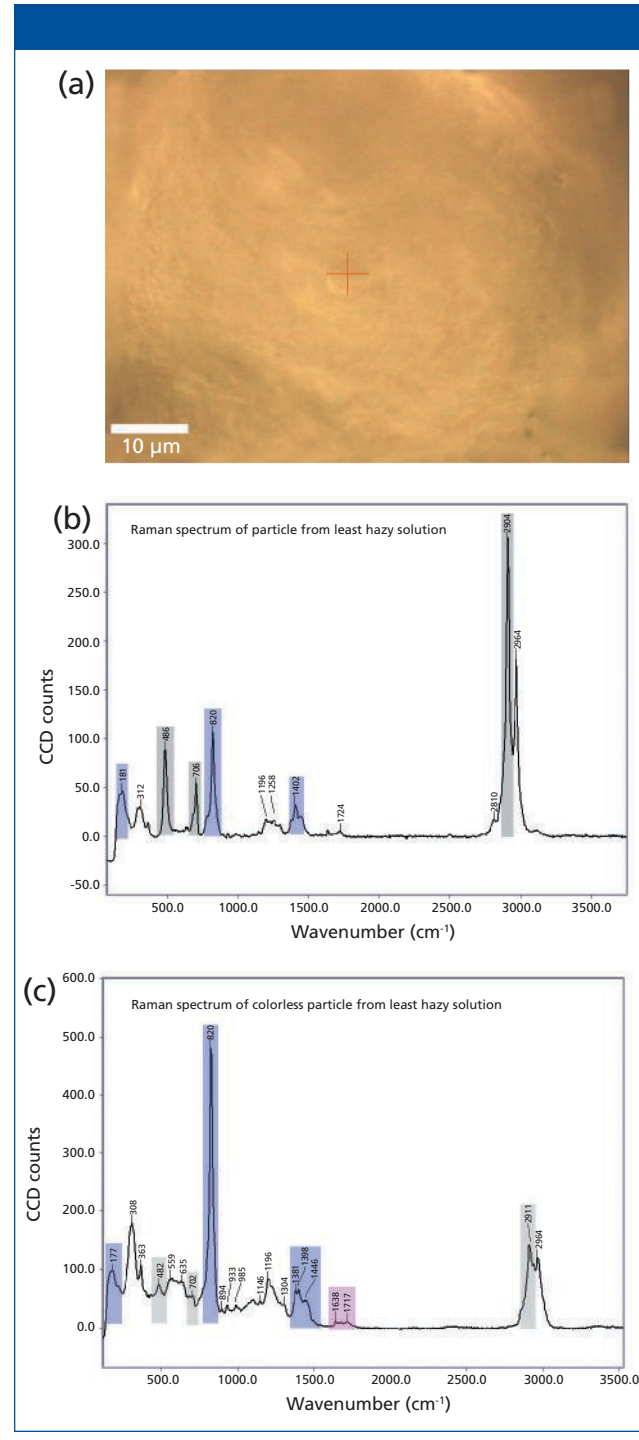

Figure 4: (a) Representative image of bumpy, textured particle selected for Raman analysis; (b) Raman spectrum of particle in (a), primarily fluoropolymer (blue) and monomer (grey); (c) Raman spectrum from additional clear or colorless particle showing a mixture of fluoropolymer (blue) and monomer (grey) with traces of isocyanate (pink). Refer to Table I for peak color codes of monomer and raw materials.

drug products (9,10). This area now extends to quality-related issues in manufacturing processes, including consumer health products, drug tablets and capsules, implantable medical devices, surgical equipment and supplies, and ophthalmic lenses.

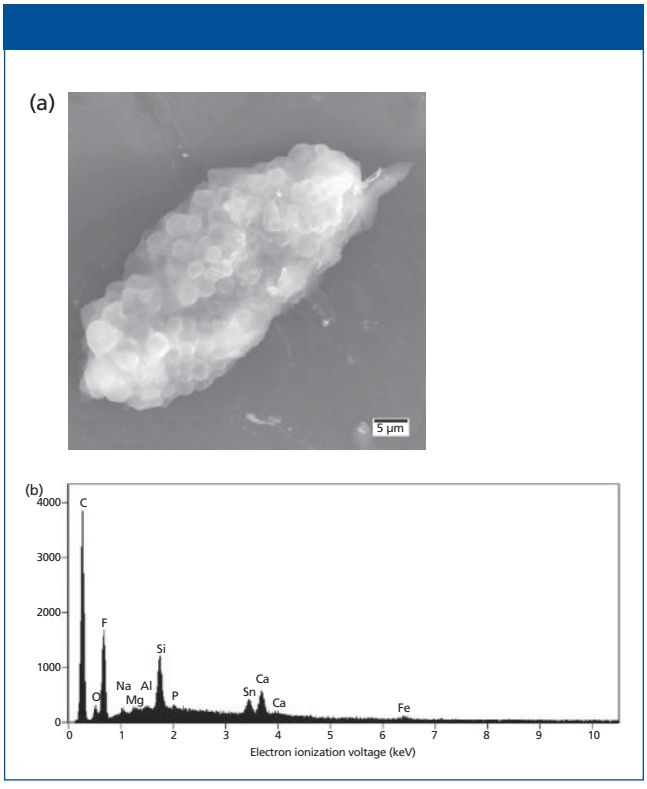

Figure 5: (a) SEM image of clear or colorless particle from the haziest monomer solution exhibiting bead-like features in a gel matrix; (b) EDS spectrum from particle indicates it is carbon (C), oxygen (O), fluorine (F), and silicon (Si) rich.

Monomer solutions are used in a variety of applications, including hard and soft contact lenses; a novel application reported in the literature is the use of contact lenses for delivery of controlled release drugs directly to the eye (11). Contamination of the monomer may reduce biocompatibility and permeability of the lens. Not only is the biocompatibility of the polymer important, it also must be produced in such a way that any residual monomer or solution does not pose a health risk (12). In general, high quality, inclusion-free polymers are equally important to all industries where a transparent polymer is required. Depending on the application, inclusions may result in reduced visibility and unintentional reflection or refraction of light.

In a recent case, inspection of monomers intended for use in the production of lenses revealed hazy solutions. These monomers did not meet the standard criteria for the final product manufacture, which requires a colorless, transparent polymer lens. MVA Scientific Consultants (Duluth, Georgia) was asked to investigate the nature of the haze in the monomer and intermediate product solutions and determine the source of the problem. The monomer is a proprietary formula consisting of multiple components, including but not limited to, silicone, fluoropolymer, organotin, acrylic, and isocyanate compounds.

This article describes the use of confocal Raman microscopy for the identification of particles in the 5–50 µm range and illustrates how it bridges the gap between micro-FT-IR and SEM-EDS analyses. The use of these complementary tech-

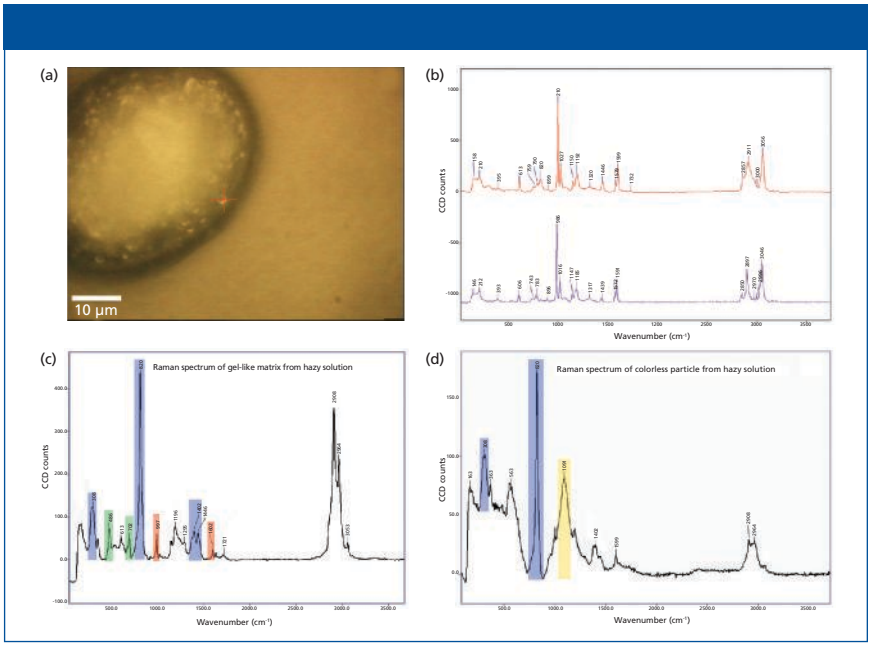

Figure 6: (a) Confocal Raman microscope image showing bead-like features observed in particles isolated from the haziest monomer solution; (b) Raman spectrum obtained from bead-like feature (upper trace) and a polystyrene reference spectrum (lower trace); (c) Raman spectrum of gel-like matrix consistent with fluoropolymer (blue), with traces of polystyrene-like compound (orange), and silicone (green); (d) Raman spectrum of clear or colorless particle consistent with mixture of fluoropolymer (blue) and isocyanate (yellow). Refer to Table I for color codes of monomer and raw materials.

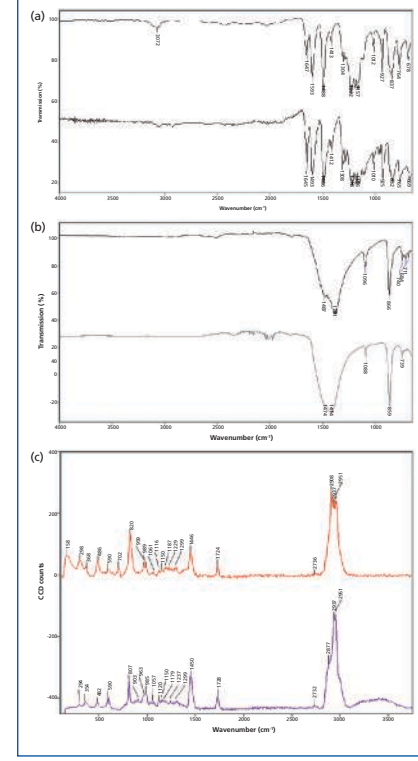

Figure 7: (a) Infrared spectrum (upper trace) of particle identified as extraneous material isolated from haziest monomer solution and polyether ether ketone (PEEK) reference (lower trace); (b) infrared spectrum (upper trace) of particle identified as extraneous material isolated from haziest monomer solution and inorganic carbonate reference (lower trace); (c) Raman spectrum (upper trace) of opaque or white particle identified as extraneous material isolated from haziest monomer solution and Carboset acrylic reference (lower trace).

niques in the pharmaceutical and allied industries is widely reported in the literature, especially for analyses and identification of small particles (6,7,10,13–16).

Experimental

Preliminary examination of the monomer solutions and particulate material was conducted using a Zeiss Stemi-C2000 stereomicroscope (Carl Zeiss Microscopy, Thornwood, New York) with a magnification range of 6.5–47×. The monomer solutions were filtered in an ISO Class 5 clean bench for isolation of particulate material using GE Water and Process Technologies (Trevose, Pennsylvania) 47-mm diameter,

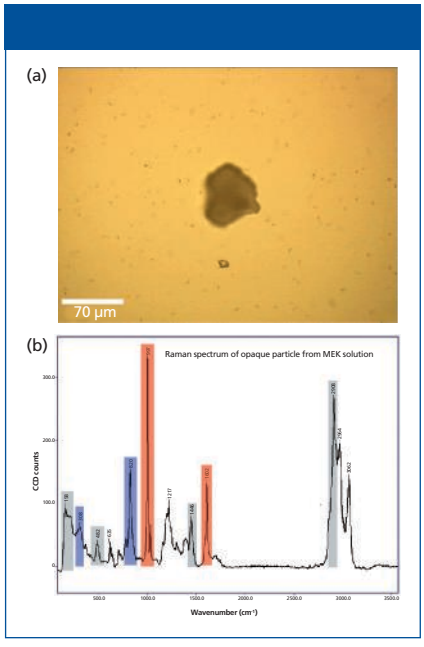

Figure 8: (a) Confocal Raman microscope image of opaque or white particle from MEK-diluted intermediate solution selected for Raman analysis; (b) Raman spectrum of particle in (a) suggests a mixture of fluoropolymer (blue), residual intermediate product or monomer (grey), and polystyrene (orange). Refer to Table I for color codes of monomer and raw materials.

0.8-µm pore size, polycarbonate track etch membrane filters. The filters were rinsed with prefiltered (0.2 µm) ethanol. Ethanol blanks and controls were prepared and examined with each sample set to ensure no introduction of significant particulate material during sample preparation. Representative particles were selected using fine tungsten microtools for analyses by micro-FT-IR, SEM-EDS, and CRM.

Micro-FT-IR analyses were conducted with a SensIR IlluminatIR Fourier transform infrared spectrophotometer (Smiths Detection, Danbury Connecticut, formerly SensIR Technologies, Danbury, Connecticut) coupled to an Olympus BX-51 compound microscope (Olympus America, Center Valley, Pennsylvania). Spectra were collected using a 50- or 100-µm aperture, a spectral resolution of 4 cm^{-1}, 128 scans, and either an all reflecting objective (ARO) or an attenuated total internal reflectance (ATR) objective.

JEOL JSM-6400 and JSM-6500F scanning electron microscopes (JEOL USA, Inc., Peabody, Massachusetts) with Noran energy dispersive X-ray systems (Thermo Scientific Noran, Madison, Wisconsin) were used for SEM-EDS analyses.

Raman spectra were obtained using a WITec (Maryville, Tennessee) alpha 300R confocal Raman microscope with a 532-nm excitation wavelength laser (NdYAG). Images of the particles were obtained before analyses. Typical spectra were collected using a 20× Nikon or a 100× Olympus objective, a 0.1-s integration time, and 100 accumulated scans. The spectrometer grating used was 600 grooves/mm. Both Raman and FT-IR spectra were processed using Thermo Electron Grams AI software (Thermo Fisher Scientific, Madison, Wisconsin).

Results and Discussion

Visual Inspection

More than 20 samples of the monomer solutions were received. The solutions were visually inspected and ranked

Table I: Raman peak frequencies (cm^{-1}) of monomer and raw materials

Isocyanate Compound 1	Isocyanate Compound 2	Silicone	Organotin	Fluoropolymer	Methyl Ethyl Ketone	Intermediate Product	Monomer
1091 (br)	3108	2904	1299	820	2921	3121	3108
559	2742	486	2854	300	755	2964	2964
2418	2425	702	1438	1454	1082	2904	2904
781	1717	186	1154	1380-1410	581	2810	2807
2538 (sh)	1638	1258	2911	177	1709	2415	2496
						1724 (w)	1721
						1450	1638
						1410	1446
						1299	1406
						1258	1295
						1082 (br)	1258
						781	855
						702	781
						482	702
						177	482
							186
							158

Key peak positions used for identification/correlation of components within mixtures
sh = shoulder, br = broad, w = weak

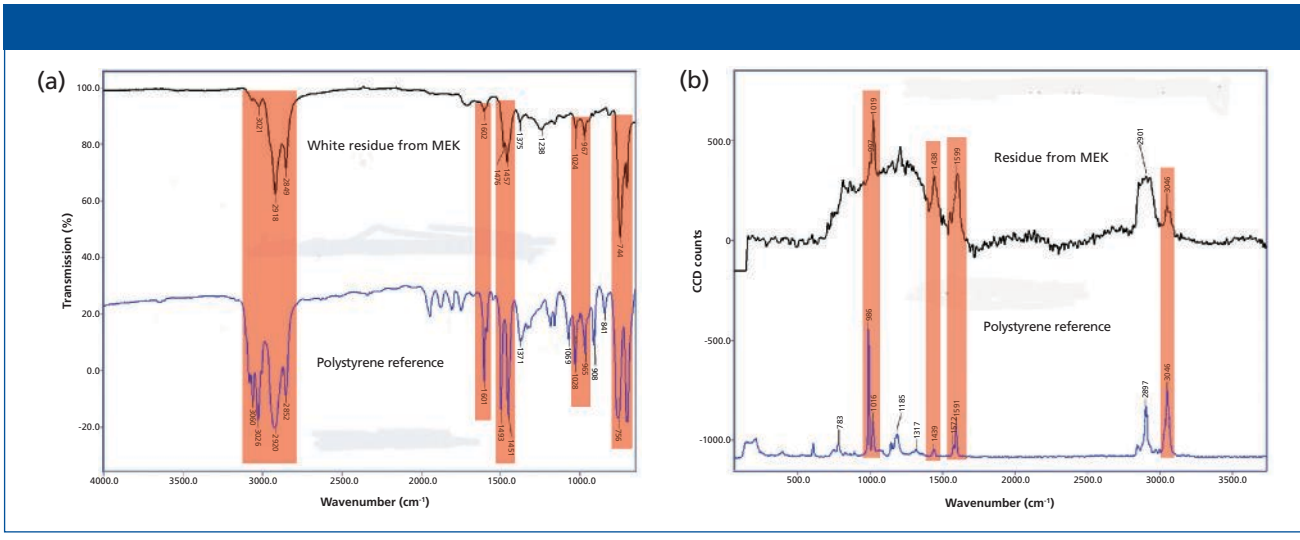

Figure 9: Infrared and Raman spectra of white residue recovered from MEK solvent: (a) Infrared spectra of residue (upper trace) and polystyrene reference (lower trace); (b) Raman spectra of residue (upper trace) and polystyrene reference (lower trace). Highlighted peaks illustrate correlation.

based on the level of visual clarity and haziness. Preliminary examination suggested the haze was caused by particles in the solutions. Representative samples of the least and most hazy solutions were selected for analyses. Figure 1 shows the representative samples.

The two solutions were filtered and particles were retained on the filter membranes, as shown in Figure 2. The predominant particles recovered from the hazy solution had a size range of approximately 20–500 µm. Stereoscopic examination of the filters revealed fine, white-to-colorless particles; opaque-to-transparent flakes and ribbons; brown, red, and orange-yellow particles; colorless, red, tan, and blue fibers; and large fibrous masses.

Examination of Particulate Isolated from the Least Hazy Solution

Particles from the least hazy monomer solution ranged in size from about 25 to 150 µm and were primarily clear or colorless and opaque or white. The approximate total weight percent of particulate (post-sampling) isolated from this sample was 0.001%. SEM analysis revealed that most of the particles had a bumpy, textured surface (Figure 3a). The elemental composition of a typi-

HORIBA Scientific

At HORIBA Scientific we pride ourselves on providing extraordinary spectroscopic solutions.

Horiba Scientific is the world-leading manufacturer of high performance Raman, fluorescence and elemental spectroscopic instrumentation.

Horiba Scientific's products offer unsurpassed precision and performance for applications in nanotechnology, semiconductors, pharmaceuticals, chemistry, photovoltaics, environmental and life sciences.

Combining our strengths in research, development and applications, HORIBA Scientific offers researchers the highest quality products and solutions.

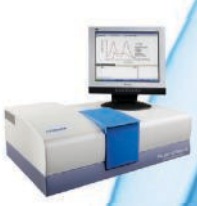

Fluorescence

Optical Spectroscopy

Atomic emission

Detectors

Raman analysis

OEM Spectrometers, gratings, hand-held Raman

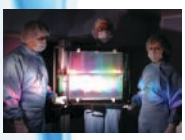

Custom gratings and VUV beamlines

X-ray fluorescence

Spectroscopic Ellipsometry

Particle Characterization

Surface Plasmon Resonance Imaging

Forensics

Pittcon 2012
Booth # 3222

horiba.com/scientific
email: adsci-specty@horiba.com

JOBIN YVON Technology

cal particle (Figure 3b) is consistent with components of the monomer solution including the fluoropolymer and silicone compounds with traces of the organotin compound and other inorganic salts. Analysis by Raman microscopy confirmed highly textured surfaces; a representative image is presented in Figure 4a. The Raman spectra suggested the particles were composed of silicone compounds and fluoropolymer with traces of an isocyanate compound (Figures 4b and 4c) — all components of the monomer solution.

Examination of Particulate Isolated from the Haziest Solution

Several clear or colorless and opaque or white particles in the 20–200 µm range were isolated from the haziest solution for evaluation. The approximate total weight percent of particulate (post-sampling) isolated from this sample was 0.004%. Examination of the 20–200 µm isolated particles by SEM revealed that most were composed of small bead-like features held together by a gelatinous material (Figure 5a). EDS analysis of these particles yielded elemental compositions rich in carbon, oxygen, silicon, and fluorine, with traces of calcium, sodium, and tin present (Figure 5b). Confocal Raman microscopy was used to characterize the small bead-like particles within the gelatinous matrix, many of which were <5 µm in diameter. This technique was especially effective because it allowed us to focus directly on the beads without further isolation from the gelatinous material. A representative particle exhibiting bead-like features is shown in the micrograph presented in Figure 6a; the corresponding Raman spectrum acquired from the marked location is shown in Figure 6b. Matching this Raman spectrum to spectral databases revealed the beads were consistent with a polystyrene-like material (Figure 6b). Raman spectral analysis of the gel-like matrix and colorless irregular shaped particles revealed mixtures of the components in the monomer solution, primarily fluoropolymer, silicone, and isocyanate (Figures 6c and 6d). The peaks at 997 cm^{-1} and 1602 cm^{-1} in Figure 6c suggest a trace of a polystyrene-like compound also may be present.

Extraneous materials were identified by micro-FT-IR and Raman spectroscopy. The FT-IR spectrum of a 70-µm clear particle indicated that the particle was a polyether ether ketone (PEEK) polymer (Figure 7a). Another clear particle was characterized as an inorganic carbonate by FT-IR spectroscopy and is presented in Figure 7b. Analysis of white particles by Raman spectroscopy with spectral matching revealed an acrylic polymer consistent with Carboset (Lubrizol Advanced Materials, Inc., Wickliffe, Ohio) products. Representative Raman spectra are presented in Figure 7c. Other extraneous materials identified by light microscopy, FT-IR, and Raman spectroscopy included skin flakes, cellulose particles and fibers (paper, cotton), polyethylene, and poly(tetrafluoroethylene) or PTFE.

Examination of Raw Materials, Intermediate Product, and Process Solvent

To trace the origin of the particles

causing the haziness of the monomer solutions, the raw materials and processing solvent were evaluated. A sample of an intermediate product of the polymer (that is, a prepolymerized, viscous liquid that had not yet been cross-linked) also was provided. Evaluation of the Raman and FT-IR spectra obtained from the starting materials, the methyl ethyl ketone processing solvent, the monomer solution, and the prepolymerized intermediate product revealed spectral peaks that could be used as markers for identification of these compounds in particles isolated from the monomer solutions. The spectra obtained from the intermediate product and the monomer solutions were quite similar and distinctions between the two were based on subtle variations of the contributions of the two isocyanate compounds. When identifying particles, the distinction between the monomer and intermediate product is not made, so both are referred to as monomer. The key peak positions for the raw materials, methyl ethyl ketone solvent, intermediate product, and monomer are provided in Table I.

Dilution of the viscous intermediate product solution with methyl ethyl ketone, followed by filtration, yielded clear or colorless and opaque or white particles that ranged in size from approximately 20 to 400 µm. Representative particles were selected for analysis by FT-IR, Raman microscopy, and SEM-EDS. FT-IR analyses of selected particles revealed materials associated with the monomer components, primarily fluoropolymer and silicone. Both surface texture and the elemental composition were evaluated by SEM-EDS. The data indicate bumpy, textured particle morphologies mainly composed of carbon, oxygen, silicon, and fluorine. Raman analyses showed that most of the particles were mixtures of the monomer components, primarily the fluoropolymer and isocyanate. (These data are consistent to the spectra presented in Figures 4, 6c, and 6d.)

Extraneous materials recovered from the viscous intermediate product following dilution with methyl ethyl ketone were identified by SEM-EDS and Raman microscopy. A representative 300-µm opaque or white particle was selected for analysis by SEM-EDS; the elemental composition is consistent with silicon. One 70–80 µm clear or colorless particle yielded a Raman spectrum consistent with an acrylic material, such as the Carboset acrylic material previously observed. An opaque or white particle exhibiting a bumpy, textured surface is shown in Figure 8a. The Raman spectrum of this particle indicates it is a mixture of fluoropolymer, residual monomer or intermediate product, and a polystyrene-like compound (Figure 8b).

The results of the preparation of the intermediate with methyl ethyl ketone led to the investigation of the methyl ethyl ketone solvent as a potential source of the polystyrene-like material. Evaporation of the methyl ethyl ketone yielded insufficient residue for analyses. A small volume (2 mL) of remaining methyl ethyl ketone solvent was mixed with particle-free deionized water to reduce the solubility of

any polystyrene, if present, in the solvent. During the addition of the water to the methyl ethyl ketone, a small amount of white residue was observed forming on the container walls, immediately above the liquid level. Evaporation of the methyl ethyl ketone and water blend yielded additional white residue for evaluation. However, the overall residue collected was minimal; the amount was estimated to be in the microgram range based on the overall weight percents of particulate collected from the monomer solutions and volume of methyl ethyl ketone used for the dissolution and evaporation study. FT-IR and Raman spectroscopy were used for analyses of the white residue and yielded spectra that suggested polystyrene or a related aromatic impurity was present in the methyl ethyl ketone solvent. The FT-IR spectra are presented in Figure 9a, and the corresponding Raman spectra are shown in Figure 9b.

Conclusion

Analyses of monomer and intermediate product solutions exhibiting particulate materials led to the evaluation of the raw materials and processing solvents as potential sources of extraneous particles. Most of the particles in the least hazy solution were determined to be related to the starting materials used in the formulation. Results indicated that most of the particles were mixtures of monomer components. Extraneous materials not related to components of the monomer were also identified.

Differences between the least hazy and haziest monomer solutions were primarily due to the presence of 2–10 µm polystyrene beads encapsulated in gel-like aggregated clumps of mixtures of the monomer components in the haziest solution. These individual polystyrene beads were identified using the high spatial resolution capabilities provided by CRM. The polystyrene-like component was rare or absent in the least hazy solution. The polystyrene contamination was traced back to the methyl ethyl ketone solvent. Although FT-IR spectroscopy suggested polystyrene might be present, Raman microscopy provided supporting results indicating the presence of a polystyrene-like material; detection of small particles of extraneous polystyrene-like material demonstrates the advantages achieved with confocal Raman microscopy.

The use of FT-IR and Raman spectroscopy along with SEM-EDS provided complementary analytical results to solve a challenging quality control problem during a contact lens manufacturing process. Identification of the particulate materials causing the haze of the monomer, as well as the source of it, assisted the manufacturer in improving the quality of the product.

References

(1) E. Caudron, A. Tfayli, C. Monnier, M. Manfait, P. Prognon, and D. Pradeu, *J. Pharm. Biomed. Anal.* **54,** 866–868 (2011).

(2) T. Vankeirsbilck, A. Vercauteren, W. Baeyens, and G. Van der Weken, *Trends Anal. Chem.* **21,** 869–877 (2002).

(3) M. Miller, M. Cavaliere, and D. Drew, "Evaluation of Controlled Release Products by Light Microscopy, Scanning Electron Mi-

croscopy and Confocal Raman Microscopy," presented at 37th Annual Meeting and Exposition of the Controlled Release Society, Portland, Oregon, 2010.

(4) M. Cavaliere, M. Miller, and T. Vander Wood, "Microscopical Characterization of Controlled Release Pharmaceuticals: A Complementary Approach," proceedings of Microscopy and Microanalysis, Portland, Oregon, 2010. J. Shields, S. McKernan, J. Mansfield, B. Foran, J. Frafjord, D. Beniac, and D. O'Neil, Eds. (Cambridge University Press, New York, New York, 2010).

(5) M. Miller, "Identification of Impurities in a Pharmaceutical API: Is Meeting USP Compendial Testing Enough?," presented at the American Association of Pharmaceutical Scientists (AAPS) Annual Meeting and Exposition, Los Angeles, California, 2009.

(6) M.A. Miller and T.B. Vander Wood, "Microanalysis in the Pharmaceutical and Biomedical Industry," proceedings of Microscopy and Microanalysis, San Antonio, Texas, 2003; D. Piston, J. Bruley, I.M. Anderson, P.Kotula, G. Solorzano, A. Lockley, and S. McKernan, Eds. (Cambridge University Press, New York, New York, 2003).

(7) T. Barber, *Instrumental Analysis of Particulate Matter, in Liquid-and Surface-Borne Particle Measurement Handbook*, J. Knapp, T. Barber, and A. Lieberman, Eds. (Marcel Dekker, New York, New York, 1996).

(8) J. Woodcock, *Amer. Pharma. Rev.* **7,** 10–15 (2004).

(9) N. Macleod and P. Matousek, *Pharm. Res.* **25,** 2205–2215 (2008).

(10) M. Witkowski, *Amer. Pharma. Rev.* **8,** 1–5 (2005).

(11) C. Alvareze-Lorenzo, H. Haruyuki, and A. Concheiro, *Amer. J. Drug Deliv.* **4,** 131–151 (2006).

(12) J. Bergin, "Contact Lens Polymers: A Technical Overview of the Development, Manufacturing, and Future of Contact Lenses," presentation from Introduction to Polymers Course, State University of New York at Buffalo, Buffalo, New York, 2000.

(13) D. Alonso, "Microscopy Techniques in Pharmaceutical and other Manufacturing Industries," proceedings of Microscopy and Microanalysis, Honolulu, Hawaii, 2005. R. Price et al., Eds. (Cambridge University Press, New York, New York, 2005).

(14) D.S. Aldrich, "Particulate Matter in Air and in Liquids- Isolation, Quantitation and Identification Considerations," proceedings of Microscopy and Microanalysis, Honolulu, Hawaii, 2005. R. Price et al., Eds. (Cambridge University Press, new York, New York, 2005).

(15) G. Torraca and Z. Wen, "Forensic Investigation of Biopharmaceutical Manufacturing Incidents by Light Microscopy, FT-IR Microscopy, Scanning Electron Microscopy and Energy Dispersive X-ray Spectrometry," proceedings of Microscopy and Microanalysis, Honolulu, Hawaii, 2005. R. Price et al., Eds. (Cambridge University Press, New York, New York, 2005).

(16) F. Adar, G. leBourdon, J. Reffner, and A. Whitley, *Spectros.* **18**(2), 34–40 (2003).

Mary A. Miller, Michelle R. Cavaliere, Ming Zhou, and **Pronda Few** are with MVA Scientific Consultants in Duluth, Georgia. Direct correspondence to: mmiller@mvainc.com. ■

For more information on this topic, please visit our homepage at: www.spectroscopyonline.com

Nanoscale IR Spectroscopy: AFM-IR — A New Technique

The combination of atomic force microscopy (AFM) and infrared (IR) spectroscopy in the technique of AFM-IR is one of the most important recent developments in the field of IR microspectroscopy and chemical imaging. The importance of IR spectroscopy to our scientific infrastructure needs no introduction given the size of the industry and the breadth of its application. However, the fundamental physical limit imposed by diffraction has prevented the use of this technique in applications requiring high spatial resolution, which is the case for many applications in polymers and the life sciences. AFM-IR uses an AFM probe as the IR absorbance sensor and hence breaks through the diffraction limit to attain spatial resolution improvements of up to two orders of magnitude over traditional IR microspectroscopy.

Curtis Marcott, Kevin Kjoller, Michael Lo, Craig Prater, Roshan Shetty, and Alexandre Dazzi

Infrared (IR) spectroscopy is one of the most practiced analytical measurement techniques in industrial and academic R&D laboratories. Unfortunately, diffraction physics limit its spatial resolution to ~5 µm. A spatial resolution breakthrough has been achieved with a novel technique that uses a nanoscale probe from an atomic force microscope acting as the IR absorbance detector (1). The nature of the IR absorbance detection results in simultaneous measurements of nanoscale mechanical properties and nanoscale morphology, along with the chemical composition. The technique also integrates nanoscale thermal property mapping, resulting in a multifunctional tool that provides nanoscale structure, chemical, mechanical, and thermal properties.

Introduction to AFM-IR

Atomic force microscopy with infrared spectroscopy (AFM-IR) is based on photothermal induced resonance (PTIR), a technique that was pioneered by Alexandre Dazzi from the Laboratoire de Chimie Physique, CLIO, at the Université Paris-Sud in Orsay, France (2–6).

The AFM-IR technique uses a pulsed, tunable IR source to excite molecular vibrations in a sample that has been mounted on an IR-transparent prism. This creates an illumination configuration similar to conventional attenuated-total-reflection (ATR) spectroscopy. As the sample absorbs radiation, it heats up, leading to rapid thermal expansion that excites resonant oscillations of the cantilever. The induced oscillations decay in a characteristic ringdown, as shown in Figure 1.

The ringdown can be analyzed with Fourier techniques to extract the amplitudes and frequencies of the oscillations. Measuring the amplitudes of the cantilever oscillation as a function of the source wavelength creates local absorption spectra; the oscillation frequencies of the ringdown are related to the mechanical stiffness of the sample.

Users of AFM-IR can quickly survey regions of a sample with AFM imaging and then rapidly acquire high-resolution chemical spectra at selected regions on the sample. As shown in Figure 2, polymer spectra acquired with AFM-IR have demonstrated good correlation with bulk Fourier-transform infrared (FT-IR) spectra.

This capability allows researchers to import individual nanoscale IR spectra into commercial IR databases where they can digitally search to chemically identify the materials at the specific sample locations measured.

Alternatively, the IR source can be tuned to a single wavelength to map compositional variations across the sample surface.

In addition to its ability to provide high-resolution infrared spectra, the technique provides information on the mechanical properties of the sample. This is accomplished, as mentioned above, by monitoring the frequency of the fundamental or higher resonant modes of the cantilever. This is analogous to the contact resonance method used for a number of years in the AFM community. The contact resonant frequency of the cantilever in the AFM-IR system correlates to the stiffness of the sample and can be used to map the modulus of the sample qualitatively. It also can perform nanoscale thermal analysis utilizing novel AFM cantilevers that incorporate a resistive heating element into the end of the cantilever. Using these cantilevers in combination with the system allows for the local measurement of the transition temperature of materials to a single point or an array of points across a sample. This can then identify or map the amorphous or crystalline content, stress, extent of cure, or other material properties which can be characterized by the transition temperature of the material.

This combination of measurement capabilities creates a multifunctional tool that provides nanoscale structure, chemical, mechanical, and thermal properties.

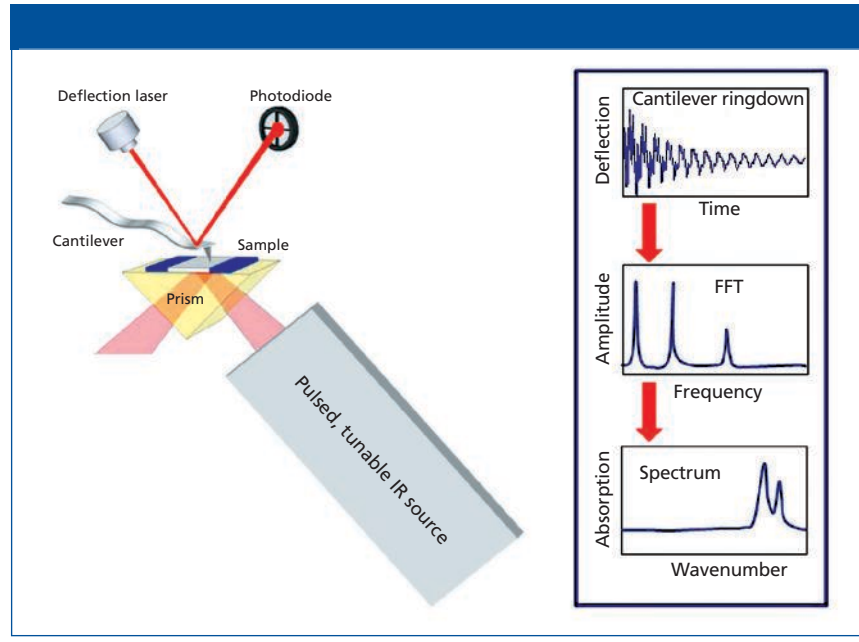

Figure 1: Operational schematic of the AFM-IR technique based on photothermal induced resonance (PTIR). The AFM cantilever ringdown amplitude plotted as a function of laser excitation wavelength produces the IR spectrum.

Experimental

The IR source in the AFM-IR system used in this study (nanoIR, Anasys Instruments, Santa Barbara, California) is a pulsed laser that is continuously tunable from 1200 to 3600 cm^{-1}. All AFM topographic images are obtained in contact mode with either an AppNano SICONA 450 µm (Santa Clara, California), TeamNanotec Improved Super Cone 450 µm (Villingen-Schwenningen, Germany) contact mode cantilevers, or ThermaLever self-heating cantilevers (Anasys Instruments). The spatial resolution of the IR spectra measured is determined by the AFM tip size, but it can deteriorate from this ideal for thicker samples because of heat transfer from regions deeper in the sample to the point at the sample

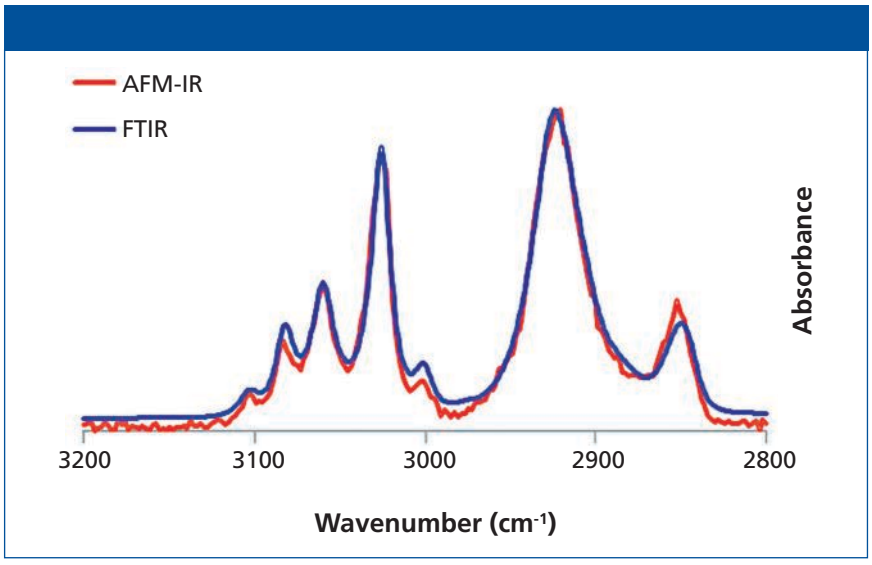

Figure 2: Spectral comparison of a polystyrene sample recorded in the CH-stretching region by AFM-IR (red) and conventional FT-IR (blue).

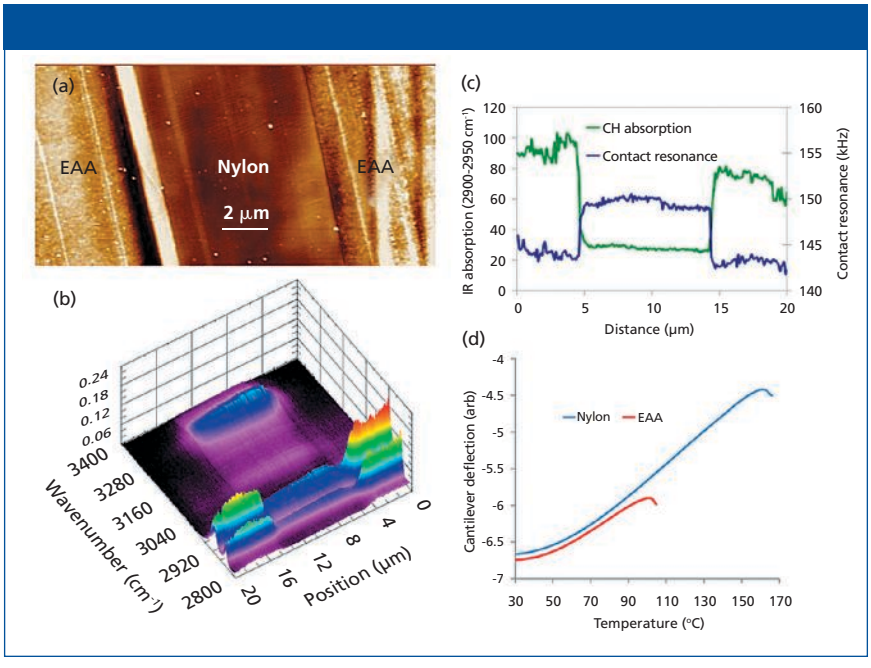

Figure 3: AFM-IR can be used to provide integrated measurements of topographic, chemical, mechanical, and thermal properties on the same sample. (a) AFM image of a laminated polymer multilayer comprising ethylene acrylic acetate (EAA) and nylon layers. (b) Line spectral map across the interfaces showing CH and NH absorption peaks. (c) Simultaneous chemical and mechanical characterization. The green curve shows the strength of the CH absorption between 2900 and 2950 cm^{-1} while the blue curve shows the relative mechanical stiffness across the interfaces. (d) Nanothermal analysis measurements performed on the nylon and EAA layers showing material softening at different temperatures.

surface where the AFM tip detects the signal. In the studies discussed in this article, sample thicknesses are typically 300–500 nm and we estimate the spatial resolution of the IR spectra to be about 100 nm.

Measurements of Polymeric Samples

AFM-IR is ideal for measuring polymeric samples in which there are local material variations (7). This includes materials such as polymer blends, multilayer films, nanocomposites, and micro- and nanoscale defects in materials. A number of examples follow that demonstrate the utility of the technique in these application areas.

AFM-IR requires a thin film sample that is deposited on the prism surface. To accomplish this, the typical sample preparation technique is to use ultramicrotomy to cut sections with thicknesses between 100 nm and 1000 nm. The sections are then transferred to a prism surface. Alternatively, the sample can be deposited out of solution, either drop cast or spin coated, onto the prism surface. Regardless of the sample preparation method, it is important that good optical contact be made between the sample and the prism surface to obtain the highest-quality spectral results.

Multilayer Films

A multilayer film example is shown in Figure 3 and demonstrates the multifunctional measurement capability of AFM-IR. This particular film has a number of layers with the central layer being nylon surrounded by two ethylene acrylic acetate (EAA) layers. Figure 3a shows the topographic image of the surface of the sample, which was created by embedding and microtoming the film.

After visualizing the different layers of the film in the topography, an array of spectra was collected across the sample surface, as shown in figure 3b. These spectra were collected over the range of 2800–3400 cm^{-1}, which includes the CH- and NH-stretching absorption bands. The two materials are clearly differentiated by their differing absorption in these two bands with a resolution of ~100 nm. The mechanical and spectroscopic data were obtained simultaneously, thus allowing direct correlation of mechanical stiffness information with chemical composition data (see Figure 3c). Note that the transitions in contact stiffness correlate extremely well with the strength of the CH absorption. The nanothermal analysis also was per-

formed on the same sample, clearly identifying softening at different temperatures for the nylon and EAA layers (see Figure 3d).

Polymer Blends

Within polymer blends, one of the challenges is in characterizing the extent of miscibility of the components and identifying the size and distribution of domains in immiscible or partially miscible blends.

Various techniques are used to image and characterize these domains, including electron microscopy, Raman microscopy, and AFM. AFM-IR brings the advantages of multiple property evaluation and the rich IR spectral information. An example of using the chemical identification capability of AFM-IR to identify domains in a blend is shown in Figure 4. The sample is a polycarbonate-poly(methyl methacrylate) (PC-PMMA) blend, which shows domain structure at the micrometer and submicrometer scale. The two components can be differentiated by the structure of the domains seen in the AFM image with one material exhibiting smooth domains after being microtomed and the other showing a rougher surface. These domains can then be identified as either PC or PMMA by the strength of the characteristic PC absorptions at 1770 and 1496 cm^{-1}. Six spectra were

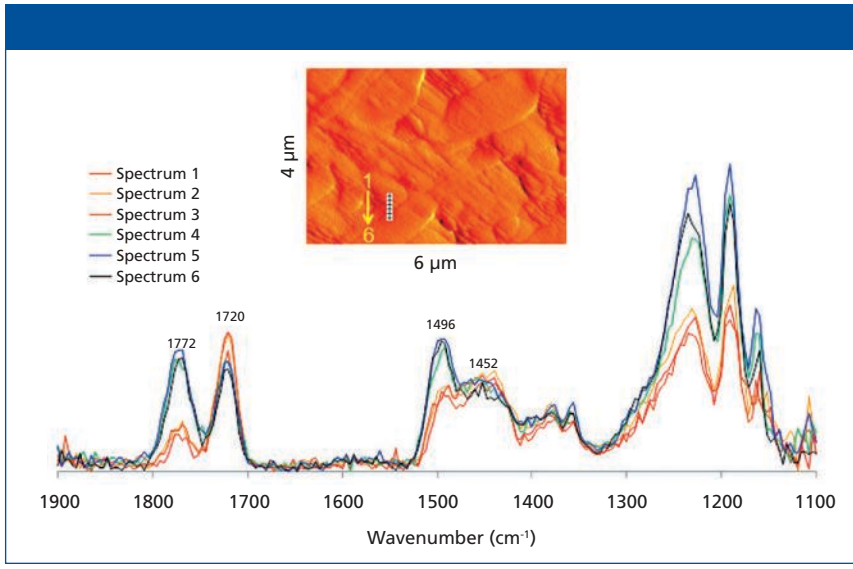

Figure 4: Polycarbonate–poly(methyl methacrylate) blend: 4 µm x 6 µm AFM image (top) and spectra (bottom) corresponding to six points spaced 100 nm apart across a transition between the two domains.

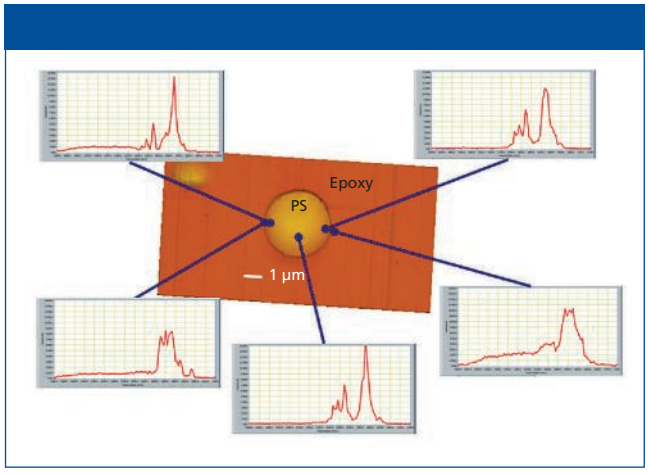

Figure 5: An AFM image and the spectra of a polystyrene (PS)–epoxy composite sample recorded in the CH-stretching region.

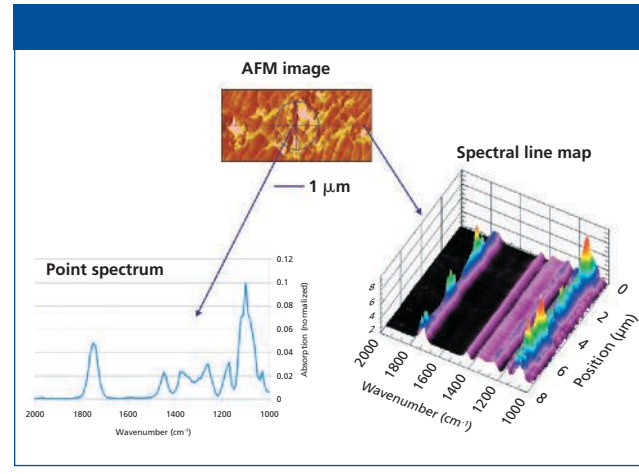

Figure 6: Spectral mapping of a degradable polymer blend.

taken across an interface between the two components with a separation of 100 nm. The PMMA dominates in spectra 1–3, while spectra 4–6 show a higher PC composition.

Polystyrene–Epoxy Composite

Figure 5 shows an AFM image with spatially resolved IR absorption spectra recorded on a thin section of a model composite of polystyrene (PS) and epoxy. The sharp transition in the spectral characteristics on either side of the PS-epoxy boundary demonstrates spatial resolution well beyond conventional IR microspectroscopy. Note that the IR spectrum collected at the center of the PS circular domain is an excellent match with the spectra recorded with 100 nm of the PS-epoxy boundary. Spectra on the lower left and right of Figure 5 collected between 2500 cm^{-1} and 3700 cm^{-1} within 100 nm of the PS-epoxy boundary show little or no evidence of the polystyrene aromatic CH-stretching absorption bands above 3000 cm^{-1}.

Degradable Polymers

Biodegradable polymers are important materials in a variety of applications ranging from tissue engineering, drug delivery, food packaging, and textiles. Such materials are increasingly complex blends of base materials and performance enhancing additives. The AFM-IR technique has been used to map, characterize, and even identify specific polymer additives. The AFM measurements allow mapping of the structure of the polymer matrix and additives. AFM-IR can then be used to spatially map variations in chemical components. In the line spectral map (Figure 6, right side), note the spatially varying intensities of the C=O carbonyl band

(1740 cm^{-1}) and the single bond C-O peak around 1100 cm^{-1}. These variations indicate the location of the two components in this material.

Summary

AFM-IR enables IR spectroscopy with 100-nm spatial resolution using AFM. It also provides high resolution topographic, chemical, mechanical, and thermal mapping. These measurements have been illustrated here using applications in polymer blends and multilayer films. Other publications have demonstrated the technique's capability with a broad range of materials and applications, including subcellular spectroscopy (8–11).

References

(1) K. Kjoller, J. Felts, D. Cook, C. Prater, and W. King, *Nanotechnol.* **21,** 185705 (2010).

(2) A .Dazzi, R.P.F. Glotin, and J.M. Ortega, *Infrar. Phys. and Technol.* **49,** 113–121 (2006).

(3) A. Dazzi, in *Biomedical Vibrational Spectroscopy,* P. Lasch and J. Kneipp, Eds. (J. Wiley & Sons, Hoboken, New Jersey, 2008), Chapter 13.

(4) J. Houel, E. Homeyer, S. Sauvage, P. Boucaud, and A. Dazzi, *Opt. Exp.* **17,** 10887–10894 (2009).

(5) A. Dazzi, *Thermal Nanosystems and Nanomaterials,* S. Volz, Ed. (Springer Berlin/Heidelberg, 2009), Chapter 16, pp. 469–503.

(6) A. Dazzi, F. Glotin, and R. Carminati, *J. Appl. Phys.* **107,** 124519 (2010).

(7) CC. Prater et al., *Microscop. & Anal. (SPM)* **24,** 5–8 (2010).

(8) A. Dazzi et al., *Ultramicroscopy* **108,** 635–641 (2008).

(9) A. Dazzi et al., *Optics Lett.* **33,** 1611–1613 (2008).

(10) C. Mayet, A. Dazzi, R. Prazeres, J.M. Ortega, and D. Jaillard, *Analyst* **135,** 2540–2545 (2010).

(11) C. Policar et al., *Angewandte Chemie Internat. Ed.* **50,** 860–864 (2011).

Kevin Kjoller, Mike Lo, Craig Prater, and **Roshan Shetty** are with Anasys Instruments in Santa Barbara, California.

Alexandre Dazzi is with the University of Paris-Sud in Orsay, France and is a scientific advisor with Anasys Instruments.

Curtis Marcott is a senior partner at Light Light Solutions (a consultancy firm specializing in vibrational spectroscopy) in Athens, Georgia, and a former research fellow at Proctor & Gamble. He has 35 years of experience in the IR spectroscopy field (including more than 100 publications). He received the Williams-Wright Award from the Coblentz Society in 1993 and was the 2011 President of the Society for Applied Spectroscopy. Please direct correspondence to: marcott@lightlight-solutions.com. ■

For more information on this topic, please visit our homepage at: www.spectroscopyonline.com

SPIE Defense, Security, and Sensing 2012

Spectroscopy previews the 2012 SPIE Defense, Security, and Sensing conference, to be held April 23–27, 2012, at the Baltimore Convention Center in Baltimore, Maryland.

Megan Evans, *Spectroscopy* Managing Editor

Jose Luis Stephens/GettyImages

At a time when security concerns are increasing around the world, the International Society for Optical Engineering (SPIE) presents the 2012 Defense, Security, and Sensing conference to offer timely material and research to help countries keep up to date with the latest tools and methods for security applications, as well as for environmental sensing. This year's conference will be held April 23–27 at the Baltimore Convention Center in Baltimore, Maryland.

Conferences

This conference features a unique setup compared to other conferences in that various topics are grouped into their own conference program tracks based on related technology topics. The program tracks include the following topics:

- IR Sensors and Systems
- Defense, Homeland Security, and Law Enforcement
- Imaging and Sensing
- Sensing for Industry, Environment, and Health
- Emerging Technologies
- Laser Sensors and Systems
- Innovative Defense and Security Applications for Displays
- Space Technologies and Operations
- Unmanned, Robotic, and Layered Systems
- Sensor Data and Information Exploitation
- Signal, Image, and Neural Net Processing
- Information Systems and Networks: Processing, Fusion, and Knowledge Generation

Courses

Another feature of the 2012 SPIE Defense, Security, and Sensing conference is the opportunity to meet with and learn from various industry experts and acquire skills you can apply to your daily work, through several courses offered. This year's program features 12 new courses and workshops, including all-new content on energy harvesting, night vision, high dynamic range (HDR) imaging, and international traffic in arms regulations (ITAR) and international trade.

Course registration includes the selected course, course notes, coffee breaks, and admittance to the exhibition. The course listings are available on the SPIE website under the various program tracks (http://spie.org/x6771.xml).

Exhibition

A conference exhibition is a great place for users to meet face-to-face with their suppliers or see new instrumentation that has become available. The 2012 SPIE Defense, Security, and Sensing exhibition is one of the biggest in this industry, with more than 500 companies expected on the show floor. Featured technologies include chemical and biological sensing; infrared sources, detectors, and systems; lasers and other light sources, laser accessories, and laser systems; cameras and CCD components; displays; electronic imaging and fiber-optic components, equipment, and systems; optical components, including specialized lenses and coating; high-speed imaging and sensing; high-precision optics manufacturing; nanotechnology applications; law enforcement technologies; robotics and unmanned systems; and new technology demos and displays. The exhibit floor with be open Tuesday, April 24 from 9:30 a.m. to 5:00 p.m.; Wednesday, April 25 from 10:00 a.m. to 5:00 p.m.; and Thursday, April 26 from 10:00 a.m. to 2:00 p.m.

Technical Program and Special Events

The 2012 SPIE Defense, Security, and Sensing conference will feature distinguished plenary speakers, workshops, panel discussions, poster receptions, and more. All conferees are welcome to attend the welcome reception on Monday, April 24 from 6:30 to 8:00 p.m. at the Maryland Science Center. There will also be a presentation and reception on "Women in Optics" on Tuesday, April 25, from 5:00 to 6:30 p.m. and an "Early Career Networking Social" on Wednesday, April 26, from 5:00 to 6:30 p.m., which all conferees are welcome to attend. Other events might require tickets.

For more information on this conference, please visit the SPIE website: http://spie.org. ■

PITTCON PRODUCT SHOWCASE

Chemical reaction monitor

The MB-Rx in-situ chemical reaction monitor from ABB Analytical Measurements is designed for use in laboratories and pilot plants. According to the company, the monitor is a plug-and-play system that provides real-time information about chemical or biochemical reaction kinetics and parameters. Data reportedly are collected with an insertion probe and can be analyzed via a software interface. **ABB Analytical Measurements,** Quebec, Canada; www.abb.com/analytical

Digital scientific camera

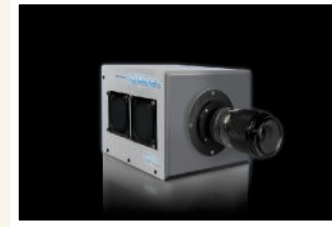

The xSCELL digital scientific camera from Photonis USA is designed for high-speed imaging at low light levels and with low dark noise requirements. Applications include fluorescence imaging, spinning disk confocal microscopy, high-throughput screening, and gene sequencing. According to the company, the camera features 1000 frames/s at a resolution of 1024 × 1024, readout noise of less than 2 e- rms, and quantum efficiency of 65%. **Photonis USA,** Sturbridge, MA; www.photonis.com

Spark atomic emission spectrometer

The OBLF GS 1000-II spark atomic emission spectrometer from PANalytical includes a spark stand design that incorpporates two counter electrodes. The design reportedly reduces total analysis time versus single-electrode spectrometers. According to the company, the instrument is capable of performing a two-measurement analysis of ferrous samples in 25 s. Samples requiring only standard carbon analysis and no nitrogen reportedly have an analysis time of 15 s. **PANalytical,** Westborough, MA; www.panalytical.com/OES

ICP accessory

Glass Expansion's Niagara Plus ICP accessory includes a six-port valve designed for simplified operation. An optional seventh port reportedly is available for automatic dilution or addition of internal standard. According to the company, software and port drivers are preloaded. **Glass Expansion Inc.,** Pocasset, MA; www.geicp.com

ICP-MS system

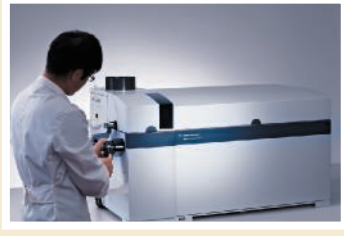

The Agilent 8800 triple-quadrupole ICP-MS system is designed to provide improved performance compared with single-quadrupole ICP-MS and to provide MS-MS operation for interference removal in reaction mode. According to the company, the system can be used to analyze elements in life-science, soil, rock, and plant materials. The system reportedly also can be set up to operate like a single-quadrupole ICP-MS system. **Agilent Technologies,** Santa Clara, CA; www.agilent.com

Imaging system

The iStar 312T imaging system from Andor is designed to provide acquisition rates greater than 15 frames/s and can be used for combustion and plasma studies. According to the company, the system also features a -40 °C thermoelectric cooling interface, low-noise electronics, and high-sensitivity photocathodes. The system's integrated digital delay generator reportedly enables low insertion delay and timing accuracy down to a few tens of picoseconds. **Andor Technology,** Belfast, UK; www.andor.com

Benchtop XRD systems

Rigaku's benchtop X-ray diffraction analyzers are intended for qualitative and quantitative analysis of polycrystalline materials. The Miniflex 600 analyzer operates at 600 W (X-ray tube), and the Miniflex 300 analyzer operates at 300 W and does not require an external heat exchanger. The analyzers reportedly are available with sample changers and are supplied with powder diffraction analysis software. **Rigaku Corporation,** The Woodlands, TX; www.rigaku.com

USB-to-Ethernet converter

The AvaGigE USB-to-Ethernet converter from Avantes is designed to enable the company's Avaspec miniature spectrometers to be controlled through an IP network. According to the company, the hardware device supports the connection of as many as 16 spectrometers (via USB hub) and a web-based configuration utility. **Avantes,** Broomfield, CO; www.avantes.com

Raman spectrometer

The RamSpec-HR 1064-nm Raman spectrometer from BaySpec is designed as a research-grade instrument for the wavelength range up to 1700 nm. The benchtop spectrometer reportedly is suited for applications such as process control, routine analytical analysis, reaction monitoring, material identification, and mixture analysis. According to the company, the instrument includes a light-tight sampling chamber, volume phase gratings customized for each specific wavelength region, and deep-cooled InGaAs array detectors. **BaySpec Inc.,** San Jose, CA; www.bayspec.com

FT-NIR spectrometer

The Tango FT-NIR spectrometer from Bruker Optics is designed as a stand-alone benchtop system with touch-screen operation. The spectrometer is intended for use in applications such as food, feed, chemical, and pharmaceutical analyses. The system is available in two versions, one for measuring solids in reflection and one for measuring liquids in transmission. According to the company, the spectrometer can be used in laboratory and dusty environments. **Bruker Optics Inc.,** Billerica, MA; www.brukeroptics.com

Diode laser modules

The MLD series high-performance laser diode modules from Cobolt AB cover a spectral range between 405 and 660 nm. According to the company, the lasers can be used for fluorescence applications such as confocal microscopy and flow cytometry, and they feature direct intensity modulation capability for applications such as optogenetics, microlithography, and metrology. All control electronics reportedly are integrated in an industry-standard-size laser head. **Cobolt AB,** Solna, Sweden; www.cobolt.se

Miniature voltage converters

The A Series DC-to-high-voltage-DC converters from EMCO High Voltage are designed to provide controllable output voltages of 100 V to 6000 V. The output power is 1 W standard, with 1.5 W available as an option. The converters reportedly occupy less than 0.1 in.^{3} of volume and have a profile of 0.250 in. **EMCO High Voltage Corporation,** Sutter Creek, CA; www.emcohighvoltage.com

X-ray sources

Moxtek's OptiMAG X-ray sources are designed for applications such as X-ray spectrometry and real-time imaging, in which collimated, high-flux, and stable X-ray output is required. The sources' focal spot reportedly is less than 800 µm and is centered on the X-ray exit window. According to the company, the sources' operate in the 4–50 kV, 0–200 µA range with a maximum output power of 4 W. The sources are intended for use in both handheld and benchtop instruments. **Moxtek, Inc.,** Orem, UT; www.moxtek.com

UV–vis spectrophotometers

UV–vis spectrophotometers from Shimadzu Scientific Instruments are designed for routine analysis and research applications. The double-monochromator UV-2700 system reportedly achieves stray light levels of 0.00005% T at 220 nm, a photometric performance range of 8 Abs, and a transmittance value of 0.000001%, which enables the measurement of low-transmittance samples. According to the company, the single-monochromator UV-2600 system features a measurement wavelength range to 1400 nm, which allows measurements in the near-infrared region and analysis of photovoltaics and other materials. **Shimadzu Scientific Instruments Inc.,** Columbia, MD; www.ssi.shimadzu.com

Dual laser source Raman module

PD-LD's LS-2 LabSource benchtop Raman module has two laser sources. According to the company, the laser sources are VBG-stabilized, and are available in standard and custom wavelengths. When the two laser sources' wavelengths are closely spaced together, the module reportedly is capable of performing surface enhanced Raman differential spectroscopy. **PD-LD, Inc.,** Pennington, NJ; www.pd-ld.com

Materials characterization database

Release 2011 of the Powder Diffraction File from ICDD contains ~747,000 unique material data sets. According to the company, each data set contains diffraction, crystallographic, and bibliographic data, as well as experimental, instrument, and sampling conditions, and select physical properties in a common standardized format. **International Centre for Diffraction Data,** Newtown Square, PA; www.icdd.com

Infrared filters

Infrared filters from CVI Melles Griot are manufactured using a sputter coating process and are designed for durability and environmental resistance. According to the company, the filters are optimized for peak transmission and blocking. The filters can be used for applications such as gas analyzers, nondispersive, or Fourier-transform instruments, spectrometers, and biomedical devices. **CVI Melles Griot,** Albuquerque, NM; www.cvimellesgriot.com

Diffraction gratings

Zeiss mechanically ruled or holographically recorded diffraction gratings from Hellma are designed using holographic exposure systems and ultrahigh-precision ruling engines. According to the company, the gratings are used with monochromators, spectographs, spectrophotometers, dye lasers, and other laser types. **Hellma,** Plainview, NY; www.hellmausa.com

ATR accessory

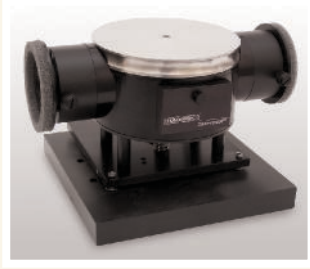

The Diamond ConcentratIR horizontal multiple internal reflection accessory from Harrick is designed for analyzing minute liquid and paste samples in quality control environments. According to the company, the compact attenuated total reflection (ATR) microsampler incorporates a diamond internal reflection element, and its infrared beam interacts within a 4-mm diameter area. The instrument reportedly has a feature that allows rapid sample exchange without interrupting the purge of the spectrometer. **Harrick Scientific Products, Inc.,** Pleasantville, NY; www.harricksci.com

Silicon drift detectors

Amptek's Super silicon drift detectors are designed for XRF applications with OEM handheld instruments and benchtop analyzers. According to the company, the detectors have 125-eV FWHM resolution, an 11.2-µs peaking time, and a P/B of 8200 with an area of 25 mm^2 and a silicon thickness of 500 µm. The detectors reportedly are contained inside the same TO-8 package and do not require liquid nitrogen. **Amptek Inc.,** Bedford, MA; www.amptek.com

Inorganic certified reference materials

Inorganic certified reference materials from SPEX CertiPrep are designed for use with US EPA and ASTM methods. The products can be used for compliance monitoring of drinking water samples and for the analysis of ground and surface water. Common methods include US EPA SW-846, Method 1310, US EPA 200.7, and US EPA 200.8. According to the company, each standard comes with a comprehensive, detailed certificate of analysis, and MSDS. **SPEX CertiPrep,** Metuchen, NJ; www.spexcertiprep.com

AA spectrometers

The PinAAcle atomic absorption spectrometers from PerkinElmer are available with a variety of configurations and capabilities, including flame only, furnace only, or stacked designs featuring both; flame, furnace, flow injection, FIAS-furnace, and mercury/hydride capabilities on a single instrument; and with deuterium or longitudinal Zeeman background correction. The spectrometers include the company's TubeView color furnace camera and WinLab32 software. **PerkinElmer,** Waltham, MA;, www.perkinelmer.com

Raman software

LabSpec 6 Spectroscopy Suite

LabSpec 6 Raman software from Horiba Scientific is designed to guide researchers through system setup, Raman spectrum data and map acquisition, measurement and data processing, and report generation. The software reportedly offers comprehensive data acquisition, processing, and display functionalities for the company's Raman, cathodoluminescence, and photoluminescence spectrometers. According to the company, the software also includes an integrated multivariate analysis module for characterization of complex datasets and on-the-fly data processing. **Horiba Scientific,** Edison, NJ; www.horiba.com

Topographic Raman imaging

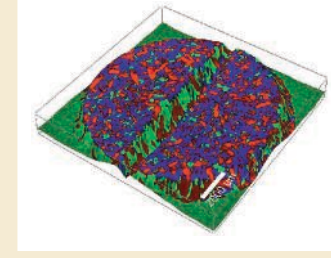

WITec's True Surface Microscopy imaging mode is designed to allow large-area topographic coordinates from the profilometer measurement to be precisely correlated with the large-area confocal Raman imaging data. This option reportedly enables samples that would normally require extensive preparation to obtain a certain surface flatness to be automatically characterized as they are. According to the company, it allows scan ranges as large as 50 mm × 100 mm with a spatial resolution of 100 nm vertically and 10 µm laterally. **WITec GmbH,** Ulm, Germany; www.witec.de

Temperature controllers

The PTC Series temperature controllers from Wavelength Electronics are designed for use in applications such as particle and droplet measurement, communications, manufacturing testing, and medical systems. The controllers reportedly operate from single power supply between 5 V and 30 V, and two models drive ±5 A or ±10 A to a Peltier thermoelectric cooler or resistive heater. The controllers mount directly to a circuit board. According to the company, the controllers interface with various temperature sensors and have an adjustable bias current. **Wavelength Electronics Inc.,** Bozeman, MT; www.teamwavelength.com

Hyperspectral imaging camera

Horiba Scientific's Verde hyperspectral imaging camera is designed to measure complete image and spectral information simultaneously. According to the company, the camera can capture the complete spectrum of every point in an image in a single measurement in 3 ms. The camera reportedly uses a 2-D dispersion element to capture all spatial and spectral information, and no averaging or repeated experiments are required. The camera has no moving parts. Possible applications are field work and industrial quality control, including plasma monitoring in semiconductor foundries, color quality control for fabrics, paints, foods, computer monitors, and televisions. **Horiba Scientific,** Edison, NJ; www.horiba.com

Mercury analyzers

Teledyne Leeman's Hydra II mercury analyzers are designed to provide configuration flexibility. According to the company, the analyzers can be configured to conduct the analysis of liquids by sample digestion followed by cold vapor atomic absorption or cold vapor atomic fluorescence, and the direct analysis of solid or semisolid sample matrices through thermal decomposition followed by cold vapor atomic absorption. **Teledyne Leeman Labs,** Hudson, NH; www.LeemanLabs.com

UV–vis microvolume spectrophotometer

The NanoDrop Lite UV–vis microvolume spectrophotometer from Thermo Fisher Scientific is designed to measure nucleic acid and protein concentrations in 1.0–2.0 µL sample sizes. According to the company, the compact spectrophotophotometer is suited for rapid, accurate, and reproducible microvolume measurements without the need for dilutions. Applications include routine measurements related to sequencing, PCR/qPCR, protein isolation, antibody production, and HLA typing. Features include local control, and a docking printer is available that prints freezer-compatible adhesive labels. **Thermo Fisher Scientific,** Waltham, MA; www.nanodrop.com

Spectrometer

StellarNet's Black-Comet-HR concave grating spectrometer is designed for high-resolution applications. According to the company, the system is available for measurements in two ranges, UV (200–600 nm) and visible (380–750 nm), and can achieve resolving resolutions of 0.4 nm. The system reportedly is USB-2 powered, shock-proof, and vibration tolerant with no moving parts **StellarNet,** Tampa, FL; www.stellarnet-inc.com

Raman microscope

Renishaw's inVia Raman microscope can be used for nondestructive testing of sperm DNA for assessing the healthiness of sperm cells. The instrument can be customized to integrate optical tweezing, which enables researchers to immobilize sperm cells with a tightly focused laser beam. The resulting Raman spectra contain information about the vibrations of molecules within the sperm cells and can be used to assess the state of its DNA. **Renishaw,** Hoffman Estates, IL; www.renishaw.com

Raman analyzer

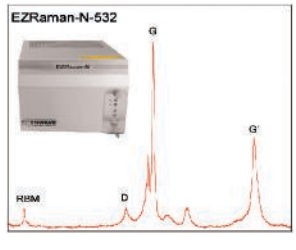

The EZRaman-N analyzer from Enwave Optronics is designed for fast carbon nanotube characterization. According to the company, the 100–3300 cm^{-1} spectral range covers full carbon nanotube bands of interest from the radial breathing mode to the G'-band. **Enwave Optronics, Inc.,** Irvine, CA; www.enwaveopt.com

Photovoltaic measurement system

Newport Corporation's Oriel IQE-200 photovoltaic cell measurement system is designed for simultaneous measurement of the external and internal quantum efficiency of solar cells, detectors, and other photon-to-charge converting devices. The system reportedly splits the beam to allow for concurrent measurements. The system includes a light source, a monochromator, and related electronics and software. According to the company, the system can be used for the measurement of silicon-based cells, amorphous and mono/poly crystalline, thin-film cells, copper indium gallium diselenide, and cadmium telluride. **Newport Corporation,** Irvine, CA; www.newport.com

Calendar of Events

February

16–20 2012 American Association for the Advancement of Science Annual Meeting
Vancouver, British Columbia, Canada
www.aaas.org/meetings/

25–29 Biophysical Society 56th Annual Meeting
San Diego, CA
www.biophysics.org/2012meeting/Main/tabid/2386/Default.aspx

27–2 March 8th Winter Symposium on Chemometrics in Russia (WSC-8)
Moscow, Russia
wsc.chemometrics.ru/wsc8/

27–2 March American Physical Society March Meeting
Boston, MA
www.aps.org/meetings/march/

March

3–6 24th Austin Symposium on Molecular Structure and Dynamics at Dallas (ASMD@D)
Dallas, TX
smu.edu/austinsymposium/

11–15 Pittcon 2012 — Pittsburgh Conference on Analytical Chemistry and Applied Spectroscopy
Orlando, FL
www.pittcon.org

25–29 243rd ACS National Meeting and Exposition
San Diego, CA
www.acs.org

28–29 International Conference on Optics, Lasers, and Spectroscopy (ICOLS 2012)
Madrid, Spain
www.waset.org/conferences/2012/madrid/icols/

28–31 10th Biennial International Conference of the Infrared and Raman Users Group (IRUG10)
Barcelona, Spain
www.ub.edu/IRUG10BCN/

April

9-13 Materials Research Society Spring Meeting
San Francisco, CA
www.mrs.org/spring2012/

16–19 SPIE Photonics Europe
Brussels, Belgium
spie.org/x12290.xml

23–27 SPIE Defense, Security, and Sensing 2012
Baltimore, Maryland
spie.org/x6771.xml

May

20–24 60th ASMS Conference on Mass Spectrometry
Vancouver, British Columbia, Canada
www.asms.org/

26–30 CSC 2012 — 95th Canadian Chemistry Conference and Exhibition
Calgary, Quebec, Canada
www.csc2012.ca/

June

3–8 Gordon Research Conference on Multiphoton Processes: Attoseconds, Intense Fields, and Ultrafast Imaging
South Hadley, MA
www.grc.org/programs.aspx?year=2012&program=multiphot

July

1–5 Euromar 2012
Dublin, Ireland
euromar2012.org/

August

5–10 Gordon Research Conference on Vibrational Spectroscopy
Biddeford, ME
www.grc.org/programs.aspx?year=2012&program=vibrspec

6–10 61st Annual Denver X-Ray Conference
Denver, CO
www.dxcicdd.com/

12–16 2012 SPIE Optics & Photonics,
San Diego, CA
spie.org/optics-photonics.xml

13–17 23rd International Conference on Raman Spectroscopy
Bangalore, India
www.icors2012.org

19–23 244th ACS National Meeting & Expo.
Philadelphia, PA
www.agrodiv.org/244th-acs-national-meeting-exposition

26–31 31st European Congress on Molecular Spectroscopy
Cluj-Napoca, Romania
www.phys.ubbcluj.ro/eucmos2012/

Short Courses

February 2012

25–26 DPOLY Short Course: Case Studies in Polymer Physics from the Industrial Research World
Boston, MA
www.aps.org/meetings/march/events/workshops/dpoly.cfm

March 2012

12 Introduction to Inductively Coupled Plasma Atomic Emission Spectrometry
Orlando, FL
www.pittcon.org

12 Side Illuminated Optical Fiber Sensor with a High Density of Sensing Points
Orlando, FL
www.pittcon.org

13 Fundamentals of Particle Size Analysis with an Emphasis on Light Scattering Techniques
Orlando, FL
www.pittcon.org

14–15 Basic Theory, Instrumentation and Applications of Vibrational Spectroscopy (Raman, Mid-Infrared, and Near-Infrared) in Materials Science)
Orlando, FL
www.pittcon.org

24–25 Analysis and Interpretation of Mass Spectral Data
San Diego, CA
www.proed.acs.org/sandiego/

24–25 Spectroscopic Method Development: Qualitative & Quantitative Techniques
San Diego, CA
www.proed.acs.org/sandiego/

26 High-Throughput Method Development for Drug Analysis by LC–MS
San Diego, CA
www.proed.acs.org/sandiego/

26–27 Infrared Spectral Interpretation: A Systematic Approach
San Diego, CA
www.proed.acs.org/sandiego/

27 Introduction to GLP Regulations and Bioanalytical Method Validation by LC–MS-MS
San Diego, CA
www.proed.acs.org/sandiego/

27–28 NMR Spectral Interpretation and Organic Spectroscopy: A Problem-Based Learning Approach
San Diego, CA
www.proed.acs.org/sandiego/

Call for Application Notes

Spectroscopy is planning to publish the next edition of The Application Notebook in September 2012. As always, the publication will include paid position vendor application notes that describe techniques and applications of all forms of spectroscopy that are of immediate interest to users in industry, academia, and government. If your company is interested in participating in this special supplement, contact:

Michael J. Tessalone, Group Publisher • (732) 346-3016
Edward Fantuzzi, Publisher • (732) 346-3015
or
Stephanie Shaffer, East Coast Sales Manager • (508) 481-5885

Ad Index

Resolution in Mid-Infrared Imaging: The Theory.

The field of mid-infrared (mid-IR) imaging has made significant developments in recent years, but the theory has not kept pace. Rohit Bhargava, an associate professor of engineering at the University of Illinois at Urbana-Champaign and the associate director of the University of Illinois Cancer Center, recently undertook studies to address that gap. *Spectroscopy* spoke to him recently about that work.

In your talk at the recent FACSS conference (now called the "SCIX conference"), you discussed the theory of resolution and image quality in mid-IR imaging. Why did you undertake this research into the theory?

Bhargava: Actually, the research started as just as curiosity, as a fundamental exploration of the theoretical basis for our field. I had been working in the area of infrared imaging for almost 10 years to that point, and we did not have a firm theoretical basis or a book where one could look up the theory of infrared microscopy and imaging. So this really started as an intellectual exercise, and took off from there.

Do the issues you have explored only arise with certain types of samples such as very small samples, at the nano- to micrometer scale?

Bhargava: The issue is present with all kinds of samples, whether it has any microscopic structure or not. The minute you take a sample and put it into an infrared microscope, the spectrum that you record will be different from that in the conventional interferometer, and that's because you don't have the approximately plane-wave geometry in which the light is slowly converging; you actually have a very highly converging beam of light in the microscope. So even if you have a uniform sample, under the microscope you will start to see some changes in the recorded data compared to the conventional spectrometer. With small samples, you get additional effects. So if the domain sizes are comparable to the wavelength, for example, you start to see distortion, you start to see a more prominent scattering effect. If the particle size becomes really, really small compared to the wavelength, you go back again and it appears homogeneous to the light off a certain wavelength. So you start getting back the sort of bulk effects that you would see with a homogeneous sample to begin with. So it's in both cases that you see some sorts of differences between a microscope and a conventional interferometer.

Can you summarize your theory?

Bhargava: Our theory actually can be thought of as a two-part process. The first is modeling the instrument and the optics itself. The second is modeling the sample and light interactions. Modeling the instrument is relatively straightforward; it's quite similar in theory to an optical microscope, for example. So we used much of the same framework. We start from Maxwell's equations, from the very fundamentals, and then we built up at each step, how light propagates from the source, to the beam splitter, to the mirrors, back again, through the microscope optics and on to the detector. As far as the sample is concerned, we again break it down into how light interacts with the sample, completely from first principles. We had no assumptions, no empirical parameters, nothing of that sort. So it's a very rigorous theory.

Now, there are two issues to keep in mind for this development. The first is how this differs from conventional optical microscopy and optical imaging. If you examine optical theory, a simplification is often made. In visible microscopy, we consider the sample to be a fairly uniform sample, with just a few, isolated points that actually scatter light. However, it's the scattering points that actually give the image contrast. On the infrared spectroscopy side, we have traditionally considered the samples to be highly absorbing but not scattering. If we examine the literature for almost all imaging techniques and mechanisms, you will see that this problem — image formation, that is — can either be broken down into places that don't have a whole lot of scattering but have absorption or have some amount of scattering and insignificant absorption. Hence, the theory is new, not only for infrared microscopy, but in general in the field of image formation.

This interview was edited for length and clarity.

To read the full interview, please visit: www.spectroscopyonline.com/Bhargava ■

2012 MRS FALL MEETING

November 25 – 30
Boston, MA

CALL FOR PAPERS

Abstract Deadline • June 19, 2012 Abstract Submission Site Opens May 19, 2012

MATERIALS FOR ENERGY TECHNOLOGIES

- A Compliant Energy Sources
- B Thermoelectric Materials Research and Device Development for Power Conversion and Refrigeration
- C Electrocatalysis and Interfacial Electrochemistry for Energy Conversion and Storage
- D Energy-Critical Materials
- E Photovoltaic Technologies—Materials, Devices, and Systems
- F Oxide Thin Films for Renewable Energy Applications
- G Materials as Tools for Sustainability
- H Small-Molecule Organic Solar Cells
- I Functional Materials for Solid Oxide Fuel Cells
- J Materials Aspects of Advanced Lithium Batteries
- K Hierarchically Structured Materials for Energy Conversion and Storage

SOFT MATERIALS AND BIOMATERIALS

- L Biomimetic Nanoscale Platforms, Particles, and Scaffolds for Biomedical Applications
- M Bioinspired Directional Surfaces—From Nature to Engineered Textured Surfaces
- N Precision Polymer Materials—Fabricating Functional Assemblies, Surfaces, Interfaces, and Devices
- O Next-Generation Polymer-based Organic Photovoltaics
- P Single-Crystalline Organic and Polymer Semiconductors—Fundamentals and Devices
- Q Functional and Responsive Materials Exploiting Peptide and Protein Self-Assembly
- R Fundamentals of Assembly in Biomolecular and Biomimetic Systems
- S Directed Self-Assembly for Nanopatterning
- T Membrane Material Platforms and Concepts for Energy, Environment, and Medical Applications
- U Colloidal Crystals, Quasicrystals, Assemblies, Jammings, and Packings

FUNCTIONAL MATERIALS AND NANOMATERIALS

- V Geometry and Topology of Biomolecular and Functional Nanomaterials
- W Carbon Nanomaterials
- Y Combustion Synthesis of Functional Nanomaterials
- Z Oxide Semiconductors
- AA Oxide Nanoelectronics and Multifunctional Dielectrics
- BB Recent Advances in Optical, Acoustic, and Other Emerging Metamaterials
- CC Optically Active Nanostructures
- DD Group IV Semiconductor Nanostructures and Applications
- EE Diamond Electronics and Biotechnology—Fundamentals to Applications VI
- FF Semiconductor Nanowires—Optical and Electronic Characterization and Applications

STRUCTURAL AND ADVANCED MATERIALS

- GG Mechanical Behavior of Metallic Nanostructured Materials
- HH Advances in Materials for Nuclear Energy
- II Atomic Structure and Chemistry of Domain Interfaces and Grain Boundaries
- JJ Intermetallic-based Alloys—Science, Technology, and Applications
- KK Complex Metallic Alloys
- LL Scientific Basis for Nuclear Waste Management XXXVI
- MM Materials under Extreme Environments
- NN Structure-Property Relations in Amorphous Solids
- OO Properties, Processing, and Applications of Reactive Materials

SYNTHESIS, CHARACTERIZATION, AND MODELING METHODS

- PP Frontiers of Chemical Imaging—Integrating Electrons, Photons, and Ions
- QQ Materials Informatics
- RR Advanced Multiscale Materials Simulation—Toward Inverse Materials Computation
- SS Quantitative *In situ* Electron Microscopy
- TT Defects and Microstructure Complexity in Materials
- UU Scanning Probe Microscopy—Frontiers in Nanotechnology
- VV Advanced Materials Exploration with Neutrons and Synchrotron X-Rays
- WW Roll-to-Roll Processing of Electronics and Advanced Functionalities
- XX Materials and Concepts for Biomedical Sensing
- YY Low-Voltage Electron Microscopy and Spectroscopy for Materials Characterization

GENERAL

- ZZ Communicating Social Relevancy in Materials Science and Engineering Education
- AAA The Business of Nanotechnology IV

The second annual **E-MRS/MRS Bilateral Conference on Energy** will be comprised of the energy-related symposia at the 2012 MRS Fall Meeting.

www.mrs.org/fall2012

2012 MRS FALL MEETING CHAIRS

Chennupati Jagadish
Australian National University
jagadish.mrs@gmail.com

Eric Stach
Brookhaven National Laboratory
stach.fall2012@gmail.com

Thomas Lippert
Paul Scherrer Institut
thomas.lippert@psi.ch

Ting Xu
University of California, Berkeley
tingxu.fall2012@gmail.com

Amit Misra
Los Alamos National Laboratory
amisra@lanl.gov

DON'T MISS THESE FUTURE MRS MEETINGS!

XXI International Materials Research Congress (IMRC) 2012
August 13-17, 2012
Cancún, Mexico

2013 MRS Spring Meeting & Exhibit
April 1-5, 2013
San Francisco, California

MRS MATERIALS RESEARCH SOCIETY
Advancing materials. Improving the quality of life.

506 Keystone Drive ▪ Warrendale, PA 15086-7573
Tel 724.779.3003 ▪ Fax 724.779.8313
info@mrs.org ▪ www.mrs.org

HORIBA
Scientific

Check out the magic in Orlando booth 3222

Pittcon 2012

HORIBA Scientific's products almost magically transform your samples from numbers to exciting research analyses and answers.

From fluorescence and Raman spectroscopy to glow discharge spectrometers, to hyperspectral illumination, find out how HORIBA's extensive line of high performance optical spectrometers, instrumentation and components can make magic for you.

Fluorescence

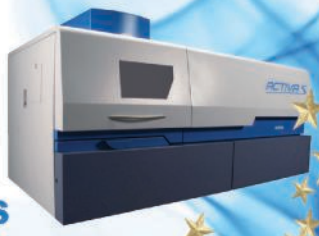

ICP & GD-OES

C/S/O/N & H Analyzers

Raman Imaging

Raman Microscopy

Particle Characterization

horiba.com/scientific
email: adsci-specty@horiba.com

JOBIN YVON Technology